# Design of a normally closed MEMS-microvalve for micropropulsion systems in PocketQube satellites

## Thesis Report

S. Agarwal

Technische Universiteit Delft

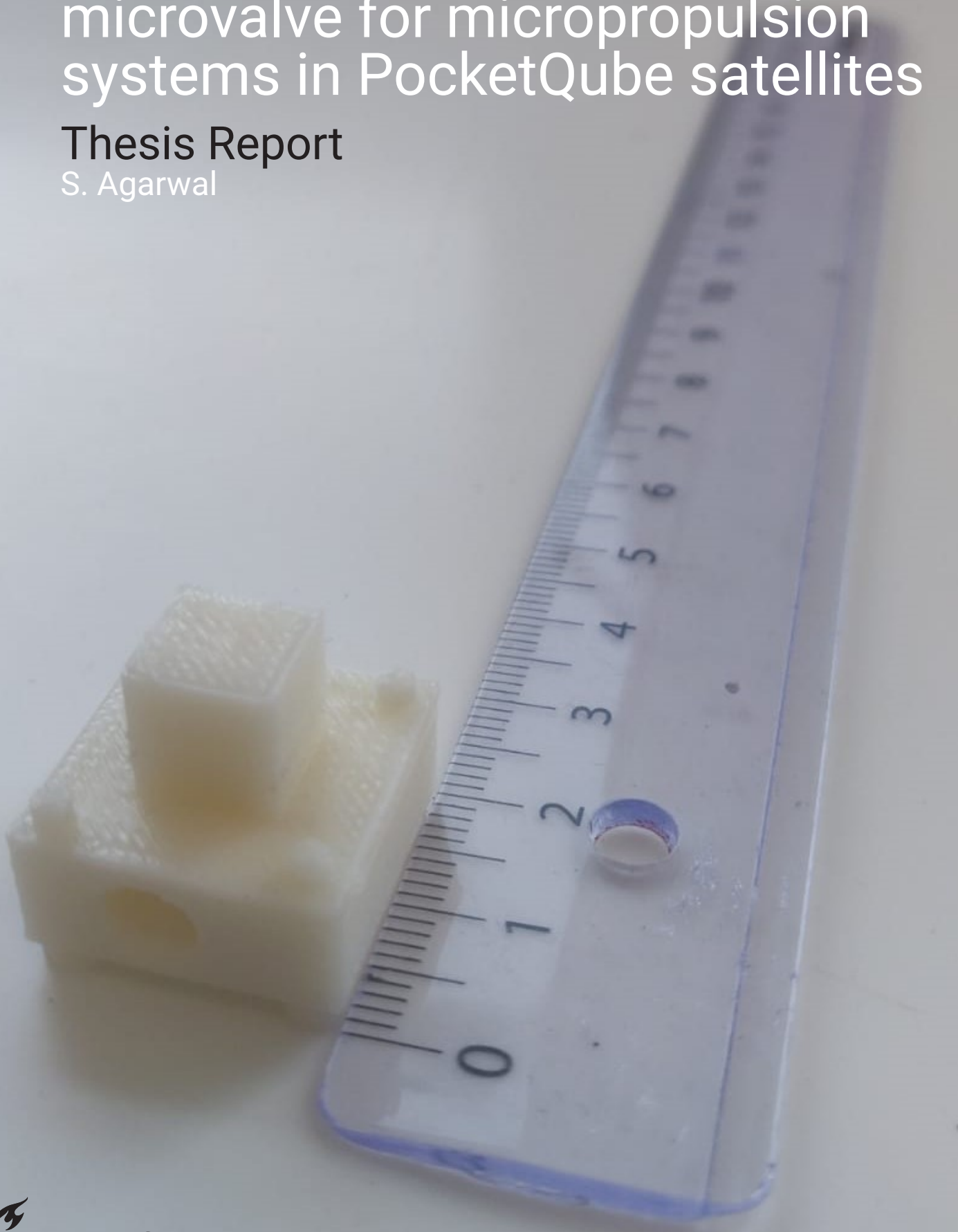

TU Delft

# Design of a normally closed MEMS-microvalve for micropropulsion systems in PocketQube satellites

## Thesis Report

by

S. Agarwal

in partial fulfillment of the requirements for the degree of

**Master of Science**
in Aerospace Engineering

at the Delft University of Technology,
to be defended publicly on Friday April 5, 2024 at 14:00 PM.


| | | |
|---|---|---|
| Student number: | 4738098 | |
| Supervisor: | Dr. A. Cervone | TU Delft |
| Thesis committee: | Dr. A. Cervone, | TU Delft |
| | Dr. A. Menicucci, | TU Delft |
| | Ir. K. Cowan, | TU Delft |




TU Delft

# Contents

# Acknowledgment

First of all, I want to contribute this thesis to an ongoing life journey towards wherever life will take me. I will always cherish my time at TU Delft, where I have been inspired so much, and have found so many wonderful friendships and connections. My time at TU Delft has been an extended one, powering through the covid pandemic and working my job at Airbus Defense and Space in the UK and France, and I am thrilled to now be able to present you this thesis report.

Thanks to my parents and my chōṭī behen, my little sister, who have given me endless support in achieving my dreams. I am forever grateful for who you are and your unconditional love for me. Also, many thanks to my friends with whom I have shared my journey in Delft. Always being there for each other, in good times and bad times, has given me so much strength, support and feelings of fulfillment. I could not have done it without you (Ash, Prem, Rajat, Pooja, Kashyap, Krishti, Abhinand, Aditi, Kaushal, Sniggs, Sampath, Kiran, Sahana). Additionally, I want to thank my boyfriend Victor, who never left my side on my endeavors and has been my rock for the past years.

Also, I had a lot of help from people in the industry. I want to express gratitude to Denis Mehmedov from Thorlabs and Francesco Stallone from EKL, who helped me to finalise the design. Your time and effort are highly appreciated.

Finally, I want to thank the people at TU Delft for making this all possible. From IT, who kept my thesis work online until the very end, to all the academic staff that taught me so much, either in or outside classes. Thanks for working with me and inspiring me. I want to mention Prof Henk van Zeijl from EWI who on multiple occasions has helped me move forward with my work. Thank you for your help. I want to thank the members of the thesis committee, Alessandra Menicucci and Kewin Cowan for being here today, to challenge my work and me for a final time. Last, but not least, I want to thank my thesis supervisor Angelo Cervone. Thank you for your help and guidance throughout this journey, and for being here to make my graduation day possible.

# Abstract

There is a growing demand for nano-satellite missions that require advancements in micro-propulsion capabilities to facilitate a wider range of orbital maneuvers. Among these capabilities, the ability to accurately control thrust would unlock new possibilities for nano-satellite applications, including missions such as space debris removal and orbit transfer.

Delft University of Technology is currently pioneering the development of an innovative green propellant-driven micro-propulsion system based on micro-electro-mechanical (MEMS) technologies for its PocketQube, known as Delfi-PQ, which features a compact form factor of 5x5x5 cm. While the thruster itself is in development, the interfacing and integration with other components are still ongoing.

Given the stringent mass, volume, and power limitations imposed by PocketQube satellite requirements, there is a pressing need for micro-scale components to realize a highly integrated propulsion system.

This thesis focuses on the design of a MEMS-based microvalve for proportional flow control in micro-resistojets. The design is conceptualised as comprising three components working in harmony: a valve seat with inlet and outlet, a flexible membrane, and a piezoelectric actuator. The valve seat with inlet and outlet, as well as the flexible membrane, utilize MEMS manufacturing techniques and are based on a silicon chip. And, a new design for piezoelectric actuators employing the d31 mode for contraction strokes is proposed.

The proposed preliminary design is a normally closed microvalve designed for a flow rate of 5g/hr, with the flexibility to accommodate higher flow rates if needed. It offers proportional flow control, ensuring precise regulation of fluid flow. Additionally, it promises a low power consumption of less than 1W and a low response time. Furthermore, this thesis provides a detailed outline of the MEMS fabrication process flow available at TU Delft's Else Kooi Laboratory for the device. It also features a comprehensive test plan aimed at assessing the feasibility of this design in future studies. Additionally, the thesis includes an elaborate risk analysis to help identify and mitigate potential risks during the manufacturing and testing phases.

The design shows promise and could pave the way for future developments of the microvalve within the department.

# List of Symbols

| | |
|---|---|
| **A** | Ampère |
| **C** | Celsius |
| **cc/min** | cubic centimetres per minute |
| **cm** | centimetre |
| **cm/s** | centimetre per second |
| **F** | Fahrenheit |
| **g** | gram |
| **g/hr** | gram per hour |
| **He** | Helium |
| **Hz** | Hertz |
| **hr** | hour |
| **kg** | kilogram |
| **kHZ** | KiloHertz |
| **kPa** | kiloPascal |
| **kW** | kiloWatt |
| **l** | litre |
| **$\mu$m** | micrometre |
| **m** | metre |
| **mA** | milliAmpère |
| **m/s** | metre per second |
| **mg/s** | milligram per second |
| **mL** | millilitre |
| **mL/min** | millilitre per minute |
| **mm** | millimetre |
| **mN** | milliNewton |
| **ms** | millisecond |
| **N** | Newton |
| **Ns** | Newton-second |
| **ns** | nanosecond |
| **Pa** | Pascal |

| | |
|---|---|
| **psi** | pound-force per square inch |
| **RPM** | Radians Per Minute |
| **s** | second |
| **scc/sec** | cubic centimeter per second |
| **sccm** | cubic centimeter per minute |
| **uF** | microFarad |
| **us** | microsecond |
| **V** | Volt |
| **W** | Watt |

# List of Acronyms

**BHF** Buffered HydroFluoric Acid

**CAD** Computer-Aided Design

**CFD** Computational Fluid Dynamics

**COTS** Commercial Off-The-Shelf

**DC-DC** Direct Current to Direct Current

**DI** Deionised

**DRIE** Deep Reactive-Ion Etching

**EDP** Ethylene Diamine Pyrochatechol

**EKL** Else Kooi Laboratory

**EWI** Elektrotechniek, Wiskunde en Informatica

**FE** Finite Element

**FEM** Finite Element Method

**FSI** Fluid-Structure Interaction

**GCI** Grid Convergence Index

**IC** Integrated Circuit

**JPL** Jet Propulsion Laboratory

**KOH** Potassium Hydroxide

**LPM** Low-Pressure Micro-resistojet

**MEMS** Micro-ElectroMechanical System

**MEOP** Maximum Expected Operating Pressure

**NASA** National Aeronautics and Space Administration

**NC** Normally Closed

**NO** Normally Open

**PCB** Printed Circuit Board

**PDMS** PolyDiMethylSiloxane

**PECVD TEOS** Plasma Enhanced Chemical Vapour Deposition TetraEthOxysilane

**PEEK** Polyether Ether Ketone

**PTFE** PolyteTraFluoroEthylene

**PWM** Pulse Width Modulation

**PZT** Lead Zirconate Titanate

**RIE** Reactive Ion Etching

**STL** Standard Tessellation Language or STereoLithography

**TMAH** TetraMethyl Ammonium Hydroxide

**TAS** Total Analysis System

**TEOS** TetraEthOxysilane

**TU** Technical University

**UV** UltraViolet

**VDC** Volts Direct Current

**VLM** Vaporizing Liquid Microthrusters

# List of Figures

# List of Tables

# 1 Introduction

The demand for a reliable, performing and mass-optimised propulsion system for small satellite applications is gaining attention. The need to improve the performance of the satellites in terms of mission lifetime and mission capabilities require a need for propulsion modules. These modules should be capable of fine tuning the delivered thrust in order to perform precise flight manoeuvres. The thrust magnitude can be controlled by controlling the propellant mass flow rate within the valve and the propellant feed system. Hence, in particular, valves are essential fundamental components for obtaining proportional flow rate control for a given differential pressure. The major challenge is the miniaturization of such microfluidic systems.

## 1.1. Motivation

There has been a rising interest over the past few decades in the development of emerging technologies in the field of small satellites thanks to to low development costs and simpler overall systems [12]. As the components become small and more powerful the trend towards small size shows no signs of stopping in the future. Space industry is moving from using one satellite for a specific mission to using distributed systems where these small satellites work together. The large missions that took several years until launch are being replaced by smaller, faster and cheaper approach to also reduce the launch cost.
In this regard, innovation is proceeding at a very fast pace in the field of miniaturization and has evolved significantly since the 1980's [21]. High level of miniaturization can be achieved by applying micro- and nanotechnology design to produce sub-millimetre to sub-micron level devices. Integrating microelectronics with mechanical components (MEMS) in small-satellite components has a huge potential in space application and is an alternative for challenging space requirements: low power consumption and low mass without significant loss in capabilities [20]. However, to ensure that miniaturization does not lead to loss in capabilities which necessitates the need for novel instruments and systems based on MEMS technologies. Hereof, institutes, Startups and Universities along with Government space agencies are working on developing innovative space platforms and MEMS technologies to include more capabilities in small packages. Application of these MEMS technologies is not limited to the space or military industry only, but can be extended to any field. For example, the MEMS Technology group at Jet Propulsion Laboratory (JPL) is currently developing MEMS technologies for biomedical devices, adaptive optics, along with micro-instruments and micro-propulsion devices [20]. Even the Automotive and mobile industry employs the use of MEMS sensors for the various functionality of their subsystems[21]. MEMS devices are also pursued in magnetic storage systems where they are being developed for super compact, high storage density discs. Moreover, they are also used in chemical and gas sensors, focal plane arrays for earth observations and in various microscopic surgeries.

The Delft University of Technology is developing a green-propellant driven micro-propulsion payload for its PocketQube satellite called Delfi PQ which is based on MEMS technologies. This satellite has a form factor of 5 cm*5 cm*5 cm. Having a propulsion system for these kind of satellites will open up new possibilities for a wide range of applications including orbital maintenance and transfer, formation flying and attitude control. Most of the micro-spacecrafts today lack a dedicated propulsion system for orbit change manoeuvres. By means of reaction wheels and small thrusters, satellites can position themselves but cannot change orbit. Having a compact propulsion system enables capabilities for future constellation missions. Due to the

strict mass, volume, and power limitations imposed by PocketQube satellite requirements there is a need for unique micro-scale components to develop a compliant propulsion system. There are two micro-resistojets currently being developed by TU Delft, one is a low-pressure free molecular concept (LPM), and the second is a more conventional one based on vaporization of liquid water (VLM) [8]. These MEMS based thrusters have been developed but its interface with other fluidic components still needs further development. Significant mass and volume savings can be achieved if these micro-fabricated thrusters can be tightly integrated with other system components. Conventional and commercially available propulsion system components are too bulky and heavy to be used in micro satellites. A promising technology is to use micro machining technologies for fabricating MEMS based components, making the integration of different components in one device smarter and less challenging. This would help achieve a highly integrated MEMS-based propulsion system with reduced volume space and better control functionality.

The successful operation of these micro-resistojets is dependent on reliable and robust micro-fluidic systems. Valves form an integral part of the fluidic components to be used in these micro-propulsion systems for precise maneuvers and high $\Delta V$ missions: thrust levels can be in the order of a few milli-newtons or less and impulse as little as $10^{-6}$ Ns [9]. To achieve such low requirements precise control of propellant flow is necessary.

In this context, there is a growing headway at TU Delft in the research and development of new microvalve with the future goal to be integrated in the same chip as the thrusters for their micro-propulsion systems. The author Leon Turmaine et al. [68] presented the design of the technology demonstrator to test the propulsion system (VLM and LPM) on a PocketQube platform. He designed the prototype to test the propulsion system, ensuring that it would fit within the Delfi-PQ volume. The design incorporated MEMS thrusters integrated with COTS based fluidic components. The author pointed the currently used COTS valve (VHS Lee Valve (INKX0511400)) as the design limiter. These valves fulfilled the performance requirements of the propulsion systems but posed great limitation to the available volume for the rest of the propulsion components in the Delfi-PocketQube's platform. In response to the above need, miniaturisation of the valves was required which can be developed in-house and employs the use of MEMS technologies to achieve a higher level of integration with the other components. Hence, this dissertation is motivated by the study mentioned above. The mass budget of the prototype design presented by Leon et al in his study was used as input for this research.

## 1.2. Overview of Manufacturing facility

The success of any design project is intricately linked to the manufacturing environment in which it is envisioned to be fabricated. This section will present a brief overview of the manufacturing facility where the proposed design will come to fruition. This will be beneficial for contextualising the subsequent discussion on the design process and the outcomes.

The Else Kooi Laboratory (EKL) located in the EWI faculty of TU Delft is the manufacturing facility for this design project. EKL specializes in MEMS production and collaborates with many research groups both internal and external to offer expertise in micro fabrication processes. The research activities in MEMS manufacturing at the EKL encompass a wide range of areas including actuators, microfluidics, biomedical devices etc. The laboratory offers lithography, thin film deposition, etching, bulk and surface micro-machining, assembly and packaging of the device. Before you can actually transform a design schematic to a device, it is important to know how the device is actually fabricated i.e. the process step sequence or flowchart. The expertise, diverse research portfolio, collaborative environment, and the proximity of the Space Engineering department to the manufacturing facility makes an ideal setting for this research to be carried out at EKL. But, it is worth noting that the fabrication of the valve chip itself is out of the scope of this thesis.

## 1.3. Objective and Method

To address the problem stated above, the primary purpose of this study is to propose a design of a small footprint valve that can comply with the mass, size and power constraints of the picosatellite mission, such as the TU Delft-pocketQube one and can be fabricated in-house at the EKL using MEMS fabrication techniques. Based on the goal of the research to be carried out the following research objective has been formulated.

*To design a MEMS microvalve that works with liquid water and that will meet the design requirements, while having the potential to be easily integrated with the thruster?*

The objective is further broken down into sub research questions as given below:

1. What are the performance characteristics of the proposed valve design?
   (a) Which components are required for the design of microvalve for VLM?
   (b) What is the characterisation of the valve with respect to the flow rate at different pressure values and power consumption?
   (c) How dynamic is the range of flows that the valve can control?
   (d) How reliable is the design of the microvalve in case of full system power failure?
   (e) What are the limitations of the design?

   Questions 1.a will be answered with the use of systems engineering tools such as: a design tree, requirement generation and trade-off analyses. Information gathered during the literature study will also be of importance in answering this question.

   From the systems requirement table generated using systems engineering approach, a detailed valve design will be accomplished. The various design parameters that affect the performance of the valve will be identified and modelled. This will be helpful in characterising the performance of the valve and to answer questions 1.b,1.c. The reliability of the design will be addressed through a comprehensive risk analysis to identify and eliminate potential risks.

2. What materials are compatible with the available micro-fabrication approach for the construction of the design?
   (a) What are the fabrication steps involved for the realisation of the valve?

   Chapter 9 presents detailed information about Question 2, which also involved generating a step-by-step flow process for the final concept. The process flow engineers at EKL were consulted to create this flow step, which will provide an understanding of the device fabrication process.

3. How can the microvalve design be verified?

Question 3 is answered by setting up a verification plan for each requirement. This results in a test plan for future researchers at TU Delft serving as a cornerstone for testing these MEMS based microvalve which is first of its kind in the Space Engineering department.

## 1.4. Thesis Outline

This section describes the outline of the thesis report based on the above objectives. The motivation for this study and the research questions of this work were outlined in Chapter 1. Chapter 2 provides a comprehensive overview of the operating principle and the design specifications which serve as the foundation for the requirements for the microvalve. Chapter 3 presents a comprehensive overview of the valve review that was conducted to explore different valve concepts and mechanisms available in literature. In Chapter 4, selection of the most suitable concept for the different valve components will be motivated. Chapter 5 presents the different micro-fluidic strategies and presents the explored valve concepts before establishing a baseline design. The design is further developed in the Chapter 6 and the analytical analysis performed for the sizing of the valve components is elaborated. Chapter 7 presents the numerical model and the results from the fluid and mechanical simulation for the design are compared with the analytical model. Further evaluation of the dynamic characteristics of the piezo valve design is also presented. The final design is proposed in Chapter 8 through the CAD model, followed by the mass budget. Chapter 9 throws light on different MEMS fabrication technique, followed by step-by-step flowchart of the fabrication process. The potential risks anticipated during the manufacturing phase are introduced as well. Chapter 10 provides the initial verification plan for the design along with the detailed test plan to be followed to characterise the design performance. Finally, the conclusions extracted from the work performed and the recommendations for future work are summarised in Chapter 11.

# 2

# Research Framework

## 2.1. Background

The need for techniques to manipulate chemical and biological reagents in chemical analysis systems led to the introduction of micro-total analysis systems (($\mu$TAS) [36]. They are utilized in a variety of applications like drug delivery, microthermal technologies, thermal cooling, propulsion systems and lab-on chip devices [44]. These devices rely on microfluidic and involve the manipulation of tiny amounts of fluids in micro-channels using microfluidic components, i.e, microvalves and micro-pumps for various analysis and purposes. These are being made smaller and further miniaturized on a single chip to increase the efficiency, reduce the dead volume, less consumption of expensive chemical reagents, decrease in reaction time and increase reliability. Microvalves are essential microfluidic components that regulate the fluid flow in a micro-channel between two ports which form the inlet and outlet of the system. A systematic network of microchannels from inlet and outlet ports can establish simple to complex microfluidic network-based devices. They form fundamental elements in various fields such as life sciences and spacecraft micro-propulsion. They are used for on/off switching, proportional flow control or sealing of biomolecules, micro or nanoparticles, liquids, gases and many others. In conjunction with a pressure source, it is used to control, direct or regulate pressure or flow rate of the working fluid within these microfluidic circuits. Valves that operate in the $\mu$m- to cm- length scales are generally classified as microvalves and are usually fabricated using micro-fabrication techniques like lithography and etching. A smaller device size, higher pressure, biocompatibility, response time, and most importantly, microtechnology, all contribute to the valve design in microscale [43].

The groundbreaking work on micro valves started in the 1970's and quickly shifted to MEMS based microvalves in the 1990's. The introduction of the miniaturised total analysis system by Manz et al [44] greatly encouraged research in MEMS based microvalve concepts. The development of the microvalves is progressing and impressive progress has been made since the last 4-5 decades. According to the proceeding from the $\mu$TAS 2005 conference there has been a rising trend in the research of developing non-traditional microvalves [44]. However, even though improvements have been made regarding the performance of these valves, still they need to be reliable and handle flows with a large dynamic range. Many valves are commercially available for on and off switching but for applications such as micro-propulsion systems, proportional flow control microvalves are the most suited. Cost effective precise proportional flow control microvalves are not readily available, moreover they generally require external peripherals making them not suited for applications with strict mass budget. Hence, their diffusion into the commercial market has been very limited making their feasibility for commercialisation not entirely successful. [71].

When designing a microvalve, the application is critical for determining the requirements it needs to respect. In this chapter, the foundation of the microvalve configuration and design concepts will be outlined in brief, followed by the setup of the intended application use. After which, based on the application, the requirements pertaining to realising a valve design will be discussed in section 2.5.

## 2.2. Basic operating principle

Microvalves are fluid control devices that regulate the flow between two ports - an inlet and outlet. Controlling the fluid flow can be compared to the change in resistance in an electric circuit. This resistance can be changed by various means: changing the mechanical geometry, using an active element to obstruct the

passage or changing the differential pressure across the ports. A valve is in principle a pressure contained device used to shut off or otherwise modify the flow of fluid that passes through it. By definition, a valve is a device which has a body to contain the fluid and its pressure, a closure element to manipulate the fluid and an actuator.
A large body of research in microvalves has resulted in their classification based on a number of characteristics. This will be detailed further in the subsequent chapter. The main criterion for classification is their method of operation. A valve can be either passive or active, i.e, they might be unpowered or powered by an actuator. Passive ones generally employ pressure differences for the opening and closing of valves. However, the basic working principle of the valve ( active/passive) remains the same and can be explained from figure 2.1.
The bottom plate is called the valve seat which has the opening called the inlet and outlet orifice to allow for the fluid flow. The top part in the valve is what covers the orifice. It will be referred as plunger throughout the report. It is shown as a vertically translating plate in figure 2.1. However, there can be different design variations of the plunger as will be discussed in section 4.2. By changing the orifice passage either by using an active element or by varying differential pressure, the flow resistance denoted by R_flow can be changed thereby in principle offering controllability for the fluid flow.

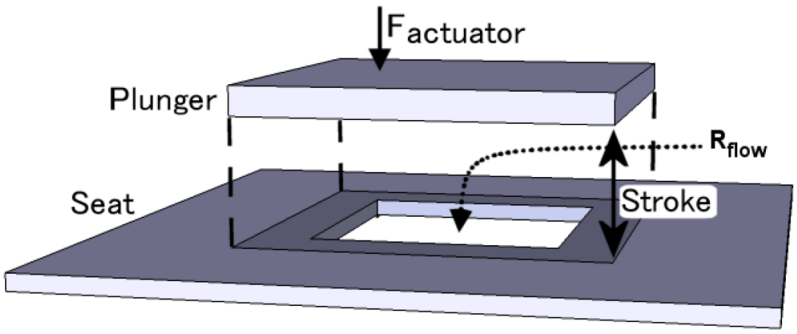


Figure 2.1: Basic structure and operation of a microvalve [24]

The force required to change the orifice volume in case of active valve is the actuating force denoted by F_actuator. The maximum separation between the plunger and the seat is defined by the stroke. The actuator is used to control the position of the valve in case of active microvalve, whereas in passive valves it is regulated by the differential pressure. The maximum flow supported by the valve depends on the fluidic channel geometry and the stroke length.

To close the valve against the fluid flow, the actuator force needed to be acting on the plunger will depend on the plunger stiffness and the maximum differential pressure across the valve since the force exerted by the fluid on the plunger needs to be counteracted by the actuator to keep the valve close. Therefore, for proper closure of the valve system and to allow for a leak tight system the maximum actuator force and seating pressure plays an important role in the design. The closing surface area, the actuating force, the surface roughness of the two plates greatly determine the leakage performance of the valve. Hence, choosing the appropriate valve dimensions and actuator mechanism plays a key role in the performance of the valve subsystem and hence the overall performance of the system.

In summary, an active microvalve basically consists of three major components: an inlet/outlet orifice for the fluid flow which is usually on the valve seat, a membrane/plate (referred to as plunger in figure 2.1) to open and close the orifice which provides the valve sealing and an actuator to provide the force required to open or close the valve denoted by F_actuator in figure 2.1. Whereas in passive valves, the deflection (stroke) is controlled by changing the differential pressure across the inlet and outlet.

## 2.3. Application

The application of a microvalve is for micropropulsion systems to be used in CubeSats or PocketQube satellites. The dual thruster propulsion system is based on water as a propellant and is currently being developed as the technology demonstrator on-board the PocketQube satellite platform to be launched by TU Delft. The two micro-resistojets concepts that are being designed at TU Delft ought to be demonstrated on the same flight and are based on two different thrust producing mechanisms: VLM which depends on heating, vaporization and expansion of pressurised liquid water in a nozzle where water enters the heating chamber in

slightly pressurised and liquid state ; and the other one, LPM based on heating and acceleration of vapour molecules in slots of simple geometry which are engraved in the chip; the slots serve as both a heating and expansion device at the same time [50],[67]. The two methods have different operating conditions and working principle hence the type of fluid flow to be controlled by the microvalves differs for both of them. The derived physical architecture of the operational envelope of the micro-propulsion system can be seen in figure 2.2 [68]. For the space propulsion system, as the propellant is being consumed over the lifetime the tank pressure reduces, the tank pressure is not maintained constant. Therefore, there is a need for continuous thrust regulation in the range from zero to maximum based on the intended application.

For this research project, the intended use of microvalve system is envisioned for the VLM thruster. The valve design is usually optimised for specific performance parameters: operating pressures, flow rates and leak ratios. The design presented in this thesis has been analysed for its suitability with liquid use. Nevertheless, the chosen materials for the design will also render it compatible for gas flows. However, it's important to note that the performance of the design will vary, as the pressure drop across the system will differ between the two media. Moreover, gas flows necessitate more stringent leakage requirements since they can escape even from microscopic openings, which may further require the consideration of different materials. The author proposes testing the same design for gas flows as well.

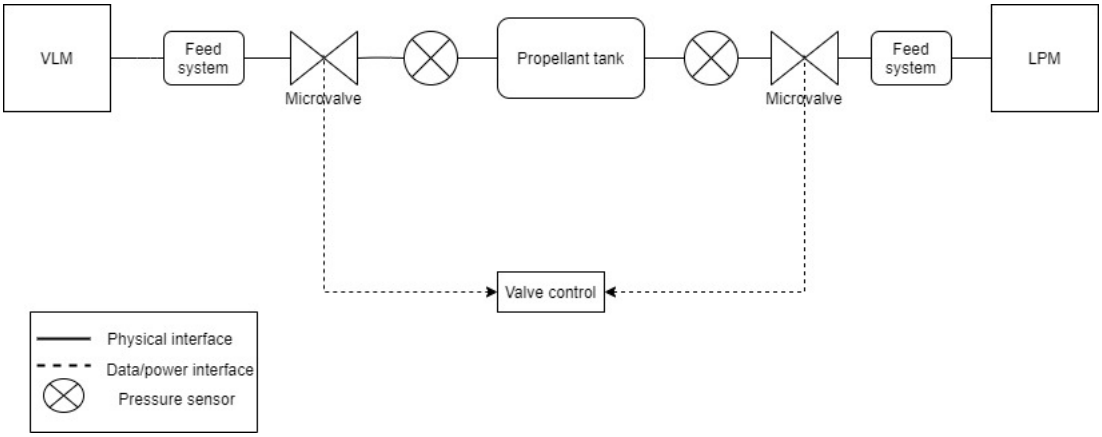


Figure 2.2: Schematic of the architecture of the system at the component level [68]

## 2.4. Design specifications

The applications for which the micropropulsion system is chosen for, places critical requirements on the subsystem level. For example, in order to achieve precise and sophisticated thrust regulation, the response time of the microvalve needs to be within a few milliseconds. Further, since the propellant that can be carried onboard is limited, the leakage requirements for the microvalve become very stringent since it directly impacts the mission lifetime hence the system capabilities. The controllability range of the mass flow rate influences the applications that the propulsion system can fulfil.
On the component level, microvalve design provides input variables for the control hardware for thrust regulation thus imposing inherent control requirements for the system, in turn characterising the range of flows. Even the PocketQube platform adds limitations in terms of mass and volume. This imposes further system and interface requirements on the propulsion system which translates to every component. Adherence to these constraints to ensure compact and flexible interfaces with the overall system and the satellite itself also adds to the challenge. The major specification bases for microvalve are leakage, power consumption, pressure range, temperature range, response time, reliability and biocompatibility. Some of the key parameters for the valve design consideration are detailed below.

1. **Leakage**: For any fluidic system it is necessary to keep a check on the leakage levels, since a very leaky system might lead to system failure. Leakage in a system is usually referred in terms of leak tight and a leaky system, their distinction based on leak rates is given below. High propellant leak rates through MEMS valves seem be an important problem in successful utilisation of these valves in micropropulsion systems [41]. However, no vacuum system can be absolutely leak tight, the essential criteria is that the leak rate must be low enough that the operating pressure and the gas pressure are not in-

fluenced. The most common leak detection method used is the gaseous helium test. It is given by 2.1

$$\Delta Q = \frac{V \times \Delta p}{\Delta t} \tag{2.1}$$

where ΔQ is the leak rate, V is the volume occupied, Δp is the pressure difference and Δt is the time difference over which it is measured. It is important to define the leak rates for the microvalve which classifies it a leaky or a leak tight system.
1 [Pam$^2$/s] ≈ 9.87 [scc/s]

$\Delta Q < 10^{-7}$ Std scc/sec is defined as a very leak tight system
$10^{-7} < \Delta Q < 10^{-4}$ Std scc/sec It is considered as a leak tight system
whereas, $\Delta Q > 10^{-4}$ Std scc/sec It is considered as a leaky system

Std cc/sec = One cubic centimeter of gas flow per second at 14.7 psi of pressure and a temperature of 77°F

In conventional spacecrafts, leak rates of $10^{-3}$-$10^{-4}$ scc/sec have been found adequate, according to Mueller [40]. But leak rates for micro-spacecrafts are much more demanding due to limited onboard propellant supply. Most of the papers surveyed aimed to reduce the leak rate to about $10^{-6}$ to $10^{-5}$ scc/sec but have not necessarily been able to demonstrate low leakage. The allowable range of leak rates for micro-propulsion systems are considered to be less than $10^{-5}$ scc/sec to consider a system leak tight and classify it as a low leakage design[.
It has also been found that the leak rates for liquid propellants for a longer duration micro-spacecrafts missions are substantially smaller than gaseous propellants. However, it is traded-off with more propellant supply onboard the spacecraft. Based on the limited actuator forces and need for seating pressures for high pressure systems, achieving low leak rates is an immense challenge.

2. **Voltage**: Typically the current large spacecrafts have bus voltage of 15-28V. However, the small spacecrafts have much lower bus voltages of 7-15 V [53]. Usually CubeSats use a bus voltage of 5V to 15V, whereas the PocketQubes have bus voltages of 3.3 V- 5V. According to the [48] The micro-propulsion system shall operate on a single unregulated voltage of 3[VDC] to 4.1[VDC]. With the current trend of miniaturisation and shift towards low power and voltage systems. The voltage constraints for the microvalve is expected to be in the range of 5V. However, no designs reported work on such low voltage. The micro-actuators that are available commercially are not powerful enough to actuate the opening/closing of the valve at such a requirement.
Typically, for MEMS based valve most of the current designs have a very high operating voltage which is one major issue for a MEMS microvalve system in case of a micro-spacecraft [40]. For small spacecrafts the available voltage is limited which means, to operate at low voltages the actuator would need to be bigger to be able to provide more actuation force and greater deflection compensating for the required high operating voltage. However, a bigger actuator defeats the purpose of a small, low mass miniaturized system. Even the seat designs have it's own limitations for the seating pressures and leak rates which poses challenges for actuating at low voltage. Hence, external power circuitry would be required to ape up the operating voltage. Depending on the required deflection, actuating force, type of the actuator and the seat design, the increased voltage requirements need to looked upon and considered in the electrical design. One possibility mentioned by Mueller [40] could be to use MEMS based transformer technology to provide the higher voltages needed for the actuator mechanisms. However, proper integration with the valve system needs to be managed in view of the size and weight constraints: which are very crucial requirements for the intended application. Another solution is using DC-DC convertors in the PCB of the micro-propulsion system to convert to required voltages for the components. However, amping the voltages way above the bus voltages has its own limitations and leads to less efficient systems.

3. **Response time** : It is the time it takes to open and close the valve, which is an important valve performance requirement for micro-propulsion systems with low thrust requirements. Such a parameter is maybe the most important from a control-engineering perspective. The valves need to have a fast response time, in other words the actuation speed of the valve must be high. Valve response time is actually the response time of the actuator. According to the requirements document[48], the thrust provided by the propulsion system shall be at least 0.12mN and a maximum of 3mN. Based on such low

thrust requirements for these micro-resistojets the propellant flow should be extremely low, of the order of 1-2 mg/s for a chamber pressure of 5 bar [8].This will require rapid actuation which means shorter valve cycle time. For lower mass spacecrafts, of mass less than 20 kg, the impulse bit is expected to be in the order of $10^{-5}$-$10^{-6}$ Ns to maintain sufficient pointing accuracy [37],[40],[41]. A large time between the thruster firings will reduce the propellant consumption by reducing the number of thruster firing thus increasing the lifetime of spacecraft operations. However, if the impulse bits in small spacecrafts increases, the rotation rate of the spacecraft becomes too high which can be seem from equation 2.2. This leads to higher thrust firings to reach the required pointing accuracy and resulting in wastage of propellant which is highly undesirable, especially for a small spacecraft with limited propellant budget.

$$\Delta I_{bit} = I\Delta\omega \tag{2.2}$$

Assuming, no external torque is acting. ΔI represents the change in impulse bit, which is essentially the change in momentum imparted on the spacecraft due to the impulse. I represents the moment of inertia of the spacecraft. $\Delta\omega$ represents the change in angular velocity (rotation rate) of the spacecraft.

$$Ibit = \int_{t_{on}}^{t_{off}} F(t)dt \tag{2.3}$$

where, $t_{on}$ is the time at which valve opens and $t_{off}$ is the time at which valve closes. F(t) is the thrust force of the rocket engine, typically time dependent over a valve cycle.
To get a first hand estimation and for the sake of simplicity we assume the thrust to be constant over a valve cycle and impulse bits of the order of $10^{-6}$ Ns. From equation 2.3, for a thruster with a maximum thrust of 3mN the valve cycle time would be around 0.3 ms and for a thruster that produces a minimum thrust of 0.12mN the valve cycle time would require a valve actuation time of 8.3 ms. Most of the current MEMS valve designs utilising especially piezoelectric actuation can perform open/close valve cycles in the order of 1-10 ms. However, with the current designs, the cycle time of less than 1 ms is highly ambitious.
The response time for most of the concepts found in the literature means for the application of micropropulsion systems that they have not necessarily been achieved or tested [10],[23],[75]. Another issue that may arise at such high actuation rates for any flow rate is the highly non-uniform fluid flow which, when expanded through the nozzle, can lead to large variations of Reynolds number leading to inefficient operation of the nozzle for the significant fraction of manoeuvre time. Therefore, the characteristics of flow through these valves at such actuation rates should also be considered and detailed numerical analysis of the propulsion system components will be necessary. Also, to get appropriate valve cycle time, the variation of thrust with time needs to be considered however, still the requirement of times less than 1ms is not very practical with the available designs.

4. **Operating Pressure**: As in any other on-board propulsion system the pressure at the valve inlet is determined by the propellant tank. The microvalve should be able to activate under a certain fluid pressure differential across it. The fluid systems are generally designed in view of the maximum operating pressure which is 4-5 bar for this application. This value is considered very high for such a small microvalve system therefore the design of the microvalve system should be able to handle this pressure. From the literature it has been found that pressures between 0.1-1bar are considered low pressures for such microfluidic valve systems. 1-2 bar is considered a moderate pressure range and usually pressures above 2 bar are considered as high operating pressure values [16],[23],[15]. In context of MEOP of 5 bar for our application, it is considered a high pressure value because of the limited seating forces available due to the size restrictions as well as the limited forces offered by most actuators. To deliver high forces, larger actuators would be required. Bonding the actuator with the valve seat to be able to obtain the required sealing force is a challenging task requiring careful design and fabrication considerations. Therefore, valve seating pressure/ force plays an important role in the microvalve design as it is the amount of force that is needed to be exerted to counter the fluid pressure acting on the valve. For high pressure systems, seating pressures must be really high in order to provide high sealing forces to be able to keep the valve closed at off condition and to avoid internal leakages [76].Therefore the valve area is an important design choice for microvalves. One of the options could be to reduce the area which will increase the seating pressures. Depending on the maximum operating pressure, calculations for the maximum

actuator force are required to cause a certain deflection that needs to be determined and likewise the contact area must be designed.

5. **Flexibility**: The flexibility of valves lies in their ability to adapt to diverse operational requirements depending on the application. Proportional flow control valves and on-off check valves used in fluidic system serve different purposes and also work differently. An on-off valve, operates in a binary matter- it is either fully open or fully closed. And they are mostly used to start, stop or divert the flow. They are often used in applications where flow control does not require fine tuning or where rapid opening and closing are not necessary. They are open used for isolating sections of the system or for initiating propulsion maneuver in the missions. On the other hand, proportional flow control valve regulates the fluid flow in proportion to the control signal and hence used in application where precise adjustment of the flow rate within a range are possible. Hence, they are used in applications requiring precise maneuvers or adjustments. Depending on the specific needs, the fluid control solutions can be tailed in order to optimise for the required performance. A proportional flow control microvalves design offer a better choice, increasing the flexibility of micro-propulsion systems to perform fine-tuned control.

Within the scope of this study, requirements for vibration, radiation levels and other environmental loads are not considered.

## 2.5. Microvalve Requirements

The specific set of demands for any microvalve design is determined by the application. In this section, the mission requirements are presented which are either derived from the micro-propulsion requirements [48], the technical budgets [49], or are based on the estimates presented earlier in design specifications. Some of the performance requirements were provided by the micro-propulsion team before the start of the project based on the performance of the thruster. These can be found in tables 2.1, 2.2, 2.3, 2.4. The rationale for each of the requirements are provided which give more insight on their source. The influence of them on the design of the valve system is also indicated. These requirements will drive the concept selection and the design phase in subsequent chapters.

### 2.5.1. System Requirements

The first requirements are set up by the micropropulsion system (VLM in this case) and the Delfi-PQ satellite. These are denominated by the **SYST** identifier and can be seen in table 2.1. Most of these requirements put forth relate to the integration of the microvalve with the system with the PocketQube.

### 2.5.2. Performance requirements

These requirements give the performance characteristics that the system should deliver such as response time and mass flow rate. These are the main requirements and the main drivers for the valve design. The list of performance requirements can be seen in table 2.2 and identified by **PERF**.

### 2.5.3. Functional requirements

These requirements cover the requirements on how the system should function. It shows how the microvalve will connect with the rest of the micro-propulsion system in order to have interface compatibility with the components. The list of functional requirements can be seen in table 2.3 and identified by **FUN**.

### 2.5.4. Interface requirements

These requirements explain how the microvalve will interface with the rest of the micropropulsion components. This influences the choice of connectors and external tubing which should be compatible with all the components. The list of requirement can be found in table 2.4 and identified by **INT**.

| MIC-SYST-100 | Mass |
|---|---|
| Type | Constraint |
| Description | The total mass of the valve+holder shall not be higher than 5g. |
| Rationale/ Comment | This is based on the assumption that the LEE valves currently used weigh around 5g. The important constraint is that the total wet mass of the propulsion system will be no more than 75g at launch, based on the requirements given in the DFF-TUD-PROP-REQ from Propulsion subsystem requirements [48], [68]. |
| Influence on design | This puts a constraint on the material properties, stiffness and actuator forces directly influencing the closing force. |

| MIC-SYST-200 | Overall Volume |
|---|---|
| Type | Constraint |
| Description | The total size of the propulsion system shall be within 42 mm x 42 mm x 30 mm (including thrusters, valve, electronic board, harness, connector and propellant storage tank ). |
| Rationale/ Comment | This requirement is obtained from DFF-TUD-PROP-REQ: Propulsion subsystem requirements [48]. |
| Influence on design | This limits the overall component design and puts strict limitations on the microvalve housing sizing . |

| MIC-SYST-300 | Volume |
|---|---|
| Type | Constraint |
| Description | The total microvalve chip size shall be no more than 10mm x10mm x 1mm. |
| Rationale/ Comment | This requirement is derived from the standard chip size that is available at EKL for MEMS fabrication. Note: Other sizes are also possible. However, the sizing should comply with the requirement :-MIC-SYS-200. |
| Influence on design | Since the objective of the thesis is a MEMS based design with the fabricability at EKL, this puts constraints on the overall sizing. |

| MIC-SYST-400 | Operating Pressure |
|---|---|
| Type | Constraint |
| Description | The valve shall be able to handle a maximum operating pressure of 5 bar when closed. |
| Rationale/ Comment | This is driven by the requirements set for the tank environment and was provided by the micro-propulsion team at the start of the project. |
| Influence on design | This puts a constraint on the material properties, stiffness and actuator forces directly influencing the closing force. |

| MIC-SYST-500 | Power Consumption |
|---|---|
| Type | Constraint |
| Description | The peak consumption of the valve shall not be higher than 4W. |
| Rationale/ Comment | This requirement is obtained from DFF-TUD-PROP-REQ: Propulsion subsystem requirements [48]. The technical budgets accounted 1 W for feed system. [49] |
| Influence on design | This influences the actuator selection and drive criteria for operating the valve. |

| MIC-SYST-600 | Voltage regulation |
|---|---|
| Type | Constraint |
| Description | The system shall be able to operate on a single unregulated supply bus voltage of 3 [VDC] to 4.1 [VDC]. |
| Rationale/ Comment | This requirement is obtained from DFF-TUD-PROP-REQ: Propulsion subsystem requirements [48]. There has to be local DC-DC converters provided to provide the required voltage |
| Influence on design | This affects the actuator selection and impacts the control circuitry. |

Table 2.1: List of system requirements

| MIC-PERF-100 | Flow rate |
|---|---|
| Type | Performance |
| Description | The mass flow rate delivered by the system shall be 5g/hr at a maximum differential pressure of 5 bar |
| Rationale/ Comment | This required is based on the thruster performance and inlet conditions and was provided by the micro-propulsion team at the start of the thesis. |
| Influence on design | This is the critical requirement of the system which influences the overall design. Influence on flow path design and required actuator stroke |

| MIC-PERF-200 | Response Time |
|---|---|
| Type | Performance |
| Description | The response time of the system shall be between 0.3 ms-8.3 ms |
| Rationale/ Comment | The response time requirement is driven by the approximate calculation presented in section 3. Even though there is no impulse bit requirement for this technology demonstrator from mission side, efforts will be made to design the system in order to keep the value significantly lower than the upper limit to achieve minimum pulse duration. |
| Influence on design | This greatly influences the actuator selection and the drive characteristics of the system. And is impacted by the peak consumption requirement:MIC-SYST-500. |

| MIC-PERF-300 | Leak Rate |
|---|---|
| Type | Performance |
| Description | The maximum leak rate shall be $<10^{-5}$ scc/s at maximum operating pressure |
| Rationale/ Comment | No requirement was provided on the leak rates in DFF-TUD-PROP-REQ: Propulsion subsystem requirements [48]. However, here leak rate requirement was determined based on literature[10]. The leak rate requirement should be careful assessed at system level |
| Influence on design | This requirement has an impact on the overall mission lifetime. Influence on the material used and fabrication technique affected by relative surface roughness |

Table 2.2: List of performance requirements

| MIC-FUN-100 | Operating mode |
|---|---|
| Type | Functional |
| Description | The system shall supply no propellant to the thruster in idle mode or when no power is supplied to the system |
| Rationale/ Comment | This requirement is obtained from DFF-TUD-PROP-REQ: Propulsion system mass, volume& power budget [49]. This necessitates the need to operate the valve in normally closed configuration |
| Influence on design | This is the critical requirement which affects the type of valve being designed |

| MIC-FUN-200 | Compatibility |
|---|---|
| Type | Functional |
| Description | The system shall be able to operate on liquid H20 |
| Rationale/ Comment | This requirement is obtained from DFF-TUD-PROP-REQ: Propulsion subsystem requirements [48] |
| Influence on design | Valve materials must be compatible with liquid H20 and also ensure that the peripheral electronics (actuator) is not in contact with fluid. |

| MIC-FUNC-300 | Flow control |
|---|---|
| Type | Functional |
| Description | The valve system shall be able to provide proportional flow control |
| Rationale/ Comment | To accommodate different mission applications, proportional flow control would be suitable where flows can be adjusted. |
| Influence on design | This requirement has an impact on the type of valve chosen. |

Table 2.3: List of functional requirements

| MIC-INT-100 | Thermal Interface |
|---|---|
| Type | Interface |
| Description | The microvalve shall stay at a temperature range of +5 °C and +85 °C during all mission phase when the propulsion system operation are required |
| Rationale/ Comment | This requirement is obtained from DFF-TUD-PROP-REQ: Propulsion subsystem requirements [48].This is to avoid propellant freezing and ensure satisfactory performance of the system. |
| Influence on design | This requirement has an impact on the valve material and overall design selection to ensure they can withstand such temperatures. |

| MIC-INT-200 | Fluidic interface |
|---|---|
| Type | Interface |
| Description | The fluidic interface of the valve system shall be compatible with both the thruster housing and the propellant tank |
| Rationale/ Comment | The valve system has to be able to connect and interface with the thruster and the tank. |
| Influence on design | This requirement puts a constraints the holder platform |

| MIC-INT-300 | Mechanical & Elctrical Interface |
|---|---|
| Type | Functional |
| Description | The mechanical and electrical interface between the valve system and other micro-propulsion components shall respect payload's technical budgets. |
| Rationale/ Comment | The valve shall comply with the propulsion system constraints as well as Delfi PQ standard. |
| Influence on design | This dictates the need to ensure the device is as small as possible while having the ability to properly interface with the other components. |

Table 2.4: List of Interface requirements

# 3

# Literature study

The following chapter reports excerpts from the extensive literature review that has preceded this thesis project. This literature study was written by the author to understand the background of microvalves and to acquire sufficient knowledge of the fundamentals that would set the framework to carry out this research. The literature study contained:

- Explored possible commercially available microvalve options
- Study of different valve concepts and actuator mechanisms
- In-depth review and summary of the all past and existing valve designs
- Implication of the different design concepts on the performance characteristics
- Information on MEMS manufacturing techniques

The part of the literature study on MEMS manufacturing techniques will not be introduced in this chapter but will be included in chapter 9 to maintain proper breakdown of the report. Although truly scarce, literature on microvalves design reported for space applications has been analysed. However, no design reported previously was found that completely meets the requirements set forth for this thesis study.

## 3.1. Classification of microvalves

Microvalves can be broadly classified as shown in figure 3.1. Further categoraisation of active and passive valves can be found in table 3.3. The use of unconventional non-mechanical mechanisms employing the use of smart materials have been excluded from the study.

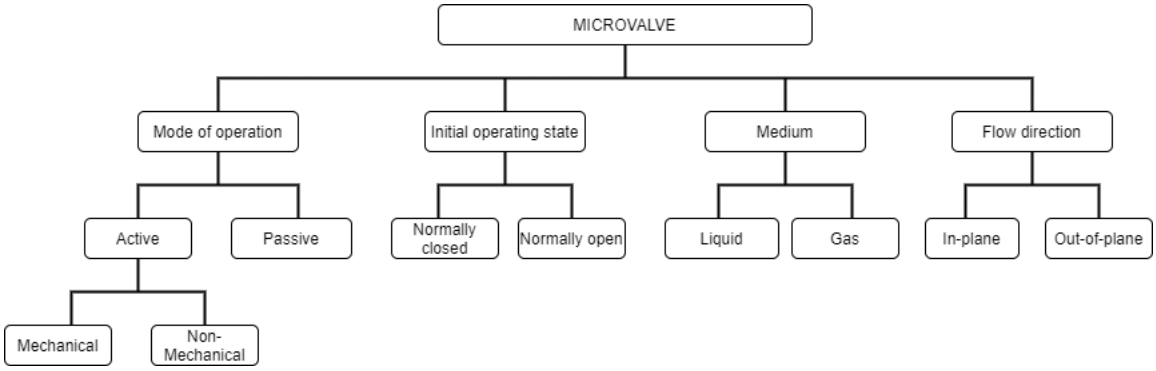


Figure 3.1: Classification of microvalves [44]

The major criterion is on the basis of operation. A valve can either be active or passive. In case of an active microvalve, the mechanically movable membranes are coupled with magnetic, electric, piezoelectric or

thermal actuation methods. The movement of membranes can also be exploited by the use of functionalized smart or intelligent materials. The actuation mechanism can be mechanical or non-mechanical in nature. More details of active microvalves can be found in table 3.3. Passive valves are unpowered and are usually used as check valves. The fluid control is entirely regulated by the differential pressure across the inlet and outlet. The flow cannot be controlled and modified which makes it undesirable for space applications and defeats the purpose of achieving precise flow control over a range of flows.
Another classification can be made based on the fluid that is modulated. Liquid microvalves generally have more stringent conditions like isolation of actuation electrodes from the fluid, compatibility of the wetted materials with the fluids and the requirement of impermeable channel to transport fluid through the valve. Traditionally, these active microvalves are fabricated using MEMS based micro-machining techniques, compatibility of the fluid with the polymers and different compounds used becomes important.
Additionally, the initial state of the valve becomes an important consideration for the design when the application requires precise dosing, low power, no flow when unpowered and good pressure performance [25]. A normally open (NO) configuration refers to the state of free flow from inlet to outlet when unpowered. The actuator needs to be actuated to create any blockage. Whereas, in normally closed configuration (NC), no flow occurs until the valve is actuated either by pressure difference or by control signal. One of the trade-offs is reduced flow rate compared to NO valves due to diminished strokes [44].
The flow direction in the microvalve is another criteria of valve classification. It determines if the valve is compatible with the microfluidic circuit. They are mostly constructed with inlet and outlet perpendicular to the valve plane. This could mean that additional off-chip tubing is required. Due to the ease of the design and better leakage performance, most of the Silicon microvalves reported tend to be out-of-plane [44].

Some of the concepts mentioned above are obviously non-compliant to the requirements and can be eliminated. This is summarised in table 3.1. The result of this high-level selection, the design is developed and motivated.

| Criteria | Requirement | Infeasible Concepts |
|---|---|---|
| Mode of Operation | MIC-FUNC-300 | Passive valve design is not acceptable since the application requires precise control of flow, which necessitates the use of an actuator. |
| Initial Operating mode | MIC-FUN-100 | Normally closed valve is not desirable, in events when the propulsion system is switched off or no power is supplied or when the propellant tank is empty |
| Medium | MIC-FUN-200 | Compatibility with water based on the requirement.<br>Also preferred for gas flows |
| Flow Direction | MIC-PERF-300 | Since low leak ratios are required, out-of-plane design concept is selected. This selection is based on the literature review conducted. |

Table 3.1: Selection status of above mentioned concepts of based on the requirements

## 3.2. COTS Options

This section will give a brief overview of the different COTS options that were researched to find feasible valve options that can potentially meet the requirements. These options were reviewed based on their performance characteristics as given in table 3.2. For space applications requiring short turnaround time and low cost components these commercially available valve options might be alternate solutions. However, the trade-off is a reduced system performance and a lack of customisation hence posing limitations on external interfaces with other components. Therefore, these COTS valves cannot offer rigid integration necessary for system reliability. Moreover, most of these valves are not based on MEMS technology, therefore they barely meet the strict mass and volume requirements set forth for this study. The valve option mentioned in column 6 of table 3.2 is the one used in the integration plan of the technology demonstrator [68]. Even though this Lee valve meets most of the performance requirements, it puts major constraints on the assembly of the other propulsion components in the PocketQube bus. The integration of the propulsion system in the test plan was centred around volume-saving options to fit in the valves with other components. The author suggested designing an in-house MEMS valve to reduce system complexities, making the integration simpler thereby, offering a tightly integrated system with potential mass and volume savings.

| **Microvalve type** | DMQ-siliQflo_TM Silicon Servo | Staiger-MI 230-001 | AST NW0.3 | Emerson-series 067 | Lee company (INKX0514003A) |
|---|---|---|---|---|---|
| **Actuation mechanism** | Electro-thermal | Electro-magnetic | Electro-magnetic | Electro-magnetic | Electro-magnetic |
| **Response time** | 50 ms | 30ms | <2ms | <10 ms | <10ms |
| **Weight** | 0.24 +/- 0.01 g | 0.45 kg | 0.016 kg w/o cable 0.004 kg w/o holder | 11.7g | 1.8 g |
| **Volume** | 10.80 x 4.84 x 2.225 mm | - | - | - | - |
| **Voltage** | 12/24 V | 6/9/12/24 V | 20/24 V pull in | 12/24 V | 4.5 VDC |
| **Power** | 5 +/- 1 W | 2.5 W | - | 2.5 W | - |
| **Max flow** | 60 +/- 5 cc/min @100psi | - | 2 l/min at 2 bar | 0.10 l/min | 0.0125 mL/min |
| **Internal leakage** | <500 cc/min @100psi N2 | - | <10-6 sccs GHe | - | - |
| **Flow control** | On/off, proportional | bistable | 2/2 way, normally closed | Proportional | proportional |
| **Maximum operating pressure** | 500 psi | 10 bar | 6 bar | 3 bar | 8 bar |
| **Medium** | Gases, most liquids | Neutral liquid, gas | Inert gases | gas and liquid | liquid, gas |

Table 3.2: Overview of performance characteristics COTS microvalve options

## 3.3. State-of-the-art microvalve designs

The design of reliable high performance microvalve system implies:

- Proper synthesis, characterisation and design of micro-systems according to their application of use and overall system requirements
- Integration of actuator with proper circuitry and sensors
- Affordable and high-yield fabrication techniques for manufacturing such systems
- Proper simulations and analysis of results

To meet these requirements, a well defined, sequential research will be carried out in the subsequent chapters based on a review of the literature survey conducted on existing microvalve design. These designs were critically evaluated based on their operating principle, performance parameters and suitability to desired application. A brief review of plunger valve concept design and actuating mechanisms will be presented separately.

### 3.3.1. Geometrical configurations: Plunger

At the micro-level, the baseline of the design of microvalves is rather similar among all analysed concepts. As mentioned earlier, the top part of the valve plate in this report will be referred to as the plunger for the sake of simplicity. A schematic representation of the most common configuration of the plunger is given in figure 3.2.

A concise narration of some of these different concepts will be provided along with the valve designs in which these were utilised. The advantages and inherent disadvantages of these concepts will also be discussed in brief.

#### 3.3.1.1. Vertically translating plate

The most frequent and simple design consists of a vertically translating plate where orifice is closed in the direction of flow. The plate is usually fabricated using hard materials like silicon/nickel, however, that leads to certain shortcomings in the performance. A leak tight system is difficult to achieve with a hard plate of high young's modulus as the two do not readily deform to match each other's structural topography causing leakage issues. So to achieve proper sealing and achieve low leak rates in the order of $10^{-7}$, high actuator

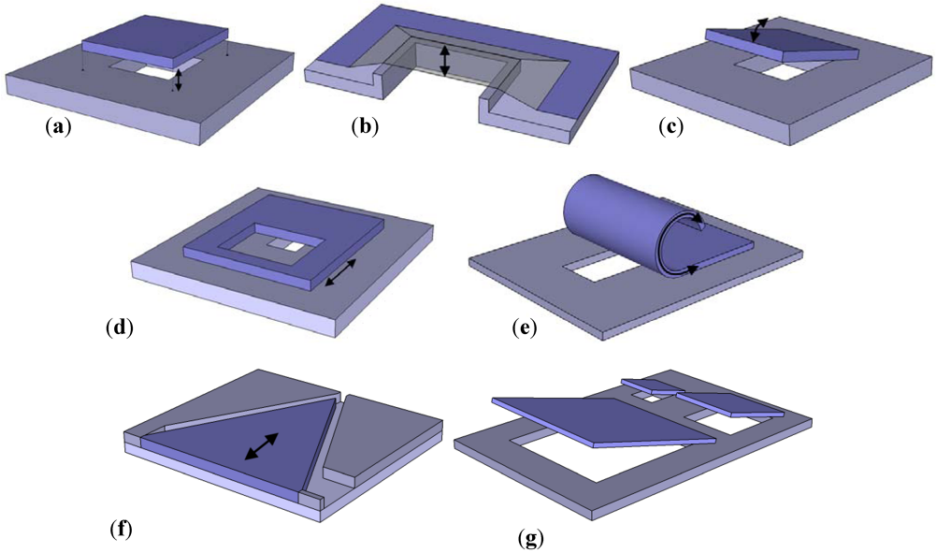


Figure 3.2: Different Valve concepts [24]: (a) Vertically translating plate; (b) Vertically translating membrane; (c) Tilting plate; (d) Horizontally sliding plate; (e) bending plate; (f) Needle; (g) Scaling valve array

pressures would be required and thus a larger actuator or higher voltage. This would then not meet the limited voltage and mass budget requirements.
Another disadvantage of such high pressure is the fact that it could damage the valve seat especially if it is made of silicon substrate. The crystalline structure of silicon is such that if a crack is initiated it could easily propagate to the entire structure breaking the entire seat. A possible solution to this problem, as mentioned in various literature could be the use of a different material along with hard materials using feasible and effective micro-machining techniques. One such solution was reported in [74] which is micro-machined on a silicon substrate to control the fluid flow. The valve seat cap was made of a softer material (NiFe). This method uses conformal layer deposition to fabricate a valve with reported leakage of $7.3*10^{-7}$ scc/s offering a really good leakage performance and it fits our requirement. Furthermore, the leakage greatly depends on the surface roughness. It has been reported that the surface of the silicon is not entirely flat but has waves which increase with the area of interest. Therefore, the larger the circumference of the valve seat, the larger are the amplitude and wavelength of the silicon surface which will lead to more fluid leakage. Therefore, even a small surface roughness could create a gap in the order of nano-metres creating leak rates in the order of $10^{-4}$ which is undesirable for space applications[34]. Another solution includes etching grooves in the hard plate thus trapping the particles in them [10], [75].

### 3.3.1.2. Vertically translating membrane

This design concept is the modification of the translating plate where the hard valve plate is replaced by the flexible thin membrane or diaphragm.These are usually fabricated of low modulus materials like silicone rubber, other elastomers and thin film polymers like Kapton or parylene. Since these materials are flexible, it requires less force to close the valve and it easily adjusts to the seat surface providing improved sealing with the seat [77],[70]. The most commonly used silicone rubber used in designs is the PDMS membrane on a glass substrate mentioned in one of the approaches [78]. An advantage of such kind of valve is the fact that the membrane can easily deform to match the topography of the seat providing better sealing and good closure. In case of soft seals the contaminants that settle on the valve can be encapsulated by the membrane making the leakage issue less challenging compared to hard plates and reducing the required actuator force to close the valve, however, this comes at the cost of an increase in the required stroke length[40].
Some of the downsides of this design include: An increased stiction due to prolong contact between the seat and the membrane which can break the system or can lead to hysteresis effect slowing down the valve. To solve the issue of hysteresis most membranes are made of silicon or other polymers and not of silicone rubber like PDMS [16]. Secondly, thin elastomer based devices carry issues of mechanical robustness [32]. Other issues include reduced chemical resistance and high permeability to moisture and gases which can wear the membrane out. As reported in [77] experimental tests performed with silicon rubber membranes

are found to be permeable to most fluids like deionized (DI) water, isopropyl alcohol, and 3M Performance Fluids (PF 5060 and PF 5070) which severely limits the application of the device. Authors have reported use of parylene or composite silicon/parylene film to solve this issue [6]. However, the fabrication process for membrane valves requires more elaborate techniques but could provide better leakage performance.

#### 3.3.1.3. Tilting plate valves

Another modification is to fix one side of the top plate to the bulk substrate as shown in figure 3.2 (c). The concept has been reported in [46] where the electrostatic actuation is used to actuate the microvalve. By choosing proper pivot points the actuator force required to open and close the valve can be reduced, leading to amplified actuator stroke compared to the vertically translating plate. Another design presented by [4] employs the design using the same concept. This valving scheme can be an alternative to the translating plate mentioned earlier when using a hard plate as the plunger. Such a design may have a potential of smaller leakage rates since the chances of misalignment of the plate during every open/close cycle is reduced. However, the choice of actuator becomes necessary to be able to employ the benefit of such a design. The designs reported employ electrostatic or thermopneumatic actuation techniques, which have their own limitations and issues which is discussed in section 3.3.2. Furthermore, leakage issues due to structural topography of the silicon, particle contamination associated with the vertically translating plate are also inherent in this valve concept. Additionally, it can lead to greater mechanical and fabrication difficulties, leading to failure of the system due to the greater stresses which might develop on the already complaint tilting plate.

#### 3.3.1.4. Bending plate valves

The bending plate concept is the adaptation of the tilting plate valve where certain kind of materials are used which bend or curl up to open the valve. This concept employs the use of material properties like the thermal expansion, piezoelectric strain or phase change memory alloys, or magnetic behaviour of materials. These valves can suffer from a large bending moment due to the fluid pressure leading to higher leakage at large differential pressure. This problem could be solved by the design presented by Watanabe et al. This type of design uses a microvalve matrix in which every valve is digitally open and close allowing the valve to control flow over wide dynamic ranges [73].

#### 3.3.1.5. Horizontally translating plate

This concept as shown in figure 3.2 (d) uses the two horizontally translating or sliding plate to overlap each other. The motion can be executed linearly, in rotation or in a pivoting structure. The latter design is reported in [24] where the thermal actuation of silicon rod pushes a perforated plate across the valve seat overlapping the orifices. Even though these valves have good control properties they suffer from a poor leakage problem since the closure and the sliding movement happens in the same plane. Such a design involves inherent trade-off between friction and closure to ensure low actuator forces and precise actuation or good leakage performance.

### 3.3.2. Actuating mechanisms

An actuator is a device that converts the electrical signals into an action by manipulating itself or it's environment to perform some function. As mentioned earlier in Section 3.1, an active microvalve is essential to allow for proportional flow control, therefore the focus of this section will be on reviewing the different actuation principles and their implications of the overall valve design. Passive valves are not evaluated as they can only be designed to control a single, specific flow [24]. The set of design requirements mentioned in 2.1,2.2, 2.3,2.4, depend to a large extent on the type and specifications of the actuator. For example, the actuator dimensions determine the maximum valve stroke and the open-loop response time of the system is also determined by the the actuator response time. Only the classes with the greatest representation in the literature have been addressed. Even though there are a myriad of other options possible, those were not explored because of their less matured technology and their unsuitability for space applications. The illustration of the working principle of the different actively controlled microvalves can be found in table 3.3.
Because the choice of the optimal actuator, the design and operation of the microvalve are mutually dependent on each other, it is difficult to choose any actuator as the best.

| | | | |
|---|---|---|---|
| Active | Mechanical | Magnetic | External magnetic field<br>Integrated magnetic inductor |
| | | Electric | Electrostatic<br>Electro-kinetic<br>Electromagnetic |
| | | Piezoelectric | |
| | | Thermal | Bimetallic<br>Thermopneumatic<br>Shape Memory alloy<br>Bimorph |
| | Non-mechanical | Electrochemical | |
| | | Phase change | Hydrogel<br>Sol-gel<br>Paraffin |
| | | Rheological | Electro-rheological<br>Ferrofluids |
| | External | Modular | Built-in<br>Rotary |
| | | Pneumatic | Membrane<br>In-line |
| Passive | Mechanical | Check valves | Flap<br>Membrane<br>Spherical ball<br>In-line mobile structure |
| | Non-mechanical | Capillary | Diffuser<br>Abrupt<br>Liquid-triggered<br>Burst<br>Hydrophobic |

Table 3.3: Classification of microvalve based on active and passive [44]

#### 3.3.2.1. Thermopneumatic

This actuation relies on the volumetric expansion of a sealed liquid or solid under thermal loading. It operates on the principle of phase change to cause membrane deflection. W. Barth [4] presents a normally closed thermopneumatic actuation mechanism, in which a liquid is trapped in a sealed cavity which contains a thin-film heating resistor on side of the cavity and a flexible membrane on the other side. When the resistor is electrically heated the fluid heats up to its boiling point after which it starts to evaporate which raises the pressure in the sealed cavity causing the flexible membrane to move outwards thus opening the valves. This type of actuation offers the flexibility of choosing the opening temperatures of the valve by choosing the required boiling point of the trapped liquid. Even though these valves offer large strokes, they concurrently achieve large forces for a microstructure. Predominantly thermopneumatic valves are not suitable for space applications since they have very slow valve cycle time of around 100-400 ms [40]. The speed of these valves are based on the temperature change of the fluid. Increasing the power provided would heat the fluid faster opening the valve quicker, but this would mean that the fluid would take longer to cool down causing very slow closing times, making the actuating mechanism infeasible for fast and precise control of propellant applications targeted here. Moreover, being strongly material dependent, any changes in temperature in the spacecraft can cause unwanted actuation of the valve which is undesirable[63].

#### 3.3.2.2. Electrostatic

Electrostatic actuation is based on the principle of attractive force between two oppositely charged plates. One of the designs mentioned in [40], which was developed by Ohnstein et al. is a normally open electrostatic valve design in which deflection of the cantilevered beam, in which one of the electrodes is formed by the conductive layer embedded in the beam, and the other electrode embedded in the silicon substrate which is essentially a parallel plate capacitor. The paper reported the valve to be close on applying 30V against pressures of around 0.137 bar and could operate at a maximum operating pressure of around 1 bar and a very

high leak rate of 6 x $10^{-}2$ sccm. It can safely operate for gases but might cause electrolysis with water or other liquid media.These performances are very poor considering the micro-spacecraft applications.
The biggest advantage of an electrostatic actuator is a fast response. However, a high drive voltage and small displacements make it difficult to integrate with microfluidic systems [43]. Other problems include that there is a certain distance required between the electrodes to avoid a pull-in effect. When increasing the voltage beyond this point the plates snap together [69], [40].This causes a high flow restriction and limits the flow that the valve can control. Also, most of the electrostatic based actuators are suitable for gas flows since they might lead to electrolysis for liquid propellants.

#### 3.3.2.3. Electromagnetic

These valves make use of the interaction of a magnetic field and a ferromagnetic element that is capable to move. The magnetic field is generally generated by a current carrying coil or by the use of permanent magnets. In one such design concept by Yangagisawa et al. which is presented by Mueller et al. in their survey [40], the valve is integrated with the spiral shaped sputter deposited thin magnetic NiFe membrane and an electromagnetic coil placed outside the tube. The magnetic field of the coil interacts with the magnetic material moving the magnetic poppet up and down which depends on the coil current direction and the generated field. Due to the limitations in micro-machining techniques a miniaturized coil carrying conductors is difficult therefore, the use of external coils coupled with a mechanically moving membrane made of magnetic material or the use of permanent magnets is typical[40] thereby resulting in a hybrid MEMS valve. In a micro-domain, as the dimensions decrease, it leads to poor actuator performance at higher levels of integration. Meckes et al. present an integrated electromagnetic coil design with the membrane for a microvalve with a diameter of 1mm, reported to generate an actuator force of 0.8mN and capable of withstanding only 8mbar of differential pressure [55].

#### 3.3.2.4. Piezoelectric

These type of valves are the most widely available and they employ the use of the strain of the piezoelectric materials when an electric field is applied through them. Theses strains are limited in piezoelectric actuators ( less than 0.1 %) but can deliver high blocking forces in the order of kilonewtons [44]. Large strokes are challenging in piezoelectric actuators even with the application of very high voltage which range from 25-50$\mu$m at voltages of >100V. Both these issues can be partially solved by using bimorph cantilever or bonded bulk PZT/stacks of thin PZT films [72], in which small deflection of each element add up yielding significant stroke with much lesser applied voltage (<30V)[54], [10]. The piezoelectric layer can be integrated on the silicon wafer in three forms: A thin film with thickness less than 3$\mu$m, thick films with thickness ranging from several microns to 50$\mu$m and a bonded bulk plate. However, integration of piezo actuators on a silicon substrate at wafer level can require a precise machining process which is limited using current technologies. Many designs have been directly depositing patterned films on the silicon substrate. However, using piezo actuators with a layer thickness of the order of micrometers requires a very high voltage and delivers very small strokes. One of the unique design concepts employing this technique is the use of a custom designed piezoelectric stack actuator developed by JPL consisting of two active zones and one inactive zone [10],[15]. This is bonded on the silicon valve components with the entire assembly contained in metal housing. The MEMs based piezoelectric design has been developed for both liquid and gas compatibility being developed for micro-spacecraft requirements. On application of 40 V the active zones vertically expand by 5$\mu$m lifting the boss centre plate which is bonded to the inactive zone of the actuator thus opening the outlet and allowing the gas to flow. The valve is reported to be tested and it successfully handles pressures up to 7 bar. The flow rate of 52 sccm at the inlet pressure of 300 psi is found at the 10 V applied voltage. Leak rates of $10^{-4}$ sccm at a pressure of 800 psi are reported with no detectable leakage at pressures below 150 psi. Another design by Fazal promises a high pressure piezoelectric design concept with flow rate of 250 ml/min for differential pressure of 4 bars. It has been shown that no hysteresis occurs and that power consumption is low. The valve accomplishes a control flow at different states with a precision of 1-2% of the full scale flow. The design makes use of static and variable resistances in series to provide flow control and to provide larger range of membrane deflections necessary for flow control [16]. Piezoelectric actuators are greatly employed for high pressure applications due to the large blocking forces and faster response time, compared to some other actuating mechanisms, making them promising candidates for space applications.

### 3.3.2.5. Shape-memory alloy

Shape memory alloys valves are another type of actuator employing the use of a thermally actuated mechanism. They provide a considerably higher stroke of around 50-100 $\mu$m by applying a special material phase change which occurs in some metal alloys like TiNi films under the influence of phase transformation temperature. Author R.H Wolf presents a shape memory film microvalve fabricated of TiNi on silicon substrates [40] and the shape memory alloy makes use of varying temperature to change its phase. When heating the Ti/Ni alloy above its transition phase, it returns to its so called parent state which is formed by high temperature annealing of the material during fabrication. Most of these valves are able to operate at high pressure ranges of about 100-400 psi exhibiting a high pressure handling capability requiring sufficiently low power and providing high flow rate [[40],[44]]. However, they suffer from the same limitations as the thermopneumatic valves with high overall valve cycle times ranging from tens of milliseconds to several seconds and a risk of unwanted actuation[24], [63]. Another disadvantage According to Soji et al., [61], these actuators can only be used for on/off flow control. Another disadvantage mentioned in the papers is that the performance of SMA valves decreases after thousands of cycles, while proportional controllers require several orders more actuator cycles during their lifespan [24]

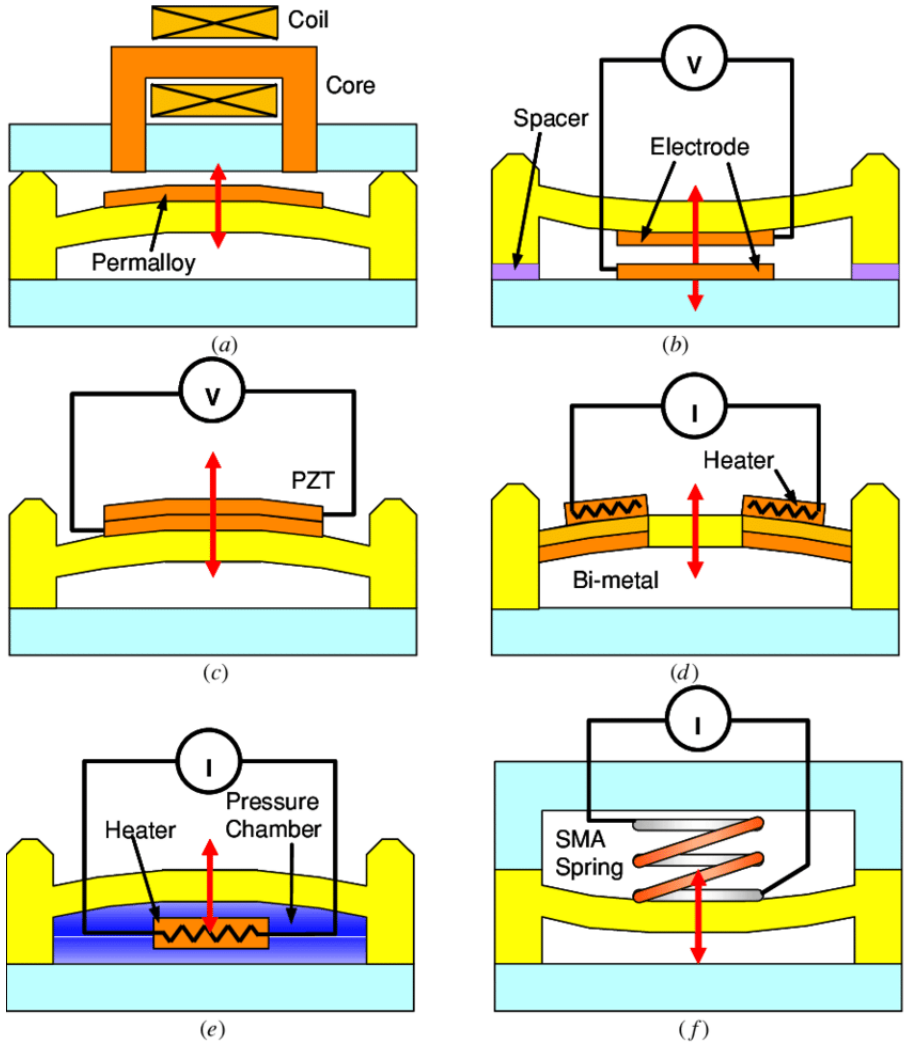


Figure 3.3: Classification of microvalves based on actuating principle [44] (a) electromagnetic; (b) electrostatic; (c) piezoelectric; (d) bimetallic; (e) thermopneumatic and (f) shape memory alloy actuation

# 4

# Conceptual Design

At the start of the microvalve design research, some important questions should be answered.

- What specifications should the microvalve meet for the desired application?
- What materials should be used for the microvalve depending on micro-machining techniques possible?
- Which actuator mechanism best suits the performance requirements and constraints?
- Which form of plunger configuration is the optimum for maximum closing pressure and for minimum leakage?

The answer to the first question has already been set forth in Chapter 2 through the formulation of the requirements table in section 2.5. Infeasible deign concepts which can be immediately eliminated since they do not satisfy the requirements are mentioned in table 3.1. To tackle the other questions, A high level option tree was presented in figure 4.1. The main objective was decomposed into different component level concepts. These concepts along with their weakest points tabulated in 4.4, 4.6, combined with methodical trade-off analysis, will give insight into the final selection.

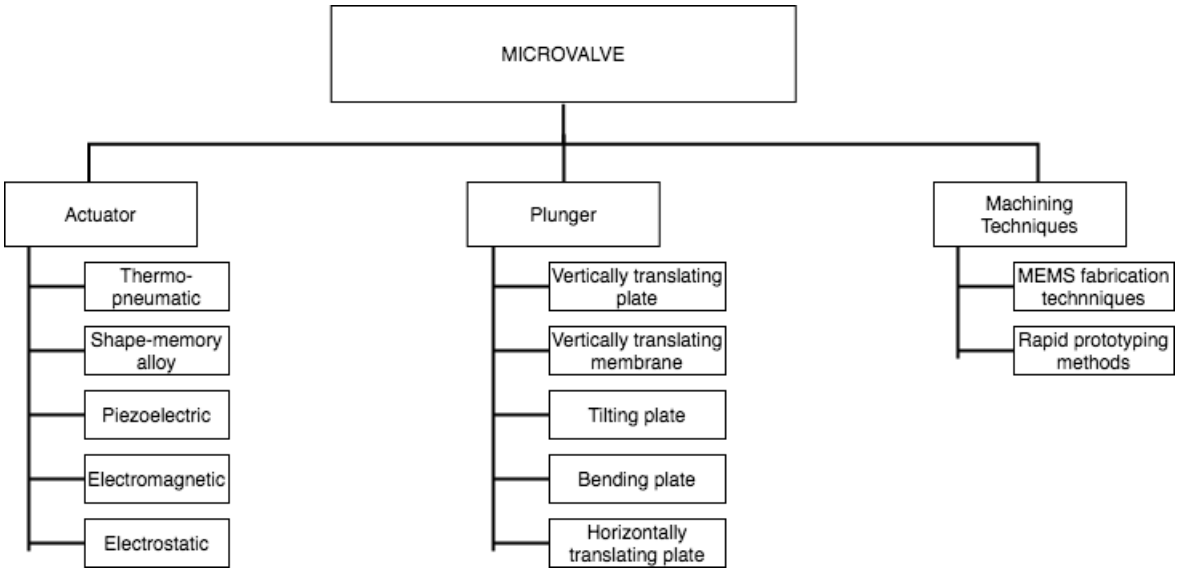


Figure 4.1: Top level design tree

## 4.1. Actuator selection

An actuator serves the following purposes in a microvalve operation [43]

1. Moving function: In case of an active microvalve, an actuator is responsible for moving the valve plate to the desired position. For which it should be able to provide enough force, displacement and controllability.

2. Holding function: The actuator should be able to keep the plunger in the desired position, which means the actuator and the valve seat must be able to overcome the inlet pressure.

3. Dynamic function: The response time of a microvalve is determined mainly by the actuator, hence it should be able to meet the dynamic requirements of the desired application.

### 4.1.1. Trade-off

A classical trade-off study by means of weighted scoring against the selected trade-off criteria is carried out. The different concepts are weighed based on their influence on the system depending on how they satisfy the criteria. At the end the weighted total average of each option is obtained. The concept that obtains the higher weighted average is the preferred choice. All the values in the trade-off are assigned based on a score of 100. The trade-off criteria selected for this analysis are in-line with the requirements of the microvalve system set forth in Chapter 2. They are tabulated in table 4.1.

| Trade-off criteria | Source | Weightage (%) | Weighting Justification |
|---|---|---|---|
| Response time | MIC-PERF-200 | 30 | A quick response to small signal changes is an important factor in providing optimum control accuracy |
| Integration | MIC-SYST-200<br>MIC-INT-100 | 10 | Minimal volume ensuring tight integration with remaining components However, commercially available actuators offer limited design freedom so integration with the MEMS chip is crucial |
| Blocking force | MIC-SYST-400<br>MIC-PERF-300 | 35 | Pressure handling capability and leak rate directly translate from available actuator force |
| Available stroke | MIC-PERF-300<br>MIC-PERF-100 | 10 | Deflection impacts the maximum flow rate that the valve can deliver |
| Ease of flow control | MIC-SYST-500 | 8.5 | Controllability of flow is another important consideration for design specifications |
| Power | MIC-PERF-300 | 6.5 | Minimising power consumption is important to be able to meet limited power budgets of the satellite |

Table 4.1: Trade-off criteria for actuator selection

To get a better understanding of the weighting for each criteria, some of the scoring method will be explained further. The blocking force is the maximum amount of force that can be provided by the actuator such that the system experiences zero deflection. In other words, it should be greater than the spring force of the plunger so as to handle the high inlet pressure. It also implies greater pressure against seating pressure leading to better leakage performance, one of the important requirements owing to a limited propellant supply onboard the spacecraft. Hence, a weightage of 35%.
The response time is another important criterion for microvalve design due to the possible capabilities required from the micro-propulsion system. Micro-spacecrafts with very tight pointing accuracy for attitude control would require thrust and impulse bits in the order of a few mN and $\mu$Ns respectively. This would require a valve that is open to have open/close cycles very fast. Based on the calculation presented in section 2.4, for an impulse requirement of $10^{-6}$Ns and a minimum thrust of 0.12 mN, a response time of less than 10 ms is required. Hence the actuator which is able to deliver such low switching times is crucial therefore, is given a weightage of 30%.
A mass flow rate of 4 g/hr at a differential pressure of 5 bar is the requirement set forth for our application. The flow rate directly translates to the deflection between the plunger and the valve seat. Since the plunger is coupled with an actuator in case of active microvalves, the deflection is directly controlled by the actuator. Therefore the deflection translates to the maximum stroke that an actuator can provide. The higher the

stroke, the higher the deflection and the greater the mass flow rate. Hence, it is given a weightage of 10%.

#### 4.1.1.1. Conclusion

| Criterion/Option | Weightage (%) | Thermo-pneumatic | Shape-memory alloy | Piezoelectric | Electro-magnetic | Electrostatic |
|---|---|---|---|---|---|---|
| **Response Time** | 30 | 30 | 10 | 90 | 85 | 90 |
| **Integration** | 10 | 15 | 25 | 70 | 40 | 60 |
| **Blocking force** | 35 | 45 | 45 | 80 | 60 | 30 |
| **Available stroke** | 10 | 75 | 75 | 30 | 40 | 20 |
| **Ease of flow controllability** | 8.5 | 10 | 25 | 80 | 75 | 55 |
| **Power requirement** | 6.5 | 30 | 40 | 85 | 60 | 70 |
| **Total** | 100 | 36.05 | 33.475 | 77.325 | 64.775 | 54.725 |

Table 4.2: Trade-off analysis for the different actuator schemes

.

As can be seen from the trade-off results the thermopneumatic and shape memory alloy actuator do not fair well in the analysis. Even though thermal based actuators have been used in various designs for different applications offering high controllable pressure differences up to around 25 bar. However, for the requirements specified it is unsuited since the power requirement and switching time are relatively large. Since their operation is based on temperature, any variation in the ambient temperature can greatly affect the working of these valves which is highly undesirable for space applications hence their suitability is questionable which explains their low weightage for most of the criterion.
From the different literature, it has been found that electrostatic actuators are fast in response with a switching time of less than 1 ms which is why they have the highest weightage for response time along with piezoelectric, but the limited drive voltage and the electrode distance in gap-closing designs makes it difficult to integrate the microvalves into the microfluidic system leading to poor control. Increasing the drive voltage up to pull-in effect voltages causes the valve seat to snap down. The closing force during this voltage is high enough to keep the valve closed against the inlet pressure. If the voltage is decreased up until the pull-up voltage the valve will open. Therefore, these valves offer poor controllability and they are generally designed as an normally open valve. This explains their low overall weightage of 54.725 hence, not very suitable.
Even though piezoelectric and electromagnetic actuators are widely used in most designs, they suffer greatly in performance in comparison to their macro-counterparts. Piezoelectric actuators offer fast response and have a high blocking force compared to other actuators, but they can handle relatively low differential pressure across the valve compared to shape memory alloys but higher than its other counterparts. Piezoelectric actuators provide very limited stroke and are limited in layer thickness, whereas an electromagnetic actuator poses disadvantage for wafer-scale fabrication as they incorporate external electromagnetic coils making the system bulky and heavy. Electromagnetic actuators can offer large deflections compared to piezoelectric, have relatively high pressure handling capabilities, fast switching time and higher voltage requirement just like piezoelectric actuators. However, since they are based on solenoid actuation, they require a magnetic core with external coils or permanent magnets to generate the magnetic field. Their integration and fabrication for small foot-print are of the chip and becomes externally challenging which is where piezoelectric actuators outperform them since integration and fabrication techniques for piezo actuators are relatively less cumbersome, therefore while the piezo score 70 in integration and electromagnetic score 40.

Although, both piezoelectric and electromagnetic actuators have their own limitations which can make it challenging to obtain the required performance. But they seem to be the most promising approaches in view of current technology based on the high blocking force, high speed and low power usage which can also be seen from the trade-off between the different actuators in table 4.5. Additional development efforts for actuator design improvements, such as stacked piezo-electric elements or piezo-bimorph options can greatly improve the available stroke and provide high differential pressure across them or a micro-fabricated high-turn number of electromagnetic coils are required.

Even though there are some piezoelectric design options available for micro-propulsion applications, they still barely fulfil the strict requirements set forth for space use. Therefore, to obtain the required performance at the manageable level of complexity, integration compatibility should be greatly improved. Voltage levels for piezoelectric actuation is a huge concern requiring up to 100V for the required mass flow rate. One solution mentioned in the literature is the use of DC-DC converters to provide the required actuation voltages. However for our micro-spacecraft with bus voltage of around 3.3 VDC-4.1 VDC, amping up the voltage to such high values might be highly undesirable making the system not very efficient.

#### 4.1.1.2. Sensitivity Analysis

A sensitivity analysis was performed on the aforementioned trade-off to ensure that the relative changes in the weighted criteria or alterations in the absolute weights do not unduly influence the study's outcome. To this end, the weighting philosophy was adjusted.

The criteria were prioritized from 6 to 1, with 6 indicating the highest importance and 1 the least. Additionally, weights assigned to the concepts ranged from -1 to 1, where -1, 0, and 1 denoted negative impact, minimal or no effect, and positive contribution to the requirements, respectively.

As highlighted above, the blocking force of the actuator is important criteria for the valve design while ensuring the actuator is able to provide required lifting or pushing forces. Hence, given the highest weightage of 6. Flow controllability and power requirements are additional criteria outlined for this thesis. However, they haven't been assigned a high weighting as they are aren't the primary driving requirements. They are also contingent on the control circuitry and failing to meet these criteria will not directly impact the mission objective. Therefore, they have been assigned a weight of 2.

Similarly, the concepts were evaluated based on different criteria, taking into account how each would impact the mission objective, and were assigned varying weightings accordingly.

For example, the response time of shape memory alloys falls within the range of 20-400 seconds, clearly not meeting the requirements for this thesis and adversely affecting the objective. In contrast, piezoelectric actuators have response times ranging from 0.1ms to 20ms, which aligns with our needs. Therefore, they have been given a relative weight of 1.

Upon closer examination, it becomes evident that piezoelectric actuators outperform electromagnetic actuators in terms of integration capability for wafer-level fabrication.

Hence, it is evident that adjusting the relative weights of the trade-off criteria does not alter the outcome, with piezoelectric actuators remaining the preferred choice.

| **Criterion/Option** | **Weighting factor ($w_{ij}$)** | **Thermo-pneumatic** | **Shape-memory alloy** | **Piezoelectric** | **Electro-magnetic** | **Electrostatic** |
|---|---|---|---|---|---|---|
| **Response Time** | 5 | -1 | -1 | 1 | 1 | 1 |
| **Integration** | 3 | -1 | -1 | 1 | -1 | 0 |
| **Actuator force** | 6 | -1 | -1 | 1 | 1 | 1 |
| **Available stroke** | 4 | 1 | 1 | -1 | -1 | -1 |
| **Ease of flow controllability** | 2 | -1 | -1 | 1 | 1 | 0 |
| **Power requirement** | 2 | -1 | -1 | 1 | 1 | -1 |
| | $\sum$ (+) | 1 | 1 | 5 | 4 | 2 |
| | $\sum$ (0) | 0 | 0 | 0 | 0 | 2 |
| | $\sum$ (-) | 5 | 5 | 1 | 2 | 2 |
| | Total | -14 | -14 | 14 | 8 | 5 |

Table 4.3: Pugh Trade-off study for the different actuator schemes

.

The round up of different actuator schemes can be seen in table 4.4.

| Actuation mechanism | Advantages | Disadvantages | Remarks |
|---|---|---|---|
| Thermopneumatic/ Shape-memory alloy/ bi-morph | 1. Large displacements<br>2. Large actuation forces | 1. Sensitive to the surrounding environment<br>2. Slow valve cycle times<br>3. Requires a cooling mechanism to close the valve<br>4. High power consumption<br>5. Suffer from the risk of unintended valve opening if valve temperatures rise too high.<br>6. Difficult to fabricate and integration with other micro-components is cumbersome | Not very suitable for space requirements |
| Electrostatic | 1. Low power consumption'<br>2. Fast response | 1. Small actuation forces possible<br>2. Small stroke available<br>3. High voltage required to actuate the valve. Possibility of pull-in effect, proportional flow control is challenging<br>4. Poor leakage performance<br>5. Cannot operate at very high fluid pressure-might lead to the opening of the valve.<br>6. Might lead to electrolysis for liquid media | |
| Piezoelectric | 1. Fast response<br>2. Very high blocking/ actuator forces available<br>3. Good pressure handling capability-can operate at high-pressure ranges<br>4. Can operate for both gas/ liquid propellants<br>5. Low power consumption<br>6. Easy integration with other components | 1. Small deflection/strokes<br>2. Leading to small mass flow<br>3. High voltage requirement | 1. Voltage issue can be solved by using MEMS based transformer circuitry<br>2. Using stacked or bi-morph to increase the stroke |
| Electromagnetic | 1. Fast response time<br>2. Small actuation voltage | 1. Use of permanent magnets or coils outside the valve chamber limiting tightly integrated systems: MEMS hybrid systems<br>2. Limited work density in micro-scale systems<br>3. Limited forces available | 1. Use of miniaturised coils or permanent magnets. |

Table 4.4: Advantages and Disadvantages of different actuation principles

## 4.2. Plunger Selection

The different valve concepts have been described in detail in section 3.3.1. One of the analogies to understand the valve concept and choose a suitable design scheme could be to consider the plunger structure as a valve spring [43]. This concept is depicted in figure 4.2. The spring force of the plunger coupled with the actuator force closes the valve. In normally closed valves, the spring force or the closing force of the plunger must be large enough to overcome the inlet pressure whereas, in normally open valve the spring constant is optimised for a lower value to be able to provide a large closing force. In this section, a trade-off analysis will

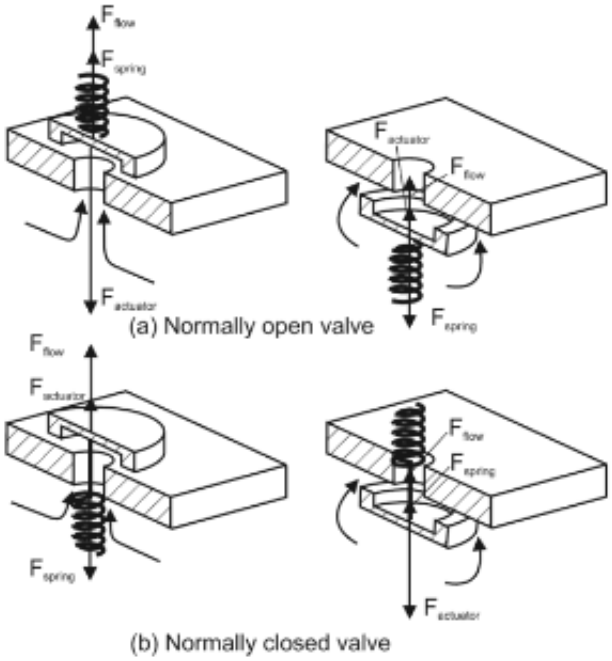


Figure 4.2: Comparison of the valve plate to a spring constant. F_actuator is the force applied by the actuator, F_spring is the pressure applied by the plate/membrane and F_flow is the force due to the inlet fluid pressure [43]

.

be conducted among various plunger concepts to determine the most suitable option for proceeding with the design.

### 4.2.1. Trade-off

In this section, the valve concepts outlined in the design tree will be presented and their rationale explained. Subsequently, a trade-off study will be conducted to determine the most suitable design concept for the plunger. A Pugh trade-off matrix will be employed, wherein the criteria have been assigned weighted scores ranging from 6 to 1, with 6 indicating the highest importance and 1 the lowest. These criteria have been carefully selected based on the system requirements, with particular emphasis placed on the manufacturability of the design. Given that the design is MEMS-based, compatibility with available fabrication techniques is paramount, while simultaneously meeting performance requirements. The motivation behind some of these weighted criteria is detailed below

Notably, leakage has been assigned the highest relative weight factor, which is understandable given its significance as one of the primary requirements for valve designs. Moreover, due to the constraints imposed by limited propellant, there are further demands on the choice of designs in terms of leakage control.

Another crucial criterion, weighted at 4, is the availability of reported performance data. During the literature review, it became evident that certain design concepts were underrepresented, leading to a scarcity of performance data. Since performance is a critical requirement for mission success, the absence of this information was deemed a crucial factor in the trade-off study.

Furthermore, as previously stated in the report, the design is envisioned to be manufactured at EKL. Consequently, the selected design concept should align with the available fabrication techniques at EKL, ensur-

ing feasibility. Additionally, simplicity in design features is emphasized to minimize manufacturing errors and enhance system reliability. Therefore, this criterion is assigned a weight of 4, reflecting its significant importance in the trade-off analysis.

| Criterion/Option | Weighting factor ($w_{ij}$) | Vertically-translating plate | Vertically-translating membrane | Tilting plate | Bending plate | Sliding plate |
|---|---|---|---|---|---|---|
| **Leakage Performance** | 5 | 0 | -1 | 1 | 1 | -1 |
| **Availability of reported literature** | 4 | 1 | 1 | -1 | 0 | -1 |
| **Ease of flow control** | 3 | 1 | -1 | -1 | 0 | -1 |
| **Freedom on actuator choice** | 2 | 0 | 0 | -1 | -1 | -1 |
| **Simple fabrication techniques** | 3 | 4 | -1 | -1 | 1 | 0 |
| | $\sum$ (+) | 4 | 1 | 1 | 4 | 0 |
| | $\sum$ (0) | 1 | 1 | 0 | 1 | 1 |
| | $\sum$ (-) | 0 | 3 | 4 | 1 | 4 |
| | Total | 11 | -8 | -8 | 7 | -14 |

Table 4.5: Pugh Trade-off study for the different actuator schemes

.

The motivation behind the weights for the different concepts will be summarised below. The weighted score have been given as 1, 0, -1 indicating positive, minimal or negative impact on the criteria, thus the mission objective.

From the discussion in section 3.3.1, it can be concluded, that both the translating plate type and the translating membrane are the widely utilised concept coupled with different actuation schemes, yielding varied performance characteristics. The vertically translating plate offers the most design freedom with widely available micro-fabrication techniques. The designs are widely available for a wide range of materials, fabrication techniques and shapes which makes it the most commonly accepted concept and therefore is awarded 1.

When considering the fabrication process for the microvalve, vertical translation emerges as favorable, especially when aiming to leverage current state-of-the-art machining techniques. These techniques do not necessitate highly intricate patterning and etching processes, facilitating relatively simpler assembly of the different wafers used in the design. However, this approach does not inherently provide added advantages in terms of low leakage compared to other concepts. Achieving zero gap height between two silicon surfaces proves challenging, requiring relatively high seating pressure to ensure low leak rates. This imposes constraints on actuator selection. Nevertheless, numerous designs reported in the literature have successfully utilized this design concept, achieving good leakage performance. Therefore, it is assigned a score of 0 for both criteria.

But particularly when a straight forward fabrication process is required, the broad design choices offered by the translating vertical plate becomes the most interesting choice. However, for better leakage performance thus greater closure, the tilting or bending plate modifications could be an alternative but the stresses developed on the already complaint plate in these cases could lead to valve failure when the inlet pressure increases.

A translating membrane could provide better closure performance by using soft, elastic membranes capable of shaping themselves to match the seat surface and allowing the contaminants to be embedded in it. But they also lead to problems of increased stiction, permeability for gases, which makes the use of harder, more resistant materials preferable at the cost of high leak rates and reduced conformity with the valve seat to provide good sealing. Furthermore, since compatibility to the gas flows is also one of the requirement, they

are not a preferred choice hence -1 for the criteria.

Precise flow control can be obtained using vertically translating plate design and needle valve. Even though needle valve has the potential of providing large strokes as well as reduced leakage. But no design has been found in literature utilising this concept thus the performance characteristics from the designs are not known. No other design than the one discussed in the study has been found in the literature to compare it with, hence implications of the different design modifications and its effect on the operation and performance of microvalves is unknown. Hence was not considered as one of the concept for the study.

Both the tilting valve and the sliding plate lead to limited design freedom and a complex fabrication process. Furthermore, there was paucity of reported microvalve designs utilising these concepts which makes it difficult to assess its feasibility.

On analysing the different designs and the subsequent discussions we can conclude that the vertically translating plate is the preferred requirement choice, however it should be noted that they vary greatly on the amalgamation of both the actuator and the design concept. A vertically translating plate would require high seating force to close the valve to reduce leakage, the low actuator forces that are available with thin sheets might not be adequate. But if a stack-type actuator or a thick film actuator are used, the hard plate would be preferred since the variable stroke and the actuator force will be amplified and would require hard seats to utilize them to provide improved sealing.

The run-down of these valve concepts can be seen in table 4.6.

| **Valve Concepts** | **Flow control** | **Leakage Performance** | **Design Freedom** |
|---|---|---|---|
| Vertically translating plate | Influenced by actuator | Depends on the spring force and actuator forces | Many designs have been reported |
| Vertically translating membrane | Influenced by actuator | Depends on the spring forces and actuator forces | Limited to thin or elastomer materials |
| Tilting plate | Large stroke due to higher fluidic resistance ratio | - | Not many reported |
| Bending plate | Depends on actuator | Material susceptible to buckling | Limited to specific actuating mechanism |
| Sliding plate | Plate position directly impacts the hydraulic resistance, hence the flow rate | Trade-off between friction and better closure | Not many reported |

Table 4.6: Summary of the valve concepts [24]

# 5

# Baseline Design

As the goal of this thesis is the preliminary design of a liquid microvalve for VLM based on micromachining for the use in future TU Delft PocketQube satellites, several different designs were analysed for various applications. It was found that only a handful designs have been reported for space applications, owing to stringent requirements and low performance characteristics, compared to their macro counterparts in terms of higher pressure valves and high leak rates.
Starting from the conceptual ideas selected in Chapter 4, this chapter unfolds based on the premise of establishing the design strategy to built upon the microvalve design in the subsequent parts of the thesis. Different approximate analytical approaches to model the fluidic behaviour in microvalves are examined which will be helpful in analysing the valve performance parameters. The chapter concludes with the design iterations that the author conceptualised. The motivations are discussed and the potential risks for the same are explored.

## 5.1. Microsystems Fluid Modelling Strategies

To determine the flow rate through the valve, it becomes important to perform a rigorous flow analysis through the complex configuration of a microfluidic network. Furthermore, the complexity increases when there are strong interactions between the fluid and structural elements which are coupled electrically to describe valve actuation. This requires specialised and costly computational fluid dynamics (CFD) analysis with a considerable expertise in theoretical fluid dynamics and associated numerical methods. However, to obtain first-hand approximation of fluid flow parameters there is a need for an analytical strategy for designing such systems. The direct calculation of the flow within the microvalves by solving the Navier-Strokes equation is not feasible without CFD software due to complicated geometries, moving boundaries, fluid surface interaction and the unsteady nature of the flow [7]. Therefore, to address this, several modelling strategies have been developed by different authors from the fluid point of view and they will be presented in this section.

One of the common approaches to estimate the flow rate is to approximate the valve as a variable area orifice model where the flow occurs through a local restriction with a variable opening area. The orifice contains a control member -such as a diaphragm- which determines the instantaneous opening area by its displacement. In this approach inertial losses dominate and an important parameter is the discharge coefficient $c_d$, defined as [63]:

$$c_d = \frac{1}{\sqrt{\zeta}} \tag{5.1}$$

where, $\zeta$ is the loss coefficient. Therefore, the flow rate can be characterised as

$$Q = c_d A \sqrt{\frac{2\Delta P}{\rho}} \tag{5.2}$$

There isn't a simple analytical expression to directly calculate the discharge coefficient. Instead, it is typically determined through calibration experiments or numerical simulations. In this model, the pressure drop $\Delta$ p becomes proportional to the square of the volumetric flow rate ( $\Delta P \propto Q^2$ ). These models give little insight into the valve geometry and require experimental validations and numerical simulations to determine the

discharge coefficient. It is one of the most common ways to describe the flow behaviour in macro fluidic components. A model was developed by Benignos [7] in which he suggests that a valve can be modelled as an orifice and he characterised the valve by three areas: the upstream flow area, the throat area, and the downstream area. The loss coefficient is then defined as a function of both the ratio of the orifice throat area to the downstream area and the ratio of the throat area to the downstream area. The developed model is described to be adherent to typical MEMS-based microvalves in order to capture the flow physics but presented only as an approximation to the correct values.

Another approach in fluid modelling in microvalves presented by many authors is to use the electric circuit analogy or the lumped parameter reduction. It is a very effective analytical approach which can provide a rapid prediction of the pressure-driven laminar flow in microchannels. However, the proposed electric circuit based fluidic models are primarily developed for single-phase flow and simplified systems [38]. This framework is based on the analogous behaviour of hydraulic and electric circuits [45], [81] with correlations of pressure to voltage, volumetric flow rate to current, and hydraulic resistance to electric resistance as can been seen in table 5.1. If N fluidic resistors are collectively in series or parallel, similar analogy as Ohm's law can be applied to calculate the equivalent hydraulic resistance.

| | **Hydraulic circuit** | **Electric circuit** |
|---|---|---|
| **Driving force** | Pressure drop ΔP (Pa) | Voltage V (V) |
| **Flow** | Volumetric Flow rate Q ($m^3 s^{-1}$) | Current I (A) |
| **Resistance** | Hydraulic resistance $R_H$ (Pa $m^3$s) | Electric resistance $R_e$ |
| **Equation** | Hagen-Poiseuille's law<br>ΔP=RQ | Ohm's law<br>V=RI |

Table 5.1: Physical analogy of microfluidics and electric circuit

$$Q = \frac{\Delta P}{R_H} \tag{5.3}$$

Many researchers have employed the lumped model analogy based on a system of hydraulic resistances for predicting the estimate of the flow rate and steady state pressure drop for a given system [16],[64],[81]. Based on the importance of this approach for the work developed in this thesis, some of these approaches will be explained further to better understand the electric analogy. From the equation 5.3, it can be seen that there is a linear the relationship between the pressure drop and the volumetric flow rate. Such flows are generally dominated by viscous losses This physics works on the assumption of the flow being fully developed laminar, viscous and incompressible, and follows a parabolic velocity profile (Hagen-Poiseuille's law).

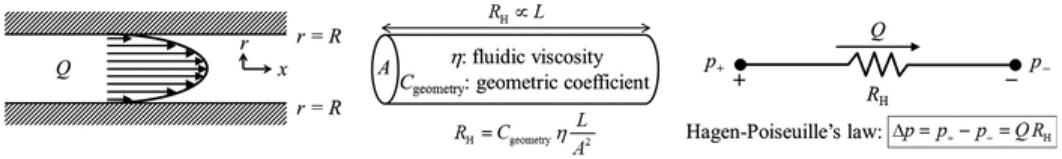


Figure 5.1: Hydraulic circuit analogy [45]

The assessment of value of hydraulic resistance is strongly dependent on the geometry as can be seen in figure 5.1. Hence, the assumption of the type of flow within the microvalve changes the geometric coefficient depending on: annular flow, circular pipe, flow between two parallel plate etc. For example, the hydraulic resistance of a a circular cross section channel can be approximated as

$$R_h = \frac{8\mu L}{\pi R^4} \tag{5.4}$$

where R is the channel radius with a finite channel length L (m).

For flows between two parallel plates (the valve seat and plunger), authors like Galambos et al. and Fazal et al. [19],[16] assumed radial flow and the relationship presented is given by equation 5.5.

$$Q = \frac{\pi h^3 \Delta p}{6\mu \ln \frac{R}{r}} \tag{5.5}$$

where h is the gap height between the valve seat and plunger, $\mu$ is the dynamic viscosity of the fluid, R is the outer radius and r is the inner radius. Alternatively, Et O Smal [64] approximated the flow between two circular spider-spring like central disk (plunger) and the valve seat as a parallel flow between two plates instead of annual flow considered by Galambos et al [19]. This is denoted by region (c) as can seen in figure 5.2. The flow model was modelled as region of cylindrical pipe, the abrupt fluid deviation and the parallel plates and was given by equation 5.6. The entrance and exit effects were not accounted for. The author presented that this analytical model gave a result very close to the 2 D finite-element analysis performed. Unsteady terms in the derivation of the average velocity were neglected but the solution developed gave a good approximation of the flow rate for the given design.

$$Q = \pi(d_c + d_i)\frac{p_2 - p_0}{d_c - d_i}\frac{x^3}{12\mu} \tag{5.6}$$

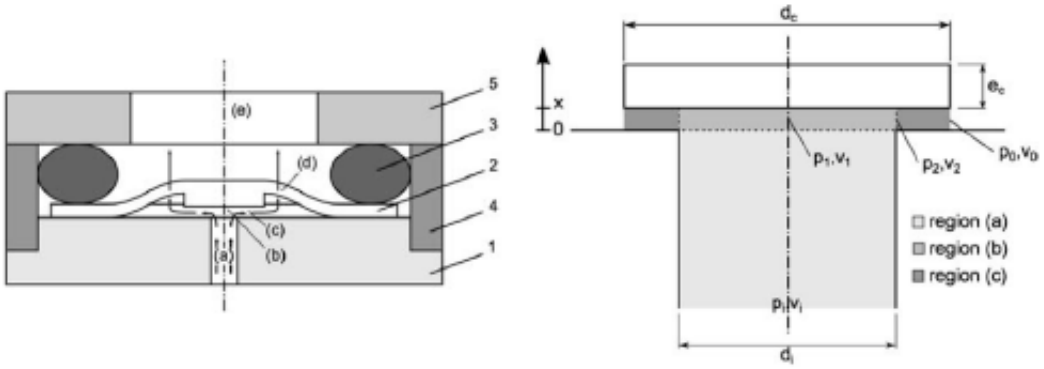


Figure 5.2: Geometrical considerations and valve sectors for analytical fluid modelling[64]

Based on a similar approach, author Zaidon et al. [81] used a network of hydraulic resistances and effectively predicted the flow rate and pressure in each system of the channel. The results from the fluid simulation in Fluent and electric simulation in PSpice were compared and they seemed to be in agreement with each other. It can be concluded that if the flow is assumed to be laminar and viscous, hydraulic circuit analogy can be engineered to predict the flow behaviour for the given channel geometry and its dimensions.

However, it should be noted that these typical orifice models as given by the two approaches do not capture geometry related sensitivities[7]. Studies about detailed fluid behaviour in microvalves remain lacking since these analytical solutions typically can be used to predict the steady state volumetric flow and the pressure drops across channels, however they do not account for the transient flows and do not provide the spatial distribution of flow velocity within the channel. For that, 2D or 3D CFD simulations need to be performed to obtain detailed flow information.

## 5.2. Valve Design versions

In line with the conceptual design ideas discussed so far in the thesis, several design options for the valve were thought of, some of which which were not pursued forward while others were developed further. A few of those initial design concepts that were not pursued further will be discussed briefly highlighting the reason why they were rejected.It should be noted that the designs presented subsequently are not necessarily presented to scale. They should be taken as mere design ideas at this stage.

### 5.2.1. Version 1

A valve design in essence constitutes of a fluid flow path including an inlet and outlet, a plunger to regulate the flow, an actuator ( in case of active valves). Based on this design philosophy, certain designs were explored. As

can be seen in figure 5.5, certain design considerations made for this initial design concept will be described below:
The design was envisioned to consist of three layers. The bottom-most layer is the valve seat containing the inlet and outlet with the fluidic path connecting the two, acting as the fluidic resistance. The middle wafer layer consists of the middle boss that is tethered to the silicon structure. These support arms are flexible extensions extending between the outer periphery of the valve body and the middle boss for supporting the boss movement relative to the valve body, to allow for the opening and closing of the fluid passage. The design employs 4 support arms, more tethers can be envisioned. Moreover, it can be important to have an even number of support arms so that the boss valve remains parallel to the valve seat, despite any out of plane stress. The more number of these tethers, the easier it is to etch using the fabrication techniques. Many tethered based boss designs were reported and patented in the literature , however most of them were reported for normally open valves.
The piezo actuator is to be bonded on top of this boss. Applying voltage to the piezo would cause the piezo to actuate vertically, thereby lifting the boss centre plate away from the valve seat. This actuation would open the passage between the inlet and the outlet to open up thus allowing for fluid flow.
The design mentioned by Choonsup Lee in [76] hinted towards the possibility of an electric short within the piezoelectric actuator when in contact with liquid, hence had introduced an additional boss to shield the piezo from the liquid. Therefore, the top most plate was introduced to this design to ensure the piezo actuator does not come in contact with the fluid which would follow the low resistance path through the gaps between the boss and the silicon tethers. However, introducing this third plate would introduce an additional force that would need to be applied to lift the boss to allow for the fluid flow. So, in order to limit the additional force while still creating fluidic barrier, the design concept of having the centre silicon etched out completely as seen in the figure 5.3a was introduced. By doing this, the piezo would still be bonded to the middle boss allowing for the free movement while the tethers in actuated state would sit in the cavity of the first plate as seen in figure 5.3b.
To ensure minimum leakage when not actuated ( in closed state), the three plates have to be compression bonded on the perimeter of the plate outside to the middle boss. This is to create a closed volume area so that the water in limited in a confined space and leakage to the environment is limited.

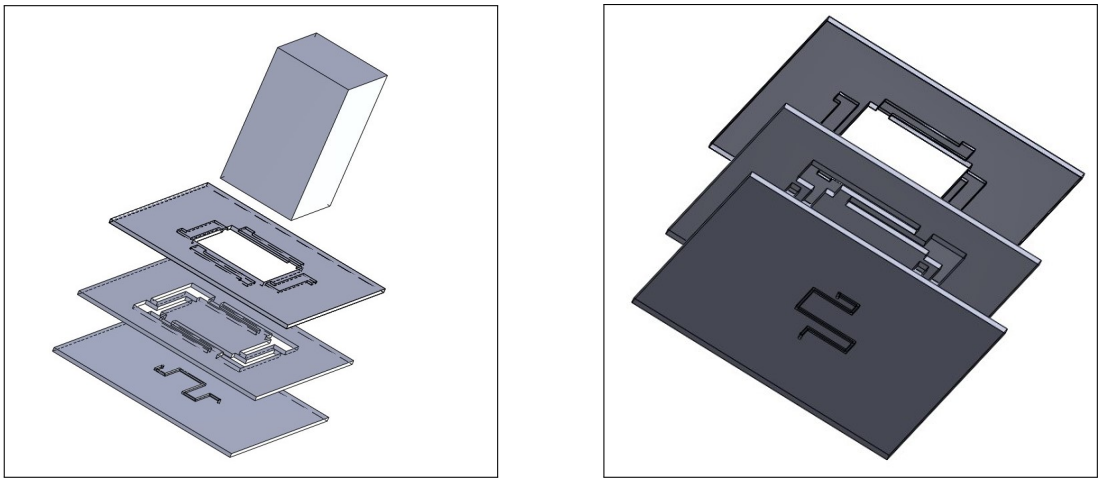

(a) Exploded view of the first design version

(b) Alternate view of design 1

Figure 5.3: 1st Version of the design concept (not to scale)

On further thought, the design was not pursued forward because of certain drawbacks. With this current design of the top plate and the piezo are bonded to the middle plate, the stroke length of the piezo would be limited by the depth of the cavity for the tethers on the top plate. This would seriously restrict the displacement length possible, in turn the mass flow rate. The introduction of these cavities also introduces manufacturing complexities. Moreover, if the tethered boss and the top cavity are not perfectly aligned, a leakage is expected from the edge of the etched closing membrane. Sealing in the corners would be extremely difficult and the sealing accuracy requirements on the tethered boss and the edged top plate cavity are very high.
Secondly, the design of tethers with the centre boss creates more stress concentration areas at the points where the tether is attached to the silicon plate. Repeated on and off cycles, during which the middle struc-

ture would be lifted vertically upwards, introduces stress at the joints eventually running the risk of structure breaking. Having such a design of the top plate does not fully restrict the flow from being in contact with the piezo. The author envisions that during the on state, when the boss is actuated along the piezo, there would still be a gap created between the piezo and the top layer and since the fluid would likely to follow the least resistance path it is likely it would flow through these gaps. Therefore, such a design does not essentially ensure that fluid would most likely follow the fluidic path towards the outlet. Hence, due to these aforementioned reasons, this design was deemed unsuitable to pursue further.

### 5.2.2. Version 2

Based on the design flaws mentioned in version 1 of the design, certain modifications were implemented. As can be seen in figure 5.4a, the opening of the edged cavity to the hollow part was sealed, this was to limit the water seeping out during the on cycles. However, in doing so, stress might be introduced at the joint of the tether and the middle boss. In order to improve the stress concentration areas where the tether is attached to the silicon plate, the thickness of the tethers were increased. The thickness of these tethers also act as a preload force to keep the valve assembly closed in the off state.
From figure 5.4b, it can be seen that the design of the valve seat was completely modified. This design drew inspiration from the valve design presented by author Pramanick et al [54]. This modified design of the valve seat would simplify the manufacturing process and would significantly minimize fabrication failures. Another major reason for such a design change was to reduce the closing area, in other words reduce the area of the valve seat that will be contact of the plunger.

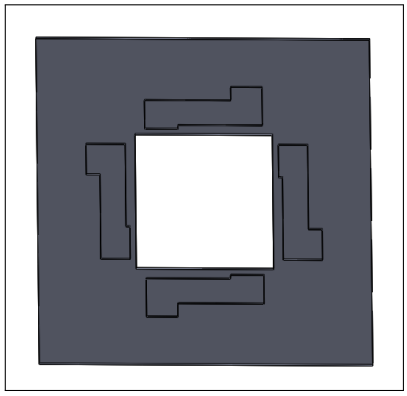

(a) The etched cavity was altered in an attempt to reduce water leakage to the environment

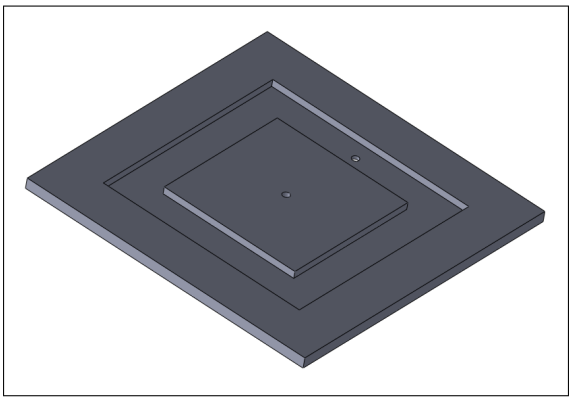

(b) Design modification to the valve seat

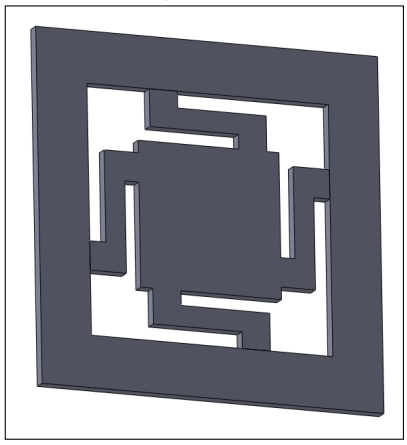

(c) The thickness of the tethers were increased as compared to design version 1

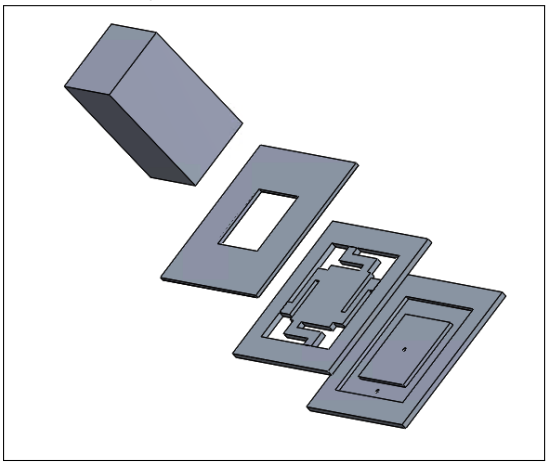

(d) Exploded view of Design Vesion 2

Figure 5.4: Design version 2: modifications made in effect to the highlighted design drawbacks of version 1

As can be seen in Design version 1, the sizing of the tethered boss would be such that both the inlet and outlet orifices are in contact to close the valve. This would imply, a bigger footprint of the boss and hence requiring large piezo actuator. On the other hand, by introducing recess that contains the outlet hole and the

boss encompasses the inlet hole, the surface area of the boss in contact with the wetted area can be reduced, which would essentially reduce required piezo footprint. Furthermore, reduction in wetted area would also reduce the stiction problems that are prevalent in MEMS design [66]. For this, the size of the tethered boss was also reduced. Another advantage of having such a design is that it helps in precisely bonding to the middle plate. Having an earlier design of the bottom plate, with the introduction of bents if not manufactured to precision, introduces areas of high pressure loss and might create zones of turbulence in the channel. Furthermore, having bents and a small channel even if easily manufactured by the MEMS process, it can be tricky to have low tolerances while etching. Hence, at this stage the valve seat design was considered optimal to be pursued further.

Since the design requires low leakage values, having tethered design of the middle plate does not create a closed fluid volume space and has increased chances of leakage. Furthermore, there are inherent complexities associated with the fabrication of the middle plate. Joachim et al in [62] used a tethered valve plate design for gas chromatography applications and he highlighted that a significant amount of time was spent on fabricating the tethers. The author decided not to pursue forward with this design version of the closing membrane (middle plate) and further attempts were made in order to simplify the design of the plunger.

### 5.2.3. Version 3

Building upon the identified drawbacks of the previously mentioned plunger design, additional attention was devoted to enhancing its functionality. Rather than employing a tethered boss, alternative design avenues were explored. In line with the concept utilized for the valve seat, a similar clamped recess structure for the plunger was conceptualized. This can be seen in figure 5.5b. The plunger design should be optimised to require minimum actuator forces, minimum stress and maximise stiffness. Such configuration of the plunger was relatively simple design compared to the tethered design as well as likelihood of reduced leakage due to clamped close volume structure. Furthermore, it would also protect the piezo actuator from any exposure to liquid. Having a recess to create a thin membrane would certainly reduce the stiffness as compared to thick plate, however, it would also reduce the required actuator forces for deformation. The valve seat and the plunger would be bonded together on the frame area such that the membrane is free to deflect. The operation of the valve would be based on controlling the deflection of this membrane via an actuator. This improved design should be properly sized and analysed for appropriate performance and this will be discussed over the subsequent chapters.

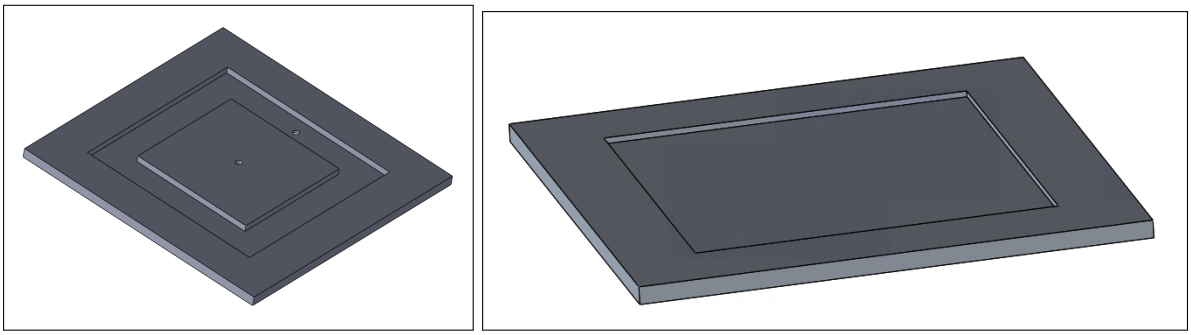

(a) Valve seat design Concept

(b) Design of the modified plunger

Figure 5.5: 3rd Version of the design concept (not to scale)

It should be noted that the design considerations for valve packaging is not considered at this stage and can introduce further modifications to this design.

# 6

# Detailed Design

## 6.1. Introduction

In this chapter, the conceptual decisions made so far in the preceding chapters will be converted into tangible results, with the help of analytical modelling. The framework of this study begins with proven configurations, with further design variations to produce a valve that meets the performance requirements. The module is split into constituent parts important for preliminary design estimation, and these are evaluated under static load cases. The requirements from Chapter 2 along with the manufacturing constraints are used as bare minimum standard for the dimensioning of the valve. Some of the design suggestions put forth in Chapter 5 will be revisited to be incorporated in the component design. Simple reduced order of analytical model (fluid and mechanical) are used as a design tool in this chapter to derive values for the key parameters required to produce a viable system. The estimation of fluid flow path for predicting the flow rate for the required pressure drop and forces on the membrane is crucial for designing the microvalve. The method used is based on subdivision of the structure into lumped elements, which are described individually using simple analytical models.

## 6.2. Model Introduction

A simple representation of the different domains in a microvalve design is shown in figure 6.1. The valve assembly reveals the piezo (shown as a spring in this representation). The green and the orange represented as the plunger and flow path, respectively. The flow path refers to the valve seat leading up from the inlet to outlet. Throughout this thesis, the plunger and membrane will be used interchangeably, and it refers to the structure sitting on top of the valve seat. The dotted line indicates the packaging/ holder unit. The double arrow indicates the interdependence between the fluid-structural response. This dependence becomes of importance for the design of the system control unit for which the valve response system is an important system parameter in order to ensure precise firing of the propulsion system for the desired application. Transient response is helpful in determining the on-off valve cycle, for which, time-dependent study involving fluid-surface interaction needs to be predicted. However, for the analytical model, loads at different states(on/off) is considered for once the steady condition is reached.

The letters indicate the different constituents of the assembly, namely:

(A) Valve seat design: A, fluid flow path for mass flow rate estimation

(B) Plunger design: B, characterised by the interactions among domain A, B and C

(C) Actuator design: C

(D) Holder: D which is essential for the sealing the valve from external environment. Owing to the external mass and volume restrictions, it defines the integration capability of the microvalve with other components of the propulsion system.

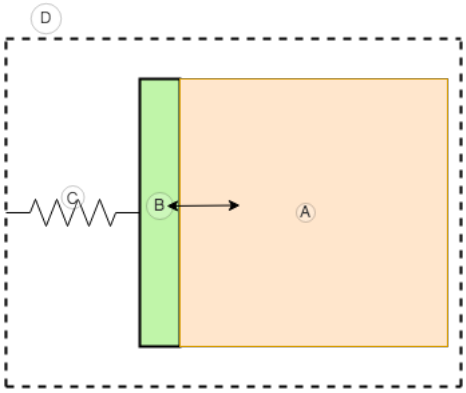


Figure 6.1: A simple representation of the constituents of a microvalve design

## 6.3. Constraints due to manufacturing

Before we dive into the design process, it is important to understand the limitations posed by the manufacturing process. Since the microsystem design is closely related and often strongly restricted by fabrication process, they must be defined at an early stage. For this, purpose, the constraints that influence the design process will be put forth so that the motivation behind some of the dimension choices can be justified. However, the detailed fabrication process for the final design will be reserved for the subsequent chapters.
The size of the chip that is shipped by the manufacturer and is available at EKL is 1.115cm x 1.115 cm. The usable design area for the silicon based manufacturing process is 9mm x 9mm, which is centred in the design. Due to the incorporation of an exclusion zone required for the mask bonding process, it is advisable to place critical elements of the design 0.25mm away from the edge of usable area which can be seen in figure 6.2. Keeping this layout requirement in mind, the dimensions are taken to be 8.5 x 8.5 mm for the initial get-go in the analytical design phase. At this stage, optimising the design size was not considered.

Although based on design requirements the fabrication process can be optimised to also support other dimensions, but for this study the standard available chip size at ElseKooi lab was chosen to avoid additional costs. The handle wafer (substrate) thickness of 300$\mu$m was chosen as the starting point in the design process. Other choices of wafer thickness are also possible which depends on the handling pressure and the yield stress of the silicon to ensure that the device does not break. However, it is recommended to not select wafer thickness below 200 $\mu$m.

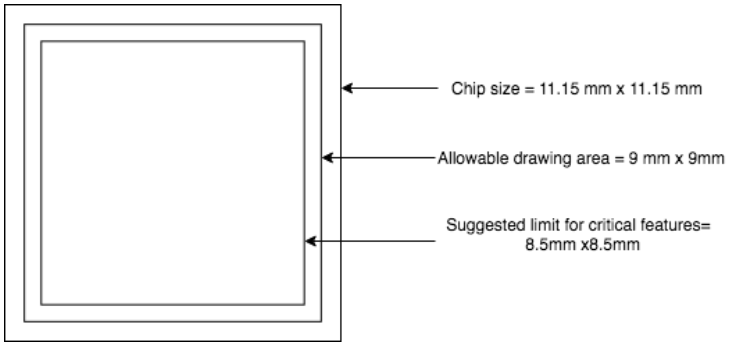


Figure 6.2: Layout Requirements[11]

Furthermore, we need to first fix the cross-section of the outlet. Even though other shapes for the outlet hole are possible, for this design a circular cross-section for the inlet and outlet hole is chosen. The minimum through hole ( inlet/outlet) diameter in the silicon substrate is 200$\mu$m with a minimum gap of 10$\mu$m between them is allowed. Therefore, for the design in this study, 200$\mu$m as the minimum inlet and outlet hole dimensions are selected.

## 6.4. PART A: Valve seat design

The discussion in this section is bound by these requirements:

- MIC-PERF-100: The valve design shall be able to provide a mass flow rate of 5 g/hr at a maximum differential pressure of 5 bar
- MIC-FUN-200: The system shall be compatible with liquid $H_20$
- MIC-SYST-200: The total size of the propulsion system shall be within 42mm x 42mm x 30mm (including all the components)
- MIC-PERF-300: The maximum leak rate shall be $<10^{-5}$ scc/s at maximum operating pressure.

Balancing these requirements is crucial to the design optimality. For this, it is important to design the flow path such that requirements are fulfilled but along with that precise proportional flow control can be achieved. Building upon the valve seat design discussed in Design version 3 of Chapter 5, the flow path from the inlet to outlet should be dimensioned. One of the flow modelling strategies explored in 5.1 will be chosen for developing the design, and the rationale behind its selection will be justified. Before diving into the sizing of the fluidic resistance it is important to understand characteristics of flow dynamics with an emphasis on channel geometry, flow conditions described by Re.

### 6.4.1. Micro Flow Dynamics

New design potential can be obtained by exploiting the positive downscaling effects of miniaturised fluidic components. In micro devices, the scaling effects come into play, which states that the surface-to-volume ratio varies as the inverse of the length scale. With the decrease in the length scale of micro-devices, the ratio of area to volume is larger than for macro systems. The area to volume ratio scaling on the flow behaviour is well described by Reynolds number. Since the volume is scaled down to power three, inertial forces are also scaled down to third power. This means inertial effects become of minor importance and viscous effects start to dominate.

Usually Reynolds number for smaller system is low and hence inertial effects like turbulence effects can be neglected, however, locally, the effect of inertial forces might still be present in the form of for example vortices at sharp corners [47]. Furthermore, due to viscous forces the energy dissipation relative to the stored kinetic energy in the flow will increase.

Since turn around times play an important role in CubeSats and test-runs to make prototype are very expensive, there is a need for modelling and design strategies to simplify this process. At this moment these tools are still in their infancy, but much effort is spent on their development [47]. Several authors have thus attempted to develop analytical flow models depending on the channel geometry to get some insight into the flow behaviour.

The precondition for successful fluid modelling using direct analytical models relies on the understanding of the flow behaviour and the correct assumption of the type of flow depending on which surface effects are dominant. However, different phenomena are observed in various work which indicate that the mechanism of flow transfer in micro-channels is not clearly understood.

There are two major forces that play an important role in micro-channels, namely viscous and inertial forces. Both of these forces can be as a measure of resistance. In case of viscous dominated flow, this resistance appears due to frictional shear forces arising during motion of molecules. When the fluid moves through the channel as a result of applied pressure gradient, generally speaking, the fluid moves more quickly in the central axis of the channel compared to the walls. This difference in relative motion of fluid layers result in the manifestation of differing amount of friction between them. On the other hand, inertia is the resistance of a volume of fluid to change its state of motion, since the fluid prefers to continue in a straight line at constant velocity. The interplay of these flows determines the flow regime at a given flow rate in any type of channel, and this can be expressed as Reynolds number. This is used to predict the range of flow rates at which the flow in the microchannels will be laminar or turbulent and comparing it to transitional number to determine which flow model to use.

Peter Gravesen et al. [22] reviewed 32 microfluidic devices mapping them based on the length to hydraulic diameter ratio and found that none of the MEMS valves operated in the turbulent regime which can be seen in figure 6.3. He concluded that most microscopic valves operate in the laminar region, making transitional or turbulent flow of little significance to microfluidic since it is difficult to achieve in microchannels. This was also found in other supporting literature [65], [60],[39]. Three different flow regimes can be defined,

$Re_t$ > Re, pressure drop is dominated by the viscous losses and the flow is laminar

$Re_t$ which is the transitional region, after which the flow becomes fully developed turbulent
Re> $Re_t$, the flow is not fully developed, and the inertial losses dominate the pressure drop across the device.

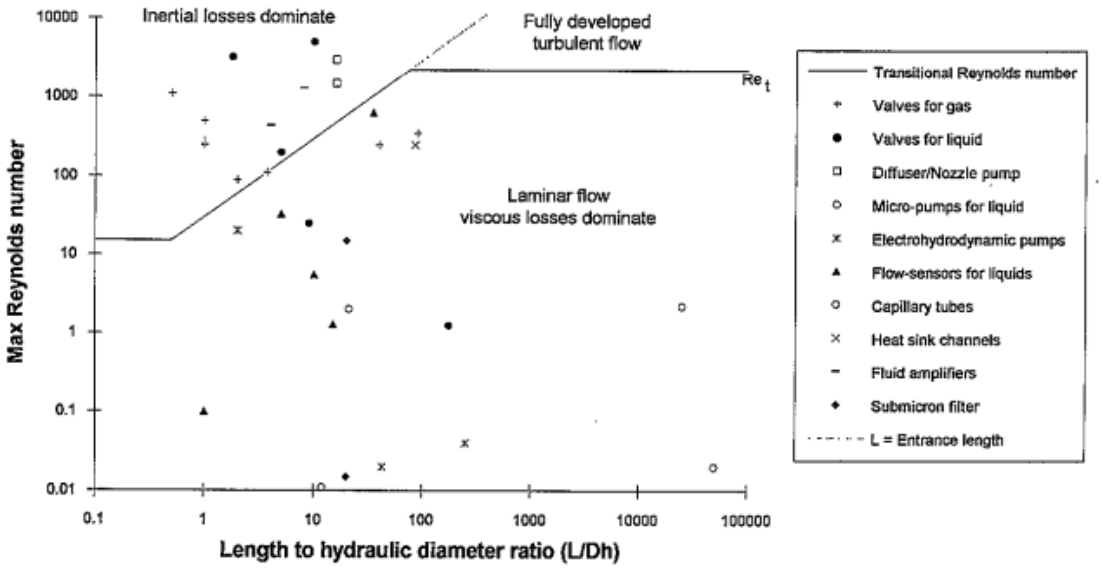


Figure 6.3: Mapping of Reynolds number vs L/$D_h$ of the 32 microfluidic devices reviewed. The points plotted represented the largest flow reported [22]

For a required mass flow rate, Reynolds number is the ratio between the inertial force and viscous force and can be used to characterise the transition between flows and is given by equation 6.1.

$$Re = \frac{\rho U L}{\mu} \tag{6.1}$$

where, $\rho$ is the density, U is the area-averaged velocity, L is the characteristic length, $\mu$ is the dynamic viscosity of the fluid, water in this case. For flow in a pipe, the characteristic length is the pipe diameter since the cross-section is circular. In case of non-circular geometries, Reynolds number is given by equation 6.2. For flow through an object with arbitrary shape, the Reynolds number can still be calculated using this formula. The Reynolds number can be assessed separately for different segments of the design to understand the flow regime. For example, if the design consists of combination of different cross-section, like circular pipes, rectangular/square channels etc, then by determining relevant parameters for each section of the flow path Reynolds number can be calculated. This will help indicate if the flow is laminar or turbulent throughout the entire flow path.

$$Re = \frac{\rho U D_h}{\mu} \tag{6.2}$$

where $D_h$ is the hydraulic diameter, which is calculated as

$$D_h = \frac{4A_v}{P_v} \tag{6.3}$$

where, $A_v$ is the cross-sectional area where the gas flows and $P_v$ is the wetted perimeter.

Generally speaking and often cited, if the valve of Re is less than around 2300, the flow is considered laminar[29]. However, there seems to be different stances for the transitional Reynolds number, some studies cited that value to be between 300-2000 [39], [43]. Whereas, for slit type orifice, the author stated this value to be around 15 [27].

The flow path may have different regions, for example, orifice, long channel, short channel, pipe flow. As can be seen in table 6.4, P Gravesen et al. presented analytical formulae relating flow and pressure drop for viscous or inertial dominant flow along with the transitional Reynolds number. This can be useful in choosing an appropriate flow model depending on which effect dominates the flow.

| Type of restriction | Definition | Viscous losses dominate laminar flow ($Re \ll Re_t$) | $Re_t$ | Inertial losses dominate ($Re \gg Re_t$) |
|---|---|---|---|---|
| Orifice | $L/D_h < 0.5$ | $Q_v = A\frac{2}{C}\frac{D_h}{\mu}\Delta P$ | 15 | $Q_v = \frac{A}{\sqrt{\xi}}\sqrt{\frac{2}{\rho}\Delta P}$ |
| Short channel | $2 < L/D_h < 50$ | | 30 $L/D_h$ | orifice: $\xi \simeq 2.6$<br>channel: $1 < \xi < 1.5$ |
| | | $Q_v = A\frac{2}{C}\frac{D_h^2}{L\mu}\Delta P$ | | |
| Long channel | $L/D_h > 100$ | | 2300 | $Q_v = A\sqrt{\frac{D_h}{L}\frac{1}{f}\frac{2}{\rho}\Delta P}$ |
| Diffuser inlet ($D_{h'}$) outlet ($D_h$)<br>($A$ is the smallest area) | $5 > L/D_h > 50$ | $Q_v = A\frac{2}{C}\frac{D_h^2}{L\mu}\frac{3\left(D_h^3/D_{h'}^3 - 1\right)}{1 - D_{h'}/D_h}\Delta P$ | 30 $L/D_h$ | $Q_v = \frac{A}{\sqrt{\xi}}\sqrt{\frac{2}{\rho}\Delta P}$<br>$0.2 < \xi < 1$ |

Figure 6.4: Flow models for incompressible liquids [22]

Prior to proceeding with the design of a microfluidic network, a comprehensive look of the physical phenomena of flow through different channel geometry shapes will be discussed.

### 6.4.2. Physics of flow in microfluidic channels

For modelling purposes when designing a fluidic system, knowledge of the physics of flow in small channels becomes essential. Questions like "*Can macro models be used to simulate resistance and flow in valves ?*" "*Which models to use and when are these models valid?*"
In order to answer this, a start is made assuming Navier Stokes equations, which mostly used in the macro-world. Assuming that the physics are still valid for channels down to few microns, these equations can be simplified. The most comprehensive set of equations governing liquid flow in the continuum region are Navier Stokes equation, which can be derived from Newton's second law. These include the conservation of mass, momentum and energy and the compact form of these conservation laws in partial differential form are [43]:

$$\frac{\partial \rho}{\partial t} + \frac{\partial \rho}{\partial x_i}(\rho u_i) = 0 \tag{6.4}$$

$$\frac{\partial}{\partial t}(\rho u_i) + \frac{\partial}{\partial x_j}(\rho u_j u_i) = \rho F_i - \frac{\partial p}{\partial x_i} + \frac{\partial}{\partial x_j}\tau_{ji} \tag{6.5}$$

$$\frac{\partial}{\partial t}(\rho e) + \frac{\partial}{\partial x_i}(\rho u_i e) = -p\frac{\partial u_i}{\partial x_i} + \tau_{ji}\frac{\partial u_i}{\partial x_j} + \frac{\partial q_i}{\partial x_i} \tag{6.6}$$

where, repeated indices in a single term indicate a summation. $u_i$ represents the flow velocity, $\rho$ is the local density, p is the pressure, $\tau$ is the stress tensor, e is the internal energy, F is the body forces and q is the heat flux

To answer the equation posed earlier, as long as the continuum assumption holds true, these well established macro models can easily be adapted for microscale problems. These Navier stoke relations can be very different for gases and liquids, however as mentioned earlier, this thesis focuses on water as the reacting specie, therefore, the above set of equations will be simplified further only for liquid flows to obtain an analytical solution.

For flows in microfluidic devices, fluids (primarily water and other aqueous solutions) can be approximated as incompressible [29], therefore, the above set of equations can be simplified considerably for an incompressible, isotropic, Newtonian, uniform viscous, Fourier conducting fluid as [43]:

$$\frac{\partial u_i}{\partial x_i} = 0 \tag{6.7}$$

$$\rho\left(\frac{\partial u_i}{\partial t} + u_i\frac{\partial u_i}{\partial x_j}\right) = \rho F_i - \frac{\partial p}{\partial x_i} + \frac{\partial}{\partial x_j}\left[\eta\left(\frac{\partial u_i}{\partial x_j} + \frac{\partial u_j}{\partial x_i}\right)\right] \tag{6.8}$$

$$\rho C_v\left(\frac{\partial T}{\partial t} + u_i\frac{\partial T}{\partial x_i}\right) = \frac{\partial}{\partial x_i}\left(k\frac{\partial T}{\partial x_j}\right) \tag{6.9}$$

Further, assuming that the flow remains at constant temperature during the operation of the microfluidic device and no body forces acting, then the energy equation (6.9) can be decoupled. When the inertial forces are small compared to viscous forces, the non-linear term can be neglected, equation 6.8, can be rewritten as [65]

$$\rho \frac{\partial \vec{u}}{\partial t} = -\rho \vec{u} \nabla \vec{u} - \nabla p + \eta \nabla^2 \vec{u} \tag{6.10}$$

where $\vec{u}$ is the velocity field denoted by $\vec{u}$=$\vec{u}(\vec{r},\vec{t})$, $\rho$ is the fluid density, $\eta$ is the viscosity, p is the pressure. Assuming flow to be fully developed, therefore in steady state the velocity field is unidirectional, laminar and there is no fluid acceleration. The convective and unsteady terms in the equation 6.10 become zero, the net pressure forces balances the viscous forces reducing to

$$\nabla p = \mu \nabla^2 \vec{u} \tag{6.11}$$

It has been suggested that the viscosity of a liquid through a small channel can be higher than the same liquid flowing through the channel at a larger length scale. However, more work needs to be done on both theoretical and experimental sides to corroborate this with certainty [43].

Considering geometric simplifications and boundary conditions (u=0 at r=R), the pressure driven flow in a long cylindrical channel with radius R is given by:

$$u = \frac{R^2 - r^2}{4\mu}(-\frac{\mathrm{d}p}{\mathrm{d}x}) = u_{max}(1 - \frac{r^2}{R^2}) \tag{6.12}$$

where, $u_{max}$ is the maximum velocity at r=0. Such a flow is termed as Poiseuille flow and is characterised by parabolic velocity profile where the flow velocity is maximum in the centre of the channel and decreases towards the outer walls. On integrating the velocity contributions from each lamina, the total volumetric flow rate for steady-state, pressure driven flow in the circular channel described by Hagen-Poiseuille's law is given by

$$Q = \frac{\pi R^4}{8\mu}(-\frac{\mathrm{d}p}{\mathrm{d}x}) \tag{6.13}$$

Hagen-Poiseuille's law typically applies only for a channel that is perfectly straight and infinitely long. However, it can reasonably be also applied to channel with finite length L. Therefore, laminar flow in a long channel can be assumed to be fully developed if L/R »1 and L/R» Re, where L is the channel length, R is the radius of cylindrical cross-section and Re is the Reynolds number [45]. For most microfluidic devices, the pressure gradient is uniform along the length of the channel, thus the term -dp/dx can be approximated as $\Delta p$/L where $\delta p$ is the pressure difference along the finite channel length of L. The equation 6.13 simply becomes

$$Q = \frac{\pi R^4}{8\mu}(-\frac{\Delta p}{L}) \tag{6.14}$$

where, $\mu$ is the dynamic viscosity, L is the channel length.
The above equation 6.14, can be re-written to give equation 5.3.

The hydraulic resistance ($R_h$) for circular channels defined as

$$R_h = \frac{8\mu L}{\pi R^4} \tag{6.15}$$

where $\mu$ is the dynamic viscosity, L is the channel length, R is the radius of circular tube.

For rectangular channels with low aspect ratio (width of the channel  height of the channel) then $r_h$ = (w x h)/(w+h). However, this estimate gives 20% error in value for square channels (w=h) [45]. For rectangular channels, an exact solution is not possible. The best possible solution is a Fourier series expansion to approximate the velocity profile, but if the aspect ratio if high (h/w «1), which is the case for most microfluidic channels, the hydraulic resistance using first order can be approximated as given below: [45], [16].

$$R_h = \frac{12\mu L}{w h^3 (1 - 0.63\frac{h}{w})} \tag{6.16}$$

where, L, w, h is the length, width and height of the rectangular channel respectively. Better results can be obtained though using second or higher order approximations, but these formulas become rather elaborate.

Design formulas of hydraulic resistance for different channel cross-section designs have been reported by Oosterbroek in [47]. It can be concluded that the internal flow resistance path determines the flow rate and required pressure drop between the two ends of the channel.
This means, in order to achieve low mass flow rate for higher pressure flows, the channel needs be designed such that the flow path is viscous, in other terms more fluid energy is lost due to viscous forces. The Hagen Poiseuille's equation is central to the design of microfluidic networks to be able to precisely control the flow rate in case of viscous pressure driven flow.

The Hagen Poiseuille's equation falls in case of low viscous flows, wide or short pipe. In this case, other flow models such as Darcy-Weisbach equation are used. In case the channel is too short and then ratio of length to the radius of the pipe is not greater than 1/48 of the Reynolds number, then the flow cannot reach parabolic velocity profile [47]. It might result in high flow rates, Poiseuille's equation is no longer valid and the flow is then bounded by Bernoulli's principle and is given by equation 5.2.

### 6.4.3. Analytical model

Having understood the foundation of the physics behind the the flow micro channels, the motivation for the design of the flow path( valve seat) will be discussed in detail in this section. The design choices are influenced by the learnings from the iterations discussed in chapter 5 and the flow physics discussed in section 6.4.2. The version 3 of the design from Chapter 5, will be further motivated and developed. This section deals with the design of Domain A, specifically, which can be seen in figure 6.11.

#### 6.4.3.1. Initial Estimates

Assuming continuum flow, from conservation of mass:

$$v = \frac{\dot{m}}{\rho A} \tag{6.17}$$

where $\dot{m}$ is the mass flow rate, $\rho$ is the fluid density, A is the cross sectional area of the inlet/outlet, v is the velocity. From the figure 6.5, it can be seen that the inlet on the middle boss is a pipe geometry with a circular cross-section.

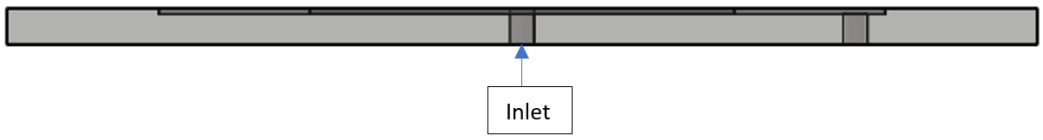


Figure 6.5: Side view of the Version 3 of the valve seat design presented in Chapter 5

From the requirements given in 2.5, desired mass flow rate is 5 g/hr, taking density of water as 1000 kg/m$^3$. With this circular cross-section of the inlet with a radius of 100 $\mu$m (minimum allowable orifice by fabrication techniques as highlighted in 6.3), the average velocity at the inlet is 0.04442 m/s.

Calculating Reynolds number at the inlet from equation 6.2, we get Reynolds number $\approx 9$. Since this value is below the transition Re, it is safe to assume that the flow falls within the laminar regime. Similarly, Re can be calculated for different sections of the geometry to ensure that the flow remains laminar throughout the flow path. The low values of Re affirm that the viscous forces typically dominate the flow and the inertial forces do not play a significant flow. Thus the resulting flows are linear, deterministic flows. These values also typically align with the ones mentioned by Todd et al. [65]. It is stated that with water as the working fluid, typical velocities of 1$\mu$m/s-1cm/s, typical channel radii of 1-100$\mu$m and the Reynolds numbers ranging between $10^{-6}$ and 10 can be expected.

Flows are basically caused by the pressure difference pushing the fluid from high pressure to low pressure. A constantly decreasing pressure is formed along the length of the fluidic channel. This pressure drop is the driver of the flow. The pressure gradient over the length of the channel has two main task, mainly to compensate for the frictional force during the flow and to accelerate the flow to achieve the characteristic flow

profile. The Hagen Poiseuile equations derived above are based on a important premise that the flow is fully is laminar, steady and fully developed. This means that the pressure gradient $\partial$p/$\partial$x only refers to the pressure drop necessary to overcome friction, so that the flow keeps flowing. In fully developed region, the pressure gradient and the shear stress in the flow are in balance and the parabolic velocity profile remains unchanged in this region.
However, these equations implicitly assume long pipes where the parabolic flow profile has already fully established. Thus, in the inlet of the pipe ( the entrance length) within which the pressure gradient has to not only compensate for the flow but also accelerate the flow, the hagen Poiseuille equation does not hold true for that part of the inlet region.

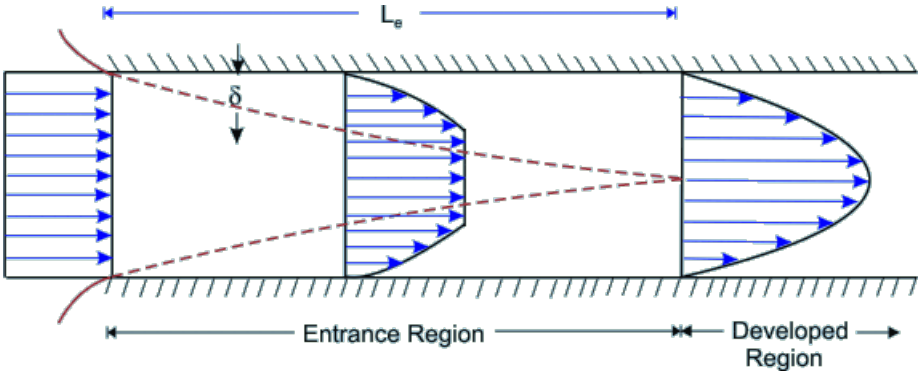


Figure 6.6: Entrance flow length in a pipe flow: Distance the flow has to travel after entering the pipe before the flow becomes fully developed [80]

As you can see from the image 6.6, the flow is usually divided into three parts:
- accelerating the flow to constant inlet velocity before the startup/entrance region
- subsequent acceleration of the flow to parabolic velocity profile in the entrance region
- Compensation of frictional forces over the entire length of the flow

In the hydrodynamic entrance region, the fluid velocity profile changes from initial profile at the entrance to an invariant form downstream. Therefore, it is important to calculate this entrance length to ensure that the length of the channel is longer than the diameter of the channel for the hagen poiseulle equations to hold true. For laminar flows this length is given by:

$$\frac{L_e}{D} = 0.0575Re \tag{6.18}$$

where $L_e$ is the entrance length, D is the diameter of the pipe and Re is the Reynolds number. With the given diameter of 200 $\mu$m and Re of 8.874 respectively (derived earlier), it is estimated that the total length of the channel should be greater than the entrance length of 0.1016 mm for the above relations to be valid. In the case in which this pressure drop due to acceleration to reach developed flow is quite low compared to the frictional work, in other words when the length of the channel is longer than the diameter of the pipe then the pressure drop is entirely due to frictional forces. This argument is corroborated by Akbari, in his paper [3] reported that for flows where $1 < Re < 35$, the pressure loss due to the developing region is less than 0.3 % compared to total measure pressure drop and hence can be neglected.

In this case, the pressure drop is simply the pressure gradient needed to be maintained between the inlet and outlet. It is very important to note though, that this is valid only in the case when there are no pressure losses due to bends, expansion and other minor effects.

Even though, the above equations are described for steady state and the analytical calculations followed in this chapter will assume steady state, Todd et al's paper [65] shed some light into the time scale to reach steady state. The linear unsteady term $\rho$ $\partial$u/$\partial$t in equation 6.10 sets the time scale required to establish steady flows. This is estimated by balancing the unsteady inertial force density with the viscous force density gives rise to equation

$$\tau \approx \frac{\rho(L_o)^2}{\eta} \tag{6.19}$$

This time required can be represented as the time required to diffuse unsteady flow over a distance $L_o$. These values are generally quite small, so for a 100 $\mu$m channel length, the pressure driven flows takes around 10 ms to reach steady state. This value sits right well with the time response requirement for this thesis.

### 6.4.3.2. Design Characterisation

Inherently, the flow needs to happen from inlet to outlet through an equivalent hydraulic resistance to obtain the required flow rate for the given pressure difference. This network of microchannels from inlet to outlet ports can readily be established using simple or very complex microfluidic network path. Broadly speaking, as the number of process to be performed by the device increases, the configuration of the fluidic channels becomes more complex. Due to which, precise control of fluid flow in each segment becomes challenging.

Some of the considerations before proceeding with analytical model are given below. The baseline design versions were presented in Chapter 5 and the considerations for the selected concept design was motivated. With that design concept in mind, further design considerations were made, which also led to further modifications. These are explained in this section, subsequently, the analytical model for it was developed.

- Once the initial design concept for the the valve seat was established, additional factors influencing the overall design were taken into consideration. Recognising that the valve packaging is crucial for the overall design, various elements were addressed. The domain D as illustrated in figure 6.1 also impacts the design of the valve seat.

  This will be summarised here, with detailed calculation in the holder design section 6.7. To mitigate the leakage and seal the fluid effectively, O-rings were inserted in the valve holder between the holder seat and valve seat.

  With the minimum O-ring size of cross section and internal diameter of 0.6mm, required gland width would be 2.10mm. The holder design includes four o-rings to ensure uniform sealing force over the valve seat. Therefore, the minimum clearance required between two gland width centres for the o-rings would be 3.20 mm as depicted in figure 6.7a, accommodating for manufacturing tolerances.

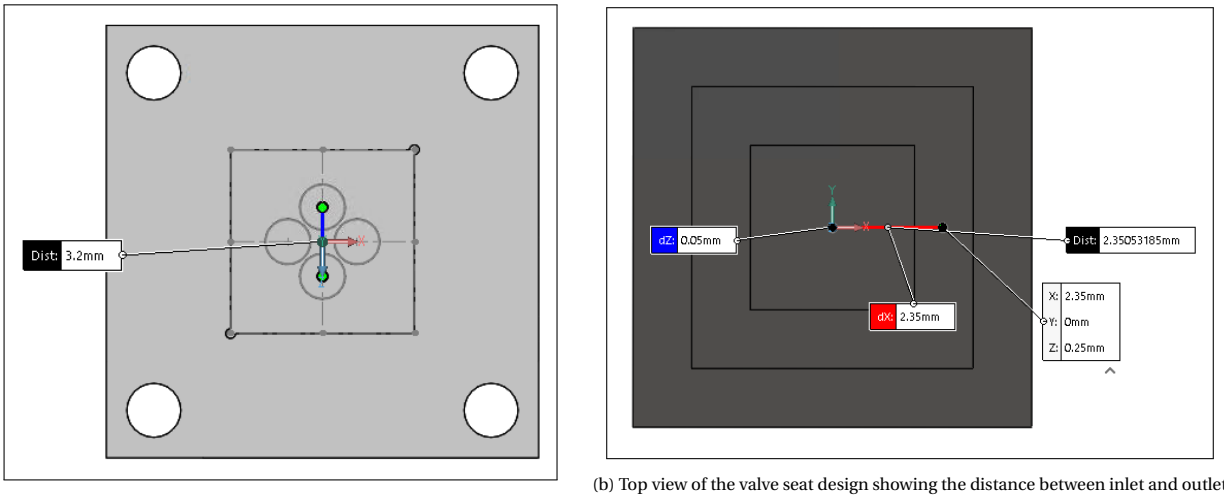


(a) Top view of the holder showing the o-ring seat design

(b) Top view of the valve seat design showing the distance between inlet and outlet orifice centres

Figure 6.7: 3rd Version of the design concept (not to scale)

This implies that the distance between the centre of the inlet and outlet orifice on the valve seat should atleast be 3.20mm. However, the baseline design, conceptualised with symmetry in mind, dictates a distance of 2.35mm between inlet and outlet. An alternative solution might involve adjusting the inlet and outlet placement to meet the required distance. However, maintaining symmetry and ensuring uniform load forces over the surfaces remained primary consideration.

This was supplemented by a design recommendation put forth by the author Fazal et al. in his microvalve design for gas flows [16]. They proposed incorporation of static regions of pressure drop along-

side variable resistance, to enhance flow controllability over a range of flows . Variable resistances refers to the resistance that can be altered by changing the plate deflection- Greater the deflection, lower is the resistance and vise versa. Conversely, static resistance denotes regions where the hydraulic resistance remains fixed for a given geometry and does not change during operation.

Hence, a segment of static resistance was introduced in the valve seat design as can be seen in figure 6.8, serving to also fulfill the holder consideration previously outlined. Following discussions with the process engineers at EKL about the necessary fabrication process for the design shown in figure 6.8, it was found that such a design would demand etching on both side of the silicon wafer, unlike design version 3. This would introduce complexities to the manufacturing process, leading to the suggestion to design a channel such that only side of the wafer required etching.

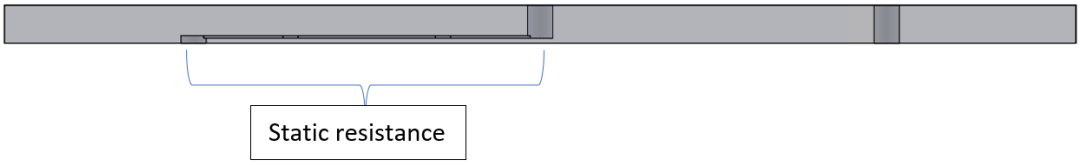


Figure 6.8: Side view of the modified valve seat design: Version 3a

Implementing the recommendation necessitated the addition of a third layer of the same thickness. While this design change would increase the overall size of the design by 300 microns, it still remained within the specified requirements (MIC-SYS-300), thus posing no issue at this stage. Therefore, the modified valve seat design design with the incorporation of the static channel is depicted in figure 6.9, while the overall valve seat design can be seen in figure 6.10.

Figure 6.9: Side view of the modified valve seat design: Version 3b

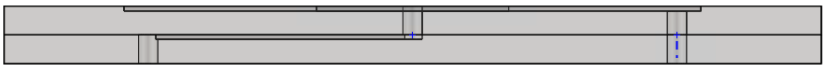

Figure 6.10: Side view of the modified valve seat design: Version 3c

- As mentioned in the Chapter 5, the valve seat depicted in figure 5.5a was designed such that only the inlet is completely blocked off by the plunger in closed state. The rationale behind this design was to was to minimise the wetted contact area and reduce the required seating forces to address the problem of stiction. It is a common problem in MEMS: When the structures are small, surface forces dominate causing the structures to stick together when the surfaces come in contact.
  One of the approaches to reduce this seating force was proposed by Eui Yang et al. in [75], which was to introduce narrow rings in the valve seat so as to reduce the fluid contact area, thereby reducing internal leakages. From literature, it was found that this design was presented for a flow rate of 52 sccm at an inlet pressure of 20 bar which is higher compared to the requirement set forth for this study. The suitability for this design feature for the current study's requirement was questionable. There was a speculation was that such a design might lead to water accumulation in the seat rings, with insufficient pressure to expel it. Hence, this design feature was not pursued further. Instead, minimizing the dimensions of the valve seat that is in contact with the plunger was considered in order to reduce the Van der waal forces while ensuring structural integrity.
- Design simplicity was a pivotal driver in the valve seat design to ensure that manufacturing complexity can be reduced. Therefore, wherever possible simple design features were implemented while meeting the requirements.

#### 6.4.3.3. Assumptions

- The flow is assumed to be laminar, incompressible and fully developed

- Viscosity of the fluid is considered to be constant throughout the channel
- Radial flow is assumed in the region between the valve seat and the membrane and existing flow model will be used to predict the pressure drop.
- Flow is modelled in a steady state domain and hence Poiseuille flow-profile is assumed over the full length of the flow path. From a preliminary transient study conducted in section 7.4, it was found that the response time of valve system was driven by the response time of the actuator itself and not the settling time of the fluid flow, which was found to be quite low.
- Inertia forces due to acceleration in the entrance region can be neglected compared to the frictional forces
- No slip boundary condition exists between the fluid and the wall
- The pressure drop due to connecting tubes: inlet and outlet manifolds in the valve holder is not considered.
- As mentioned earlier, the membrane(plunger) deflection constitutes as variable resistance. This will change based on the required deflection. In real scenario, the membrane plate would be deformed based on the actuator displacement. However, for the analytical model it is assumed the membrane once displaced remains parallel to the seat at a particular instant.

#### 6.4.3.4. Description of flow

From the design considerations discussed in the above sections, the concept design of the valve seat was further developed, which can be found in the figure 6.10. In this section, the analytical model will be developed for this design in order to properly size the flow path for the required performance requirements.

The cross-sectional view of the design is given by fig 6.11 in open closed condition. The diagram depicts the different domains of the valve design. Domain A represents the valve seat design, Domain B and Domain C represents the plunger and the piezo actuator respectively. Upon actuation by the actuator, the membrane is lifted up thus creating a open path and the fluid flows from inlet towards the outlet. The distance to which the membrane deflects is referred to as deflection.

The fluid first flows through a small channel of cylindrical cross-section (diameter = 200$\mu$m). After which, the fluid enters the series of rectangular channel. Next, the fluid flows through another cylindrical channel. The flow then deviates when the fluid hits the central boss of the top layer when it flows through the section created by deflection of the plunger away from the valve seat. Then, the fluid eventually flows through the outlet section (diameter = 200$\mu$m).

The flow in these regions can be characterised as follows:

- region (a) is the inlet flow in a cylindrical channel
- region (b) is the flow through the rectangular channel
- region (c) flow through the middle cylindrical channel
- region (d) flow causing to abrupt fluid flow deviation due by valve opening
- region (e) flow through the outlet cylindrical channel

When the valve is open, the valve boss causes the flow to occur into two sequential paths: 1) a restriction in the interior of the valve through the channels, 2) The restriction between the valve boss and the valve seat. Two main sources of pressure drop exist in systems. a) Friction loss and wall shear stress, b) Minor loss, caused by the changes in the geometry.

$$\Delta P = (\frac{f_D L}{D_H} + \sum K) \frac{\rho V^2}{2} \tag{6.20}$$

where, the first half of the equation is due to frictional losses and the summation of K denotes all the local losses due to bends, expansion or contraction etc. The pressure drop in laminar, viscous flow is caused by friction and minor losses owing to changes in the geometry. For fully-developed flow in channels, frictional

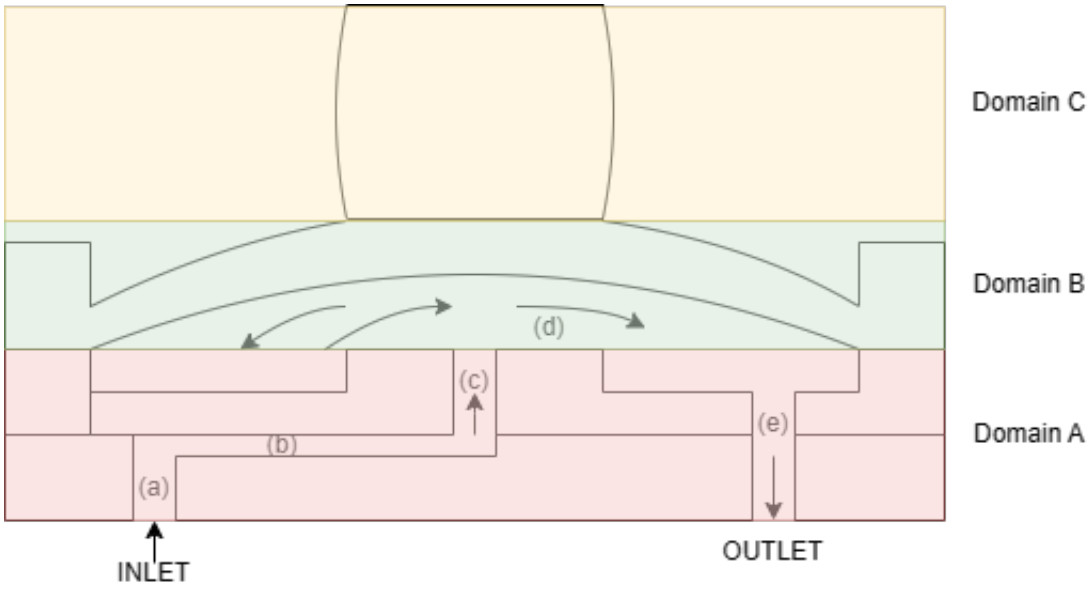


Figure 6.11: Description of flow in a valve structure in an open position

pressure drop can be calculated from Darcy-Weisbach equation which relates the flow characteristics, properties of the fluid, channel dimensions and friction factor. In this equation 6.20, $f_D$ is the Darcy friction factor, D and L are the channel diameter and length respectively. The friction factor is usually a function of Reynolds number and is expressed as,

$$f_D = \frac{C}{Re} \tag{6.21}$$

where friction coefficient (C) is geometry dependent and is equivalent to 64 for circular pipes in the laminar region. Whereas, for non-circular cross-sections, the hydraulic diameter can be related in terms of cross-sectional area and perimeter with the equation 6.3. The frictional coefficients for non-circular pipes lie between 48-96. Making this substitution in the Darcy Weisbach equation, the equation is equivalent to the Hagen Poiseuille equation 6.14. The loss coefficient in the minor loss is usually found from pressure drop experiments, and there are uncertainties associated based on the instrumentation and the technique used to determine it. The total pressure drop is directly proportional to uncertainty in estimating the friction factor and the minor loss coefficient. It is observed that for micro-tubes, this uncertainty in pressure drop measurements varies from 0.1% to 5% [30].

Researcher Akbari [3] mentioned that the minor pressure loss associated with inlet, exit connecting tubes and bend losses can be given by

$$\Delta P_m = \frac{\rho Q^2}{2A}[K_c + K_e + 2K_b(\frac{A}{A_l})^2] \tag{6.22}$$

where $K_c$ and $K_e$ are the loss coefficients of the channel and connecting tube. A and $A_l$ are the cross-section area of the channel and connecting tube. $K_b$ is the loss coefficient due to 90 degree bend and is recommended as 1.2.

Frictional pressure drop in the valve as given in figure 6.11 can be given as

$$\Delta P_f = (P_1 - P_2) - \cancelto{0}{\Delta P_{df}} - \Delta P_m - \Delta P_{un} \tag{6.23}$$

$\Delta P_f$ is the pressure drop due to frictional forces, ($P_1$ - $P_2$) is the pressure difference between inlet and outlet which is $5*10^5$ Pa, a requirement set forth for this research. $\Delta P_{df}$ is the pressure drop in the developing region. $\Delta P_m$ is the minor losses due to bends and other inlet and exit losses. $\Delta P_{un}$ is the uncertainty in pressure drop estimations, and is assumed to be a maximum of 5% of total pressure drop.
As long as the length of the circular pipe is greater than 0.1016 mm (from the calculation in section 6.4.3.1),

the pressure drop in the developing region will be negligible compared to the total pressure drop, and therefore it will not be accounted for going forward in this study instead a certain level of uncertainty is considered in the analytical model and a long pipe would be designed. Furthermore, since the Hagen Poiseuille equations are developed assuming perfectly straight channel with minimum bends or other losses, including an uncertainty would account for these slight deviations from the theoretical values.
Since the main driving factor is the frictional force to drive the flow, it is modelled as a series of rectangular, circular channels constituting as the static resistance: since the geometry does not change during operation and valving chamber constituting as the variable resistance: which is governed by the deflection.

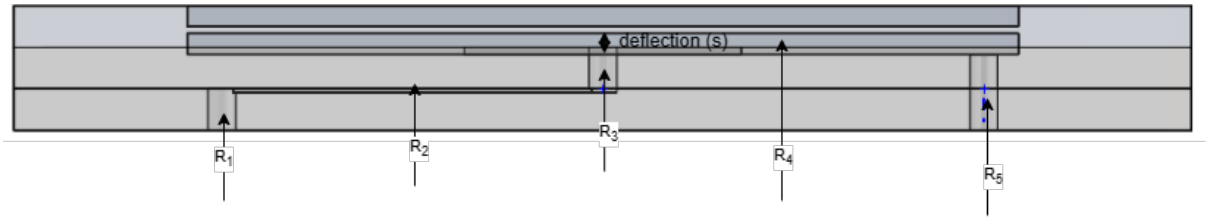


Figure 6.12: Side view of the hydraulic system network showing the different resistance constituting the flow path
R1,R2,R3-> denotes the hydraulic resistance in the circular pipe. R2->denotes the hydraulic resistance in rectangular channel.
R3->denotes the hydraulic resistance in valving chamber Deflection (s) is the gap height between the valve seat and membrane in open state

Reynolds's number and length to hydraulic diameter ratio was estimated for each segment of the design, and was found to be in the laminar region throughout the flow path. Detailed calculation can be found in Appendix A **??**. The observed values for the different geometries align well with those reported in the literature for different designs [17]. As described earlier, when the flow is predominately viscous, the lumped model can be applied. In such case, the different resistance in the flow path can be added up akin to an electric circuit. As can be seen in the figure 6.12, the resistances are in static and can be added up. $R_1$,$R_2$,$R_3$,$R_5$ constitutes the static resistance ($R_s$) whereas the $R_4$ represented the variable resistance ($R_{var}$). The total hydraulic resistance can be given by:

$$R_{total} = R_s + R_{var} \tag{6.24}$$

The volumetric flow rate Q can be calculated as [16]:

$$Q = \frac{\Delta P_f}{R_{total}} \tag{6.25}$$

To derive the characteristics of the variable resistance, an existing flow model is used, which considers radial flow through the orifice. Flow model between two parallel discs with inner radius $r_0$ and $r_1$ at a vertical distance of h, is used as a reference in order to evaluate this resistance [28] and is depicted in figure 6.13. This resistance is calculated analytically with the equation given below:

$$R_{var} = \frac{6\mu \ln \frac{r_0}{r_1}}{\pi s^3} \tag{6.26}$$

where, $r_1$ is the inner radius and $r_0$ is the outer radius and s is the height of the valve chamber. A detailed derivation of this formula can be found in [14]. In this model, the gap height 's', which control the fluid flow, is assumed to be parallel to the valve seat. However, in real world scenario, the structural deformation of the valving membrane dictates the gap height. To achieve a more accurate control over fluid volume and the required deflection for a desired mass flow rate, a fluid-structure interaction simulation needs to be performed. The above formulae is valid for small Reynold's number and Newtonian fluids. The analytical relation uses circular disc as reference instead of square plate geometry. This premise might lead to deviations from the numerical results because the mass flow will also depend non-linearly on the surrounding conditions such as fluid velocities, wall distances, fluid viscosity and the fluid control volume but in simplistic approach it is deemed to be sufficient to evaluate the flow rate for the micro-channel design. This is because the model tends to be pessimistic, yielding results higher than reality. In order words, the model might over-estimate the required deflection.

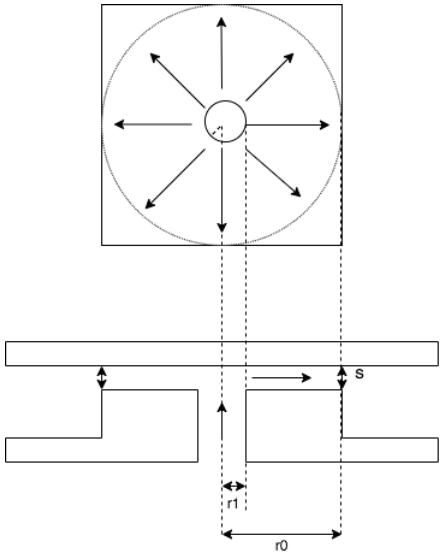


Figure 6.13: Analytical depiction of the radial flow: Variable resistance [28]

For the static resistance, there are existing flow models for the designed geometries. The hydraulic resistance for circular and rectangular channels is given by equations 6.15 and 6.16 respectively. From the equation 6.25, it is evident that hydraulic resistance must be designed to meet the requirement: MIC-PERF-100. The variable resistance is dependent to the cube of the deflection, so, higher the deflection, lower is the resistance and vise versa. The deflection is driven by the actuator specifications, this means, higher the variable resistance, lower will be the required deflection, which in turn would mean small actuator footprint. This is desirable to ensure the volume of the device is as small as possible. Hence, the strategy of increasing variable resistance and reducing static resistance was employed. However, this would necessitate larger channel dimensions, which again is not most desirable. As static resistance decreases, the flow rate becomes predominantly governed by variable resistance. Consequently, altering the channel dimensions has minimal effect on the flow rate.

Hence, dimensions of the static resistance were optimised with the objective of minimising dimensions while maintaining manufacturability. The flow field in rectangular channel is more complicated than the circular channel, because the flow fields depend on cross-sections coordinates and is a function of aspect ratio. Aspect ratio 'r' of the structure is defined as the ratio of height over width is an important consideration in MEMS fabrication. The higher the aspect ratio, the more challenging it is to manufacture the channels. The mechanical stability during manufacturing is compromised for channels with high aspect ratio, usually higher than 0.5. Since the number of methods for creating a very thin and deep channel is limited, the dimensioning of the channels was chosen such that the aspect ratio of the structure is low, with aspect ratio of 0.2 to also allow for tolerances during fabrication. Furthermore, it was found that the friction factor increased with increasing H/W and hydraulic diameter [18]. The rectangular channel $R_2$ should be designed long enough so that fully developed flow is dominant and non-linear effects due to bends or other minor losses can be avoided.

With the above points in mind, the hydraulic resistances were designed. The dimensions of each of these can be found in table 6.1. One of the design considerations involved deciding between straight path or zigzag configuration for the rectangular channel, as depicted in figure 6.14. It can be observed that for the small deflections the two cases align with each other but as the gap height increases, the two start to diverge from each other. This is expected to happen, in case of zigzag channel path, the deflection value changes to the power of cube, additionally the bends add more losses and the channel length is higher. Overall fluidic resistance increases thereby decreased mass flow rate compared to straight path for the same deflection. For instance, at a deflection of 5 micron, flow rate close to 30 g/hr can be obtained with a straight channel compared to a channel with more bends. The design is dictated by the specifications required, as can be seen from the figure, even though for a mass flow requirement of 5 g/hr both of the designs would require the valving chamber close to 2.4 micron. The straight channel offers lower static hydraulic resistance compared to the zigzag path, aligning with the aforementioned approach. Thus, to avoid flow irregularities and ensure fully developed flow can be achieved, a straight path was decided upon.

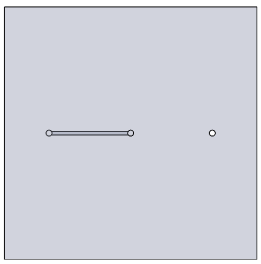

(a) Top view of the plate with straight rectangular channel

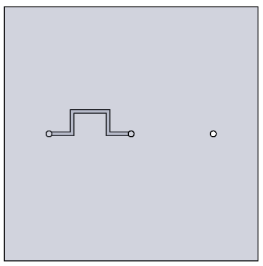

(b) Top view of the plate with zigzag rectangular channel

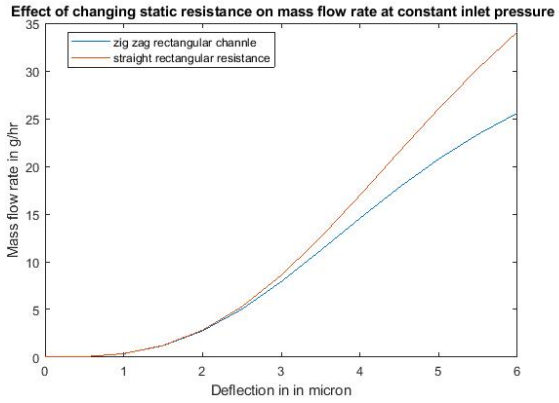


(c) Variation of deflection vs mass flow rate for the two different channel configurations shown above (same aspect ratio). Note: Deflection refers to the distance between the valve seat and plunger in open state.

Figure 6.14: Effect on the mass flow rate for different channel geometries

From the Matlab script developed which can be found in Appendix A **??**, it was found that the pressure drop in the static region was only around 5% compared to the total pressure drop. Again, changing the dimensions of the static resistance region would not have a much impact on the flow rate for small deflections.

It has been previously emphasized in the design considerations the importance of incorporating static resistance into the flow network design. This is further corroborated by Figure 6.15, where the flow rate sharply increases with deflection. This indicates that small changes in deflection would result in significant changes in the flow rate, which is not ideal for applications requiring precise propellant control.

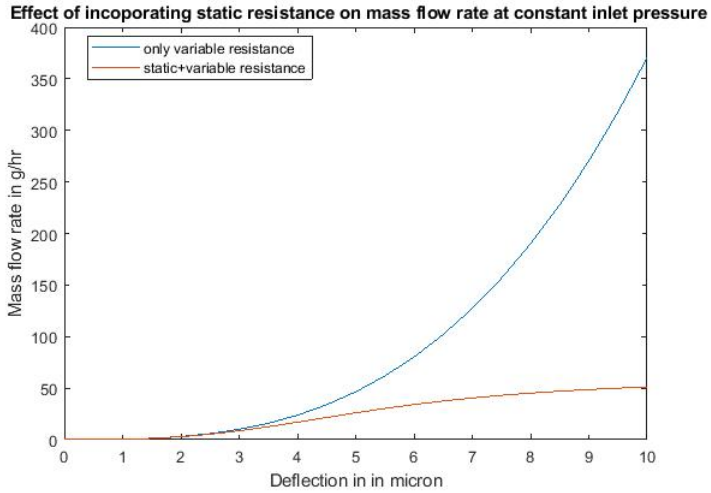


Figure 6.15: Variation of deflection vs mass flow rate: with and without static resistance Note: Deflection refers to the distance between the valve seat and plunger in open state.

From the figure 6.15, it is evident that for deflection <3.5 micron, the two cases exhibit similar behaviour, however as the deflection increases, the mass flow rises steeply for the case with no static resistance. By in-

creasing static resistance while proportionally reducing variable resistance, we can achieve more linear flow control with minor changes in deflection. Therefore, although both designs fulfill the requirements outlined for this research, the latter offers linearity across a broader range of flow rates, making it suitable for applications with higher flow rate demands in the future. However, opting for the latter design results in a 300-micron increase in the overall height of the valve chip, albeit still within the specified requirement.

It can be seen from the graph, that for smaller deflections static resistance controls the flow whereas for larger openings the variable resistance dominates.

| **Resistance** | **Resistance value ( Pa s m-3)** | **Region** | **Channel type** | **Dimensions( micron)** |
|---|---|---|---|---|
| R1 | 6.7991e9 | a | Cylindrical | Length- 300<br>Diameter-200 |
| R2 | 1.6981e13 | b | Rectangular | length= 2590<br>width=120<br>height=25 |
| R3 | 7.4790e9 | c | Cylindrical | length=330<br>diameter=200 |
| R4 | 3.2168e14 | d | Variable | r0=1500<br>r1=100<br>s=2.3 |
| R5 | 1.2465e10 | e | Cylindrical | length=550<br>diameter=200 |
| **Total Resistance** | 3.3869e14 Pa s m-3 | | | |

Table 6.1: Design parameters for the fluid path

The minor pressure loss in the system is around 5.0% (including the uncertainty assumed) and has negligible contribution. Since the design of the internal flow channels is fixed for a given geometry, the only variable controlling the mass flow rate is the variable resistance, which is dependent on the gap height/deflection. As can be seen from the table 6.1, the deflection required to achieve the desired mass flow rate is around 2.3$\mu$m. This lays the requirement for the selection of piezo actuator, which should be able to provide minimum stroke of 2.3$\mu$m.

## 6.5. PART B: Plunger Design

Determining the forces acting on the membrane is crucial in designing a valve membrane. To ensure sophisticated pulsating flow, the forces acting on the membrane should be known so that the valve can work as desired with minimum leakage and the careful design selection of the driving actuator can be made. It is important to ensure that the membrane is able to withstand the stress experienced and is within the yield stress of the material properties.
The discussion in this section is driven by these key requirements:

- MIC-SYST-400: The valve design shall be able to withstand a Maximum operating Pressure of 5 bar
- MIC-PERF-300: The maximum leak rate shall be <$10^{-5}$ scc/s at maximum operating pressure
- MIC-FUN-100: The system shall supply no propellant to the thruster in idle mode or when no power is supplied to the system
- MIC-SYST-300: The microvalve chip size (without the packaging) shall be within 10mm x 10mm x 1mm
- MIC-SYST-200: The total size of the propulsion system shall be within 42mm x 42mm x 30mm (including all the components)

### 6.5.1. Design Considerations

From the concept selection in Section 4.2, it was established that an out-of-plane design configuration is better suited for leakage minimisation compared to in plane designs. From the trade-off study in section 4.2.1, it was concluded that a vertically translating plate made of hard material like silicon or thin membrane

using soft elastomer like silicone, PDMS would be suitable candidates. Going forward, soft valve plate were not pursued further due to following reasons: permeability issues reported in literature, increased stroke requirement from the actuator owing to loss of stroke when conforming to the valve seat, stiction problems, poor mechanical robustness and elaborate fabrication procedures. Therefore, hard plate plunger made of primarily silicon substrate was considered and steps were made in the design to overcome some of their drawbacks as mentioned in 3.3.1.1.

For this, different designs of out-of plane configurations for the vertically translating plate were explored before settling on the current design. Summary of these plunger design versions is motivated in 5.2. The design considerations made for the design of the plunger pursued further are populated below.

- As mentioned in section 6.3, The initial dimensions for the size of the plunger are set at 8.5mm x 8.5 mm. No attempt has been made to optimize the design in this study, as the current design meets the specified requirements.
- As explained in Chapter 5, Closed volume design concept for the valve is crucial for low leakage in case of normally closed valve at off state. To accommodate this, similar to the valve seat design, a clamped plate structure is chosen for the plunger. Since piezo electrodes are sensitive to humidity, such a design was also to ensure the piezo electrodes are away from the contact of water to avoid short circuit.

  Therefore, the baseline design of the plunger developed in Chapter 5 as illustrated in figure 5.5b was considered in this section for further analysis.

#### 6.5.1.1. Force analysis

In this section, a simplified analytical strategy for the valve membrane design will be developed and the motivation behind those choices will be explained, ultimately moving closer towards a valve design choice. Here, the term "membrane" refers to the plate with reduced thickness, and moving forward, it will be used in this context.
The valve plunger (domain B) can be thought of as a spring. In a normally closed valve, usually only the restoring force of the plunger will close the valve. In other words, this plunger stiffness should be large enough to resist the inlet pressure whereas the actuator force is responsible for the valve actuation which also acts against the plunger restoring force (spring force) in actuated state.
There are two forces that can be characterised to be acting on the valve structure.

– Fluid forces acting on the structure, which will be denoted as $F_{f-s}$

– Structure forces acting on the fluid, which will be denoted as $F_{s-f}$

The forces are calculated for three states. It should be noted that this formulation accounts for steady-state cases.

- off state 1: This is the condition in which the valve will be in un-powered state. This means, it will be closed until actuated, the leakage should ideally be zero. Estimating leakage analytically is difficult as it depends a lot on manufacturing process and material morphology and this requires testing.
- on state: This is the state when the valve will be actuated and the fluid will flow. The piezo will actuate, lifting the membrane up from the inlet, thus creating a flow passage. Important to note is that the on state here is referred to the equilibrium condition after required deflection is achieved.
- off state 2: This is the state when the valve will go to off state (closed condition) from on state, reaching off state 1. When the flow is abrupted to close the valve, the forces acting at the transition state from "on state" to "off state 2" will be different. Hence, it is important to also account for it, so that the membrane can be designed to minimise leakage in both off states and handle the stresses induced in both cases.

The different states and the forces acting on the membrane during these state can be seen in figures 6.17a, 6.17b.

CASE 1- **Off State 1: Unpowered**:
Neglecting the small pressure drop along the channel (makes up only 5% of total pressure drop) and assuming fluid pressure acting on the membrane(in closed state) as 5 bar. The wetted area of the plunger is simply the area in contact with the fluid which is the projection of the inlet area on the membrane, equivalent

to $\pi$ $r^2$. However, this inlet area assumption is an ideal case scenario because in practice, due to fabrication defects, if there exists a physical separation (in the direction of actuator travel) between plunger and plane of inlet on the valve seat, the wetted area would then include the entire membrane area. But the pressure acting on the membrane in this case would not be 5 bar, rather a pressure drop would be experienced owing to the frictional loss in the channel and volumetric change due to gap height.

Considering a constant fluid pressure, reducing the area of the plunger in contact with the fluid, reduces the relative fluid force acting on the valve structure. This drives the design choice towards small membrane dimensions.
Another design criteria for the plunger design is the required seating force, defined as the force required to keep the valve closed against a certain fluid pressure. For normally closed valve, this is predominately driven by the stiffness of the plunger structure. If no actuator is considered, The plunger stiffness is the only contributing force to keep the valve closed, which depends on the dimensions and the thickness of the membrane itself. For a flat plate with clamped edges and constant thickness with uniform load over the entire plate, the stiffness of the plate is given by equation [79]:

$$k_m = \frac{Et^3}{\alpha a^2} \tag{6.27}$$

where, $k_m$ is the stiffness of the plate, $\alpha$ is 0.0138, a is the side length of the plate, E: Young's modulus, t: plate thickness, $s_{max}$ is the maximum deflection of the plate at the center.

It can be seen from the above equation, the stiffness of the plunger increases as the length decreases and the thickness increases.

The Requirement MIC-SYST-200 is steering the design towards reduced overall footprint size. Simultaneously, MIC-PERF-300 promotes a design with smaller length but bigger thickness. Balancing the two requirements is optimal in choosing a suitable plunger dimension for optimising membrane stiffness and thus the required seating force. However, it's important to ensure that the stiffness of the membrane isn't excessively high. This is because a higher stiffness would necessitate a larger force to pull it away to open the valve, potentially resulting in a larger actuator.

Considering, free body force diagram in figure 6.17a,

$$F_1 = (K_m + K_P)s_1 + P_s \tag{6.28}$$

where $F_1$ refers to the fluid force acting on the membrane with area equivalent to the inlet area. $s_1$ denotes the displacement between the valve seat and membrane caused by the fluid force, $k_m$ is the stiffness characteristic of the membrane and $k_s$ is the stiffness characteristic of the piezo actuator. $P_s$ represents the pre-stress force. The rationale for this pre-stress will be further explained. As the specifications required for the piezo actuator will be further developed in this section,given that they are currently undetermined, we will not consider the piezo contribution at this stage.

From the above equation, in order to achieve zero deflection, albeit, no leakage, the stiffness of the plate should be infinite, which is impossible. Furthermore, in real case scenario due to fabrication processes, there might be further introduction of separation between the valve seat and the valve plunger due to surface roughness of the solid bodies. Additionally, the material properties of the surfaces further add to the cause. For this case, the wetted area exposed to fluid would increase. Even though it is not desirable, it is unavoidable, hence it is important to design a system that would improve the leakage ratio. It is difficult to accurately quantity the leak rate due to these manufacturing induced imperfections, using an analytical model. The approach taken by Claudia et al. in [14] was to study this contact problem of two solids with surface roughness squeezed against each other, leading to a separation given by equation 6.29.

$$u(p_{\text{contact}}) = \gamma\alpha^{-1}h_{rms}\log(\beta\epsilon q_0 h_{rms}\frac{E^*}{p_{\text{contact}}}) \tag{6.29}$$

Assuming perfectly elastic deformation, $\alpha$ and $\beta$ are surface roughness constants, $h_{rms}$ is the root-mean-square of surface roughness, $\epsilon$ is the power spectrum constant of surface roughness, whereas $q_0$ is the lower limit of cut-off wave surface vectors. $E^*$ is the plain-strain modulus and $p_{contact}$ is the contact pressure between valve seat and diaphragm. However, for this approach the surface morphology must be known and also greatly depends on the young's modulus of the material.

A major drawback of normally closed microvalve, is the leakage issue. Some ways to enhance sealing is using a piezoelectric actuator that exhibits high forces so that the contact pressure on the valve seat exerted by the diaphragm can be increased. But the force applied by the piezo is zero when unpowered, therefore the only contact pressure is the spring force exerted by the plunger diaphragm and piezo assembly, which can be increased by increasing the thickness or decreasing the membrane length as seen from equation 6.27.
Another option, mentioned in literature, is to use coatings of parylene-C to improve the surface properties in order to increase the sealing behaviour [14].

The the amount of leakage would be dependent on how much the membrane is deformed, it could be speculated that the membrane might exhibit a very small bow, leading to very small leakage flow. In ideal case, in closed valve scenario the wetted area is equivalent to $\pi$ $r^2$, then the fluid force acting on the membrane is 16 mN. Then from equation 6.30, the maximum deflection at the centre of the membrane can be estimated.

$$s_{max} = \frac{\alpha_2 F_1 a^2}{E t^3} \tag{6.30}$$

where, $\alpha$ is 0.0611 in case load is uniform over a concentric circle of radius $r_o$, a is the side length of the plate, E: Young's modulus, t: plate thickness, $F_1$ is the fluid force acting on the circle, $s_{max}$ is the maximum centre deflection.

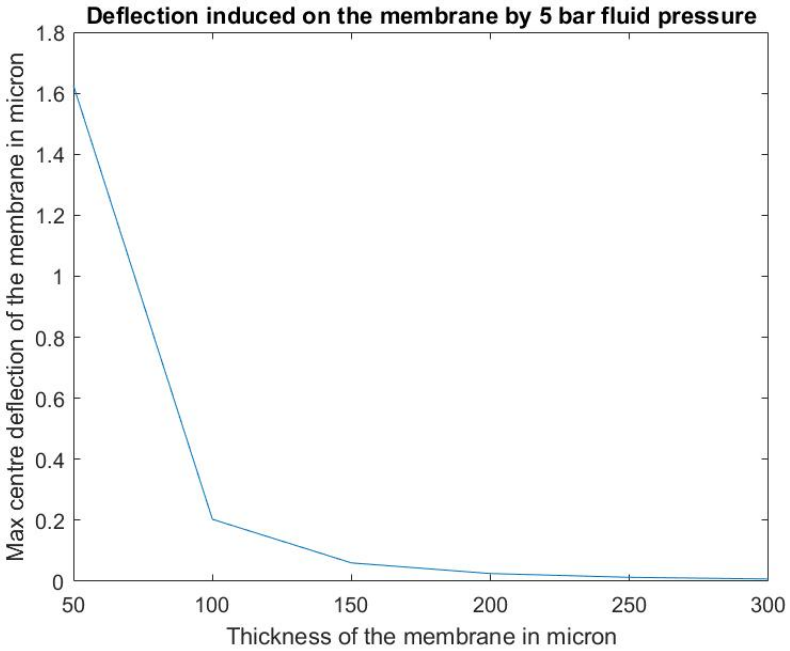


Figure 6.16: Estimation of the induced gap height between the valve seat and valve membrane in the valve in closed condition. The fluid force is supposedly acting on the membrane uniformly over a circle of radius 100 micron.

From the above graph, it is evident that a thicker plate would result in smaller deflection. The choice of membrane thickness will tend towards a thicker plunger. For instance, with a membrane thickness 200 micron, the membrane deflection is less than 30 nm. With such minimal deflection, one can estimate the theoretical mass flow rate using the analytical model presented in valve seat design section. It was determined that the estimated mass flow rate is on the order of $10^{-6}$ g/hr. These values are extremely low, indicating that the system can be considered as leak tight.
The scenario described above considers an ideal situation, but manufacturing processes may introduce additional cavities, leading to increased separation between the two surfaces and consequently higher leakage rates. Achieving zero leakage is practically impossible without any stopping force. The contact between the two surfaces depends on the pressure that squeezes them together. When the applied contact pressure p is increased, the average surface separation(u) is decreased, so the pressure p is again a function of u. To ensure blocking of the fluid, the force exerted by the plunger system must be larger than the force exerted to it by the pressure of the fluid. This can be achieved by applying a pre-stress force denoted as $P_s$, which is applied to the actuator during mounting to the membrane. This pre-stress force can be applied either by applying some

reverse voltage or mechanically. However, due to the MIC-FUN-100 requirement, applying power in the off state is not possible

So, in worst case scenario, the pre-stress force denoted by $P_s$ in figure 6.17a should at most be equal to the fluid force acting on the membrane. Therefore, as mentioned above the pre-stress required would than be around 16mN which is equal to the fluid force acting on the membrane. Now, assuming manufacturing errors and rough surfaces causes 10% deflection of the required stroke, then from the equation 6.27, then the required pre-stress would be around 1N. It can be observed that the required pre-stress in case 2 is higher than in the earlier case. This is because, in this scenario, it is assumed that due to manufacturing defects, the gap created would increase the wetted area. Consequently, the fluid pressure will act on the entire surface of the membrane as opposed to just the inlet projection in the earlier scenario. These calculations has been derived from the analytical model for the valve seat design and can be found in Appendix .

This is the upper limit value of the force required to close the valve in the closed case because the piezo and membrane stiffness will in effective reduce the required pre-stress force. Since piezo-stack actuators are characterised by very high stiffness values of up to several hundred newtons per millimetre. The height to which the piezo would be required to press against the membrane would be very small for the required pre-stress force. This value can also be tuned accordingly when bonding the piezo to the membrane but needs to be carried out precisely to not damage the structure itself.

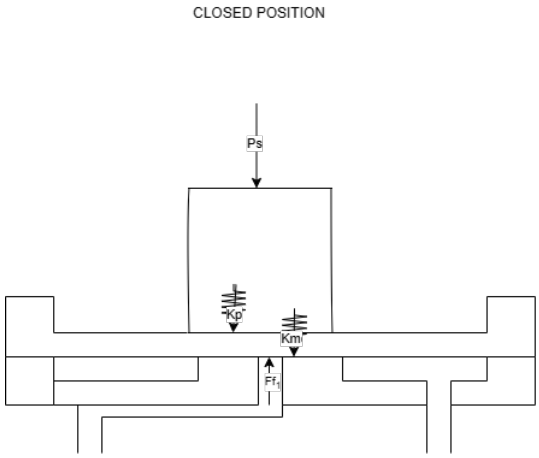


(a) Normally closed valve configuration in off state

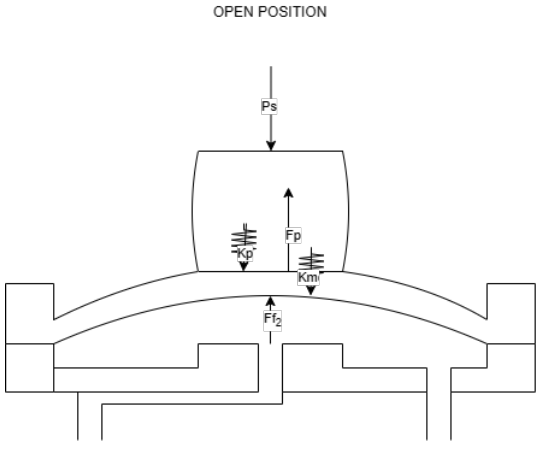


(b) Valve configuration in on state

Figure 6.17: Functions of valve spring and force balance.The figures demonstrate the section view of the valve states (not drawn to scale): $F_f$ is the fluid force acting on the wetted area of the membrane, $F_p$ indicate the piezo force to lift the membrane, $K_p$ denotes the piezo actuator stiffness, $K_m$ denotes the membrane stiffness

CASE 2-**On State: Powered**

From force balance:

$$F_p = (K_m + K_p)s_2 + P_s - Ff_2 \tag{6.31}$$

$F_p$ denotes the force exerted by the actuator to deflect the membrane. $Ff_2$ represents the fluid force acting on the membrane when it is open. $P_s$ is the acting pre-stress force applied during closed state. The open state of the valve is a transient state, with the forces acting on the membrane changing with time from zero deflection (unpowered) to a certain deflection. The equation 6.31 describes the force required by the actuator to deflect the membrane. As discussed in preceding sections, the fluid force acting on the membrane is a function of deflection. As the deflection increases, fluid force acting on the membrane decreases. This is because greater pressure drop is experienced by the fluid with increased deflection, resulting in a reduction of pressure acting on the membrane and consequently reducing the force. Furthermore, this fluidic pressure might not change uniformly across the entire membrane surface and must be decomposed into other lateral components.

Taking into account the design of internal channels, the fluid pressure acting on the membrane can be computed for a deflection (s2) of 2.3 $\mu$m (as obtained from Table 6.1). With P$i$ set at 5 bar, this can be calculated using Equation 6.32.

$$(P_i - P_f) = (R_1 + R_2 + R_3 + R_4)\frac{\dot{m}}{\rho} \tag{6.32}$$

The fluid force would then be the pressure acting on the entire cross-section of the membrane. One can see from the force balance equation, the fluid force aids in further opening the valve. So if we neglect the fluid force, we get the over-estimated force required to deflect the membrane. One can observe from the equation that the fluid force contributes to further opening the valve. Neglecting the fluid force leads to an overestimation of the force required to deflect the membrane. From Equation 6.27, the force required to pull the membrane up by 2.3 microns (as calculated in Table 6.1) when it acts over a central square/rectangular area can be calculated. This area will depend on the cross-section of the piezo actuator. It should be noted that the force estimation from this equation assumes maximum deflection at the center. However, in the case of a piezo actuator, the entire central area of the membrane bonded to the actuator would deflect parallel to the valve seat. Therefore, force required in the latter case would be higher than that estimated using the simplified bending deformation equations.

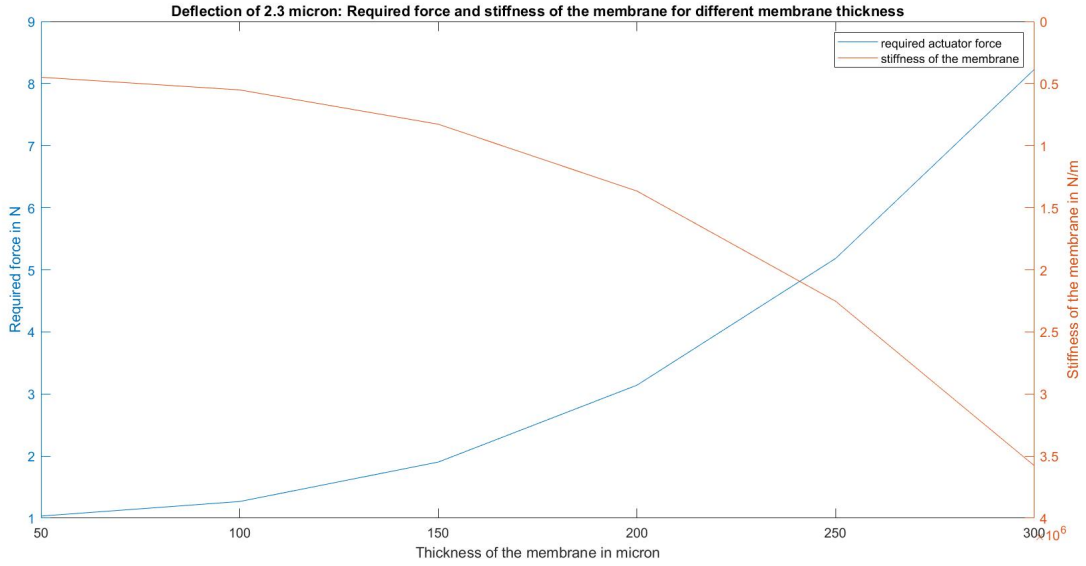


Figure 6.18: Required actuator force to deflect the centre of the membrane by 2.3 micron. Input parameters and calculations can be found in Appendix

From the graph above, it's evident that a stiff membrane would be the preferred choice to ensure high seating forces, thus driving the choice towards greater thickness. However, this would also increase the force

required to deflect the membrane for valve actuation, necessitating a larger actuator. Therefore, as a trade-off, a thickness of 200 microns for the membrane was chosen.

It is interesting to note though that computation of these fluid forces becomes important when the requirements for accurate and precise proportional flow control. For missions with stricter mission requirements, it becomes necessary to have a feedback loop in the design such that based on the fluid forces, the deflection of the membrane due to the piezo can be adjusted. This can be done by making use of mass flow sensors and having a robust control system design in the entire propulsion system design, so that the mass flow rate can be regulated to the desired deflection by regulating the voltage supplied to the actuator.

CASE 3- **Off State 2: Unpowered** As mentioned earlier, this scenario is a juxtaposition of Case 1, where the membrane had to shut against the fluid forces acting on the entire membrane. In Case 1, the valve had to shut against the assumed pressure of 5 bar on the valve seat inlet, neglecting the pressure drop in the static region. However, in Case 2, there's a lower pressure acting on the membrane over a wider membrane cross-section. Therefore, the pre-stress force should also be accounted for in this case.

From force balance:

$$P_s = Ff_2 + F_p - (K_m + K_p)s_2 \tag{6.33}$$

In closed condition, $F_p$ would be zero, since no actuator force would be applied. Furthermore, neglecting the stiffness of the piezo, the worst-case pre-stress force required would be equal to the fluid pressure acting on the membrane at the deflection when the membrane is opened. Again, the fluid force can be computed from equation 6.32. This pre-stress was calculated to be around 0.9N, again, the calculations can be found in the appendix .

Nonetheless, this pre-tension needs to adjusted carefully to ensure not enough stress is being applied on the membrane to break it, neither it is less as to allow leakage. This needs to be verified experimentally, by doing a flow test in off-state and measuring the flow rate and the equivalent deflection.

In summary, the above explained scenarios are geometrical simplifications which accounts for worst-case scenario estimation of different design aspects. Estimations due to Possible manufacturing-induced imperfections are also accounted in the design phase and hereof designing to mitigate potential issues in its reliability in space applications.

## 6.6. PART C: Piezo Actuator

The discussion in this section is driven by these requirements

- MIC-SYST-100: The total mass of the valve+holder shall not be higher than 5g
- MIC-SYST-200: The total size of the propulsion system shall be within 42 mm x 42 mm x 30mm
- MIC-SYST-500: The peak consumption of the valve shall not be higher than 4W
- MIC-SYST-600: The system shall be able to operate on a single unregulated supply bus voltage of 3[VDC] to 4.1[VDC].
- MIC-PERF-200: The response time of the system shall be between 0.3ms-8.3ms

The preceding sections outlined the specifications for the piezo actuator, including the necessary deflection and force requirements. Now, we will delve into the selection process for the actuator. This study focuses solely on choosing a commercial Off-The-Shelf (COTS) piezo actuator. The actual design of the piezo itself falls outside the scope of this study.

The operation of the valve is driven by the utilisation of the indirect piezoelectric effect, in which physical displacement is produced as a result of applied electric field as can be seen in figure 6.19. Piezoelectric actuators are fabricated from materials exhibiting piezoelectric effect. Most common piezoelectric ceramics include lead titanate and lead zirconate which are identified as PZT.

Piezoelectricity can be described as a linear interaction between mechanical stress and electric states given by:

$$D_k = d_{kij}T_{ij} \tag{6.34}$$

$$S_{ij} = d_{kij}Ek \tag{6.35}$$

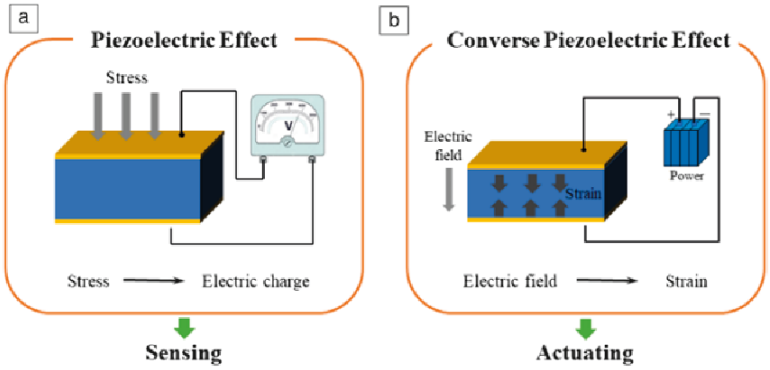


Figure 6.19: (a) Direct piezoelectric effect provides electric change when mechanical stress is applied, whereas (b) converse piezoelectric effect is the situation where strain is developed upon application of an electric field [59]

where $D_k$ is the electric displacement, E is the electric field component. S is the strain component, T is the stress component and d is the piezoelectric charge constant. A material can be transformed into a piezoelectric material if it is subjected to strong electric field along a chosen axis, this is known as poling. The influence of the field will change the material along the poling axis. Piezoelectric ceramic is a anisotropic material, therefore the direction of applied electric field affects the induced strain. The figure below, the direction of forces that can affect the piezoelectric element. In most cases, the positive polarization of the piezo is usually made to align with the z axis.

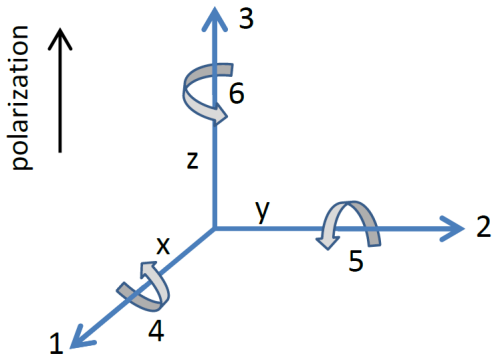


Figure 6.20: Direction of forces affecting the piezoelectric element

However, in practise, two main strain modes, $d_{31}$ and $d_{33}$. d is an important indicator of a material's suitability for strain-dependent applications.
$d_{33}$ - denotes induced strain in direction 3 per unit electric field applied in direction 3.
$d_{31}$ - denotes induced strain in direction 1 per unit electric field applied in direction 3.
This can be visualised in figure 6.21 for a rectangular block

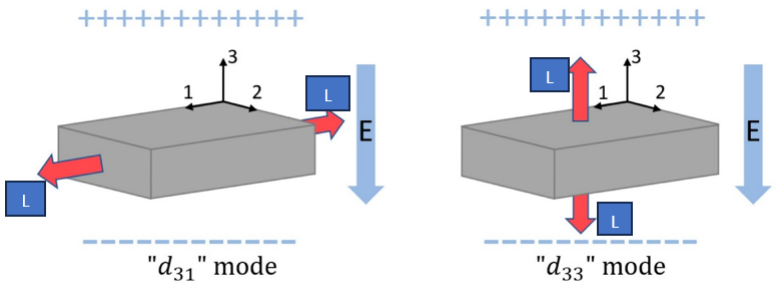


Figure 6.21: Visualisation of d33 and d31 mode for piezo material operations

Finding an actuator that meets the design requirements and can work in harmony with the design is crucial for the overall working and to meet performances.

The valve operates on the following principle: when the actuator is not powered, the microvalve remains closed, preventing any fluid flow. Upon activation from the actuator, it pulls the membrane away, thus creating a passage for fluid flow. As mentioned in the previous section, the top surface of the piezo should be pre-loaded to ensure the valve is closed when not powered. On the other hand, the bottom face of the actuator is bonded to the membrane which when contracts exerts a pulling force on the membrane.

As described in the section 6.5, the main forces involved in a valve system are:

**Fluid force on the membrane**: The fluid force acting on the bottom face of the membrane generates a pressure distribution across the membrane. This pressure distribution results in a force that tries to push the membrane upwards

**Lifting actuator forces due to piezo contraction**: As the piezo actuator will contract due to an applied voltage, it will generate a force that acts to lift the membrane attached to the boss. This lifting force is the direct result of the contraction of the piezo material

**Membrane stiffness**: The stiffness of the membrane would act as a resistance to the displacement. When the force is applied to deform the membrane, the stiffness of the membrane resists that deformation and generates a restorative force opposing the deformation.

Note: Most of the actuator companies specify the blocking force in their data-sheet. This refers to the maximum force that the actuator can overcome. Blocking force is the opposing force that acts against the deformation of the piezoelectric actuator. In the open state, the actuator needs to overcome the mechanical loads in the system or any resistance that the actuator encounters as it tries to move. The fluid force will aid in the opening of the membrane. Whereas, when the actuator is trying to close the membrane, the actuator will also have to overcome the fluid force acting.

Referring to the data presented in Table 6.1, it is crucial to identify a piezo actuator capable of delivering a minimum stroke of 2.3 microns. Another vital aspect in selecting the piezo is its ability to generate sufficient force, surpassing the forces exerted upon it, to ensure proper system functionality. In the preceding section, the pessimistic force value necessary to displace the membrane and open the valve was determined through analytical derivation, neglecting fluid forces acting on the membrane. From the figure 6.18, it was established that for a membrane displacement of 2.3 microns, an actuator force of approximately 3N was required. However, it's important to note that this force calculation only accounted for maximum deflection at the center of the membrane, which may not accurately represent real-case scenario. In reality, the entire central area of the membrane would deform due to the piezo, with maximal deformation decreasing towards the frame area. These actual forces are likely to exceed the analytical estimates significantly.

These forces were analyzed through numerical structural simulations detailed in Section 7.3. By examining the reaction force at the displacement boundary face, the necessary force to lift the membrane to the desired position was determined. The chart below illustrates the relationship between required force and displacement, aiding in understanding the force variation.

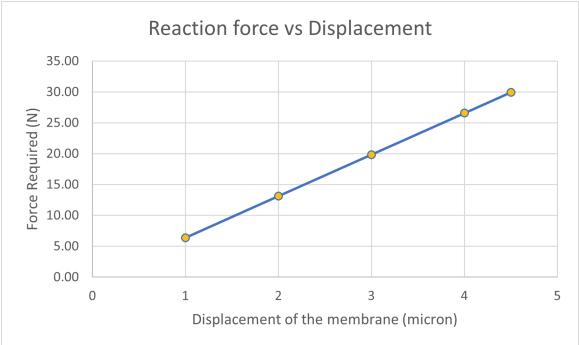


Figure 6.22: Required force to be applied on the membrane to open the valve. Displacement refers to the gap height between the valve seat and plunger

From the above figure, it can be seen a force of around 15N is required for a deflection of 2.3 microns. This implies, that the piezo should atleast be able to generate this much force. So we need to choose a piezo with blocking force higher than 15N.

A comparative analysis was conducted among various piezo actuator types to determine the most suitable actuator configuration that fits the requirements. Summary of this is depicted in Figure 6.23

Bending actuators typically comprise two piezoelectric plates bonded together, with one end fixed on a cantilever support while the other end is free to deflect. One plate is biased to expand while the other to contract. These can also be biomorph benders with different materials for the two plates. Bending mode actuators provide significant displacement but have a smaller force capability than multi-layer actuators, typically no more than a few N's.

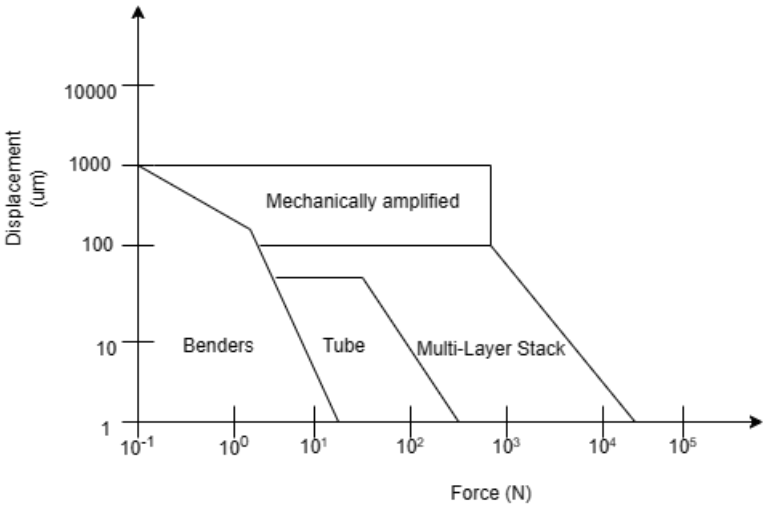


Figure 6.23: Force vs Displacement performance of various piezo actuator types

Amplified flextensional actuators offer enhanced displacements and can achieve strain amplification of about 4–5 times compared to other actuators. However, they tend to be bulky and are not well-suited for small devices. Multi-layer stacked actuators exhibit increased blocked force compared to single-layer conventional piezoelectric actuators. However, their displacements are limited compared to benders. It is noteworthy that force and stroke usually follow a linear relationship. With increased stroke, the amount of force that can be generated by the piezo decreases, and vice versa. Another important consideration is the presence of a load. The stroke mentioned in the datasheet represents the free stroke (without the presence of any load or mass). Under load, both effective force and stroke are reduced. This aspect must be considered when choosing a piezo actuator

Some of the commercially available bender actuators, although could meet the required force and displacement criteria, were not pursued due to unsuitable dimensions. After numerous technical discussions with the piezo manufacturers, it was determined that multi-layer stack actuators are most suitable for the requirements and design objectives. Multi-layer or stack actuators are composed of multiple piezo elements layered on top of each other, capitalizing on the combined expansion of each element. The most commonly available stack actuators employ d33 polarization for producing displacement, meaning they are mostly optimized for expansion of 0.1% of their height at voltages of a few hundred volts. The possible contraction is only 20%e of this maximum displacement at the maximum allowed negative voltage. However, increasing the negative voltage beyond this threshold can cause permanent depolarization due to the manufacturing process of the piezo. This is known as the butterfly effect, wherein even after applying a negative electric field, the piezo will produce positive extension instead of compression. This mode makes it nearly impossible to achieve the envisioned operating mechanism for this design. Therefore, it is suggested to employ a different polarisation coefficient of the piezo actuator. And a new custom piezo design from Thorlabs company is proposed as illustrated in figure 6.24, where d31 polarization of the piezo is employed in such a way that under positive fields, the piezo produces contracting stroke. Such a design eliminates the risk of depolarization, and strains around 0.05% are possible.

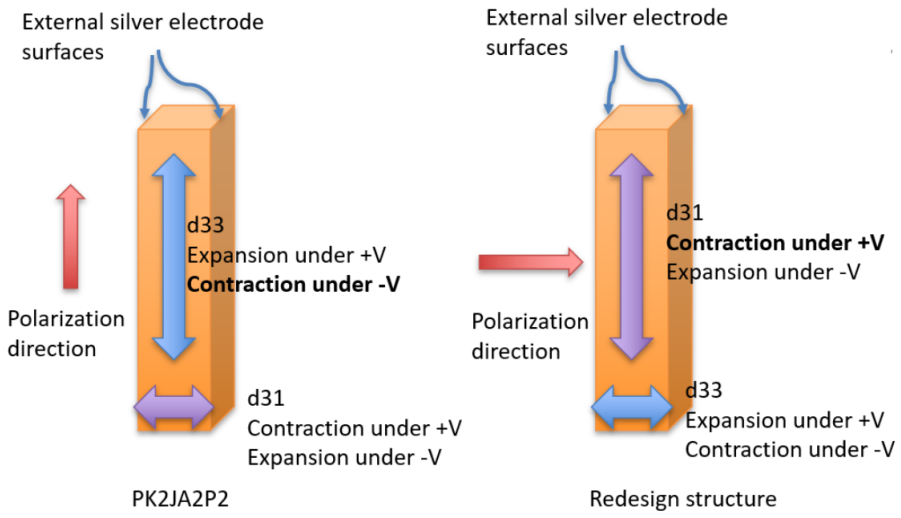


Figure 6.24: New design of the piezo stack actuator. PK2JA2PA is the model number of the existing stack actuator at Thorlabs and the Redesign is the design modification provided by the design engineer at Thorlabs

Some simple calculations can be made to theoretically characterise the piezo actuator properties, shown in figure 6.25. The strain is an important parameter of the piezo actuator which determines what an actuator can do. If this strain is multiplied by the length of the actuator, this will result in maximum free stroke. Similarly, the piezoelectric stress constant when multiplied with electric field gives the stress. This multiplied with the cross-section area of the actuator determines the blocking force. The required stroke and force requirements needed for the actuator were derived in the previous sections.

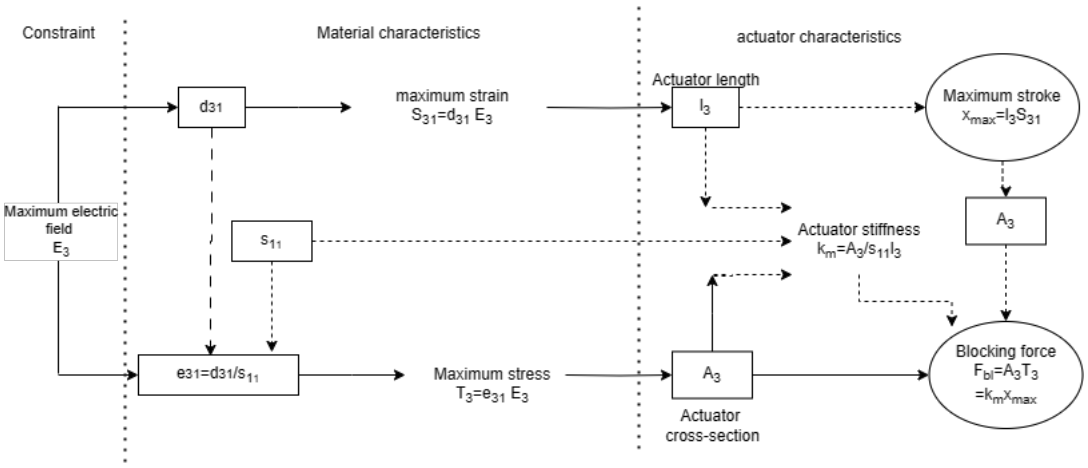


Figure 6.25: Constitutive equations for multi-layer piezo actuators. e33 is the piezoelectric stress constant, d31 is the dielectric constant

The Thorlab manufacturer provided the material characteristics for the actuator, namely the $d_{31}$ and $s_{11}$ . This design of the actuator can provide around 0.05% strain. From the figure 6.25, it is implied that for stroke of 2.3 micron, the piezo height of atleast 5mm is required. In addition, the cross-section area of the piezo stack actuator was selected to be 3mmx3mm, since this was the minimum that was possible by the manufacturer.

As have been highlighted earlier, piezo's free stroke is defined as the stroke in the absence of any load. The effects of pre-loading/loads affect the performance of the piezo actuator. The working curve for an actuator changes with no load or load with stiffness. The approximate displacement of the actuator under load is given by:

The manufacturer, Thorlabs, has provided material characteristics for the actuator, the d31 and s11 coefficients. Additionally, the cross-sectional area of the piezo stack actuator was chosen to be 3mm x 3mm, as this was the minimum available from the manufacturer. This actuator design is capable of achieving approx-

imately 0.05% strain. Figure 6.25 suggests that a piezo height of at least 5mm is required for a stroke of 2.3 microns.

As mentioned earlier, the free stroke of a piezo refers to the stroke in the absence of any load. The performance of the piezo actuator is influenced by pre-loading and external loads, which alter its working curve. The approximate displacement of the actuator under load is determined by:

$$\Delta L = \Delta L_{FS} \frac{k_A}{k_A + K_B} \tag{6.36}$$

This necessitates the need for an actuator length longer than 5mm. Equation 6.36 reveals that the reduction in stroke depends on the stiffness. The higher the stiffness of the piezo compared to the load, the smaller the change in stroke. The stiffness of the membrane actuator can be estimated from the load-deflection curve in Figure 6.22. It was found that for a piezo with the above specifications, the stroke would be reduced to about 0.2-0.3 microns. Furthermore, to account for manufacturing tolerance, a worst case stroke reduction of 15% is assumed. This would imply that this actuator length may not meet the required stroke requirement. Since the proposed piezo design presented here is untested, real data on stroke are not available; therefore, the worst-case scenario is considered.

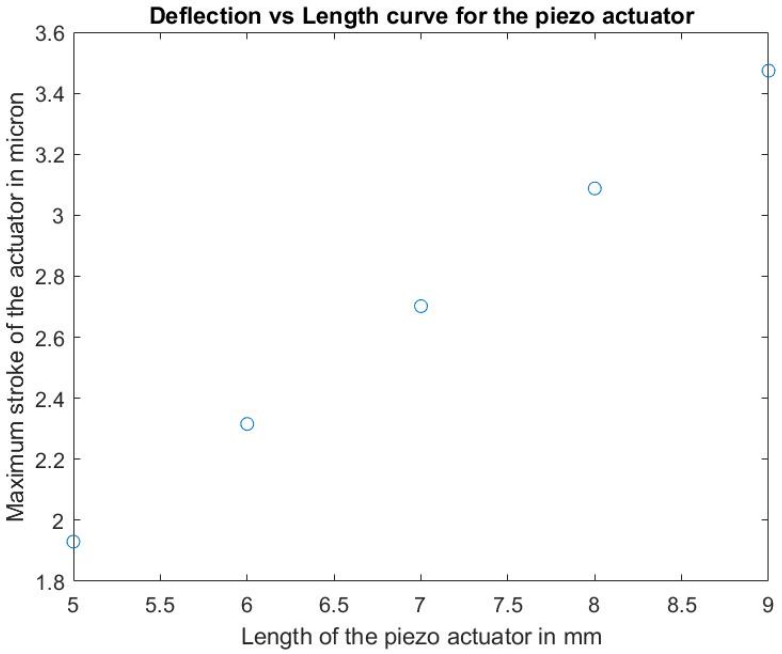


Figure 6.26: The graph shows the length-stroke curve for the actuator design. Here stroke refers to the maximum stroke provided by the actuator under load conditions and hystersis

Based on the graph above, it is evident that a length of 6 mm would just meet the stroke requirement, making it appear to be the preferred choice. However, to accommodate pre-stress load conditions, to allow for potential higher flow rate requirements for future applications, as well as, any unforeseen design considerations, the author opted for a length of 9mm for the actuator.

| **Piezo specifications** | **Value** | **Units** |
|---|---|---|
| Dimensions | 3x3x9 | mm^3 |
| Free Blocking force | 264 | N |
| Free stroke @ 75V | 4.5 +/-15% | micron |
| | | |
| **Unit price** | **Non-Recurring Cost** | **Lead Time** |
| $53.91 | $1,500 | 3 months |

Table 6.2: Proposed Piezo stack actuator specifications

The summary of the proposed piezo actuator are provided in table 6.2. The piezo stack actuator consists of an electrode layer of 2 micrometers with each piezo layer of 34 microns. Along with that, there is a top and bottom protective layer of 200 microns. PZT's are particularly vulnerable to pulling and shear forces and can cause cracks in the piezo ceramic. The pre-stress on the piezo as detailed in section 6.5.1.1 applied by the mounting structure to avoid displacements during operation would be an advantage and increase its pulling perform ance and overall dynamic push/pull application. This increases its lifetime and aids in reliable operation.

It is important to highlight that the specifications mentioned are theoretical estimates and require testing for full piezo characterization. In summary, many of the valves mentioned in research papers for space applications utilize the extension capability of the piezo, resulting in a somewhat bulkier overall structure.

This customized solution from Thorlabs presents a promising design choice that meets the design requirements.

## 6.7. PART D: Holder design

The design of the valve housing is driven by these requirements:

- MIC-SYST-200: The total size of the propulsion system shall be within 42 mm x 42 mm x 30 mm
- MIC-INT-200 The fluidic interface of the valve system shall be compatible with both thruster housing and propellant tank

This section will discuss the design of domain D in figure 6.1. Device holder has two primary purpose: provide controlled environment for the operation of the valve and enable interfacing between microvalve and microfluidic systems (sensors, fluid reservoirs, thruster etc). Furthermore, it protects the valve chip from damage or other contamination.

Since, the foremost objective would be to characterise the valve itself and test it independently for flow measurements, the valve holder was designed to integrate with the existing testing rig. The microfluidics interfacing was done by incorporating 1/4"" threaded ports into the holder design. This was done in order to be able to use Elveflow 1/4"-28 TPI microfluidic connectors (can be seen in figure 6.27) to easily connect the valve with the flow sensors and reservoirs.

Figure 6.27: 1/4-28 fittings connector for the connection with microfluidic components

It should be noted that if other fluidic connectors are used over the course of the full system testing, the holder design can be adapted to mate with those interconnections. For this thesis, the envisioned test setup rig is as mentioned in 10.2 where the priority was set to the component testing without rest of the propulsion systems, however at the later stage, if the setup or the connectors are changed the holder must be designed to fit the valve to the rest of the fluidic system.

Since, the housing needs to be compatible not just with the overall microfluidic system but also with the valve. This puts some design constraints on the valve design, and this will be mentioned in this section.

Microvalve interfacing also requires leak-proof connection. In order to prevent fluid leakage into the environment when the valve is mated with the holder inlet, o rings have been placed in the recess design to ensure fluid seal. An O-ring closes the gap through the mating components through the deformation of the seal material and the media pressure. The seal assembly consists of an elastomer O ring and a groove(which contains and supports the o-ring). The groove must be designed in order to incorporate the o ring. There are certain guidelines for the o ring groove which are based on the assumption if the seal/sealed surfaces is moving or stationary. The shape of the seal groove is generally unimportant as long as the there is enough seal compression when mating. Since this is a case of static face seal: when there is no gap between the mating surfaces and the sealing surfaces are stationary.

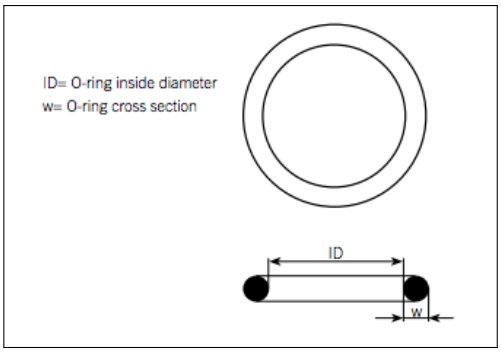


(a) Cross-section of the o ring

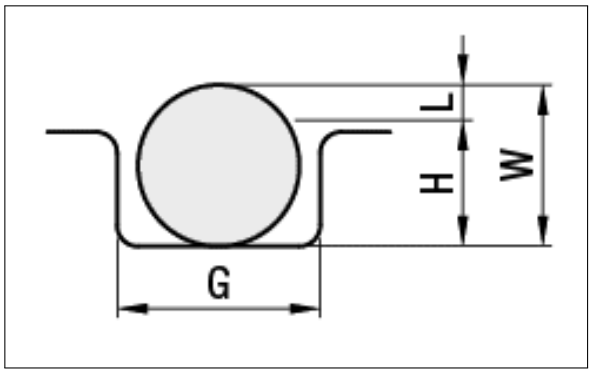


(b) Cross-section of the groove with the o ring installed, L is the compression ratio, H is the height of the groove, W is the CS of the o ring, G is the width of the groove

Figure 6.28: Holder groove design

The ID of the o ring should be smaller than the width of the gland so that the o ring can be stretched when installed. Since, the o rings will compress from the surface placed above it, the width and height of the groove is designed to allow for that compression. For this, the compression ratio is usually determined to achieve the desired squeeze of the o ring. This ratio usually lies between 5-35 %. Groove height:

$$Compressionratio = \frac{OringCS - Glandheight}{oringCS} = \frac{W - H}{W} \tag{6.37}$$

Since the footprint of the valve should be as small as possible, the smallest o ring is chosen. It was found that readily available commercial o ring from Eriks had the smallest dimensions, CS and ID, of 0.6mm. A compression ratio of 20 % was chosen. From this, a gland height of 0.45 mm was considered.
The cross-section of the groove has a rectangular area. The total volume of the o ring, which creates the rectangle to hold that volume. Gland fill is the percentage of the groove that is filled by the o ring. The recommended gland fill usually lies between 65-75, % with a maximum of 85 %. The gland fill design recommendations incorporates several factors that could impact the volume necessary to house the o ring. These include thermal expansion, swell due to fluid exposure and other tolerance variations. Keeping above in mind, gland fill of 70 % is chosen.

$$Glandfill(\%) * Glandcrosssectionarea = \pi R^2 \tag{6.38}$$

where R is the outer diameter of the o ring. From the above equation, a gland width of 2.1 mm is considered. The overall design of the valve along with the holder can be found in section 8.

# 7

# Numerical Analysis

## 7.1. Introduction

The design process started with the analytical characterisation, where simplified equations were used as a baseline for the development of valve design, such as internal flow resistance for mass flow analysis and the force evaluation. The analytical model in the Chapter 6, which is based on several assumptions, has to be validated with the aid of numerical simulations using sophisticated tools. Even though the analytical model is a first step in the design process, which is a powerful tool in estimating the device behaviour. It requires validation due to the fact that many assumptions have been made in the process which might deviate from how the system will behaviour in real life. However, validation of that can only be done via experiments, which is out of the scope of this work. The purpose of the work is to present a preliminary design satisfying the design requirements. To this extent, the validation process makes use of sophisticated numerical tool in confirming the system behaviour, comparing analytical to numerical and is also corroborated with similar designs in literature.

Simulating the behaviour of the valve is a classic example of fluid-surface interaction (fsi). The phenomenon is characterised by interactions between the deformable moving solid structure and the surrounding internal flow. When the fluid flow encounters a structure, stresses and strains are exerted on the solid object-these forces can lead to deformations. These structural deformations can be quite small or large, depending on the pressure and velocity of the flow and the material properties of the structure. Similarly, the structural deformations that are driven by the actuator will vary with time and depending on the control system can be greater than a few cycles per second. Because of these deformations, the velocity and pressure fields will change as a result. This makes this problem as a bidirectionally coupled multi-physics analysis.
However, solving 3-dimensional 2-way coupled fsi problem involves dealing with different interfacing physics: electrostatics, structural and fluid flow, there is an inherent complexity involved owing to non-linear behaviour and different material properties. Such a simulation is complicated and computationally expensive, requiring a lot of processing power. Due to lack of computational power to run heavy files, the simulation was split. Decoupling the flow and deformation is a relatively quicker way and less computationally and time expensive than multi-physics analysis to tune the parameters to get a rather optimal design.

Hence, to simplify the 3D simulation process, the following assumptions were made in order to decouple the physics involved.

- The transient fluid structure behaviour was not captured, and it was assumed that once the fluid reaches a steady state in case fully open valve, the effects on the fluid behaviour because of the structure will be negligible. Therefore, only steady state simulation was conducted, and the transient behaviour is not studied.

- Since the velocity fields is quite small according to analytical results, it is speculated that the deformation on the structure due to the fluid flow would be very small, moreover, the forces exerted on the structure account for forces by the fluid and is designed to be much higher than the fluid forces. This is to ensure that the structure is rigid and experiences negligible structural deflections due to the fluid flow.

The two decoupled simulations, fluid and structural, are studied separately but in an iterative process. The inputs from one simulation are used for other simulation. The work-flow of this analysis has been organised in a step-wise approach, which can be seen in figure 7.1. Some of the parameter results from the Matlab model developed in chapter 6 serve as input for the model definition in the numerical analysis. This methodology is employed to come up with a valve design that will meet the system requirements.

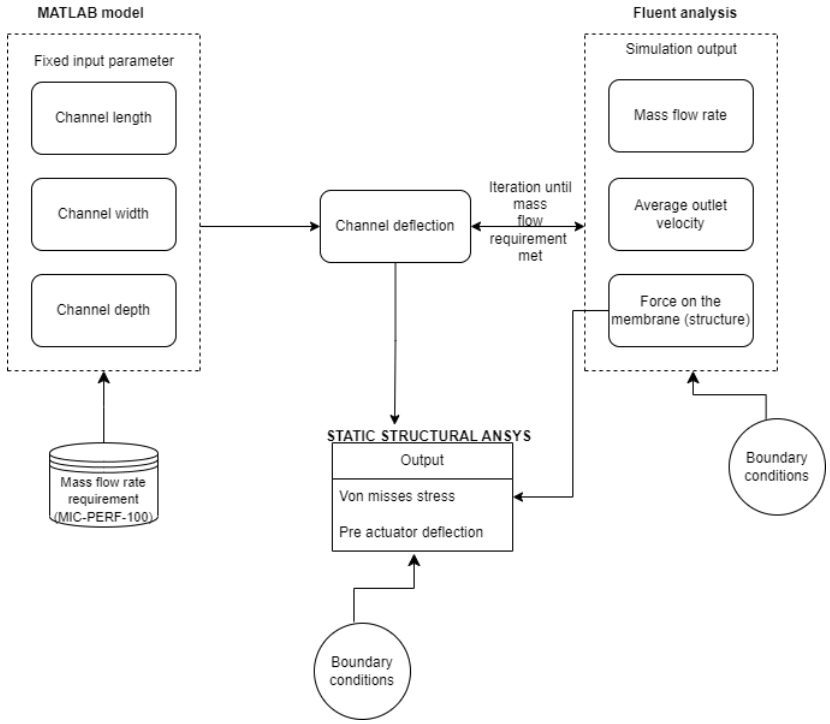


Figure 7.1: Methodology for numerical analysis for fluid and structural simulation

## 7.2. Fluid simulation

This section focuses on the modelling efforts for understanding the behaviour of the microvalve design. Steady state simulations are performed in this section to observe the values of local parameters (e.g. pressure, velocity). A numerical approach using a computational fluid dynamics (CFD) software package, ANSYS FLUENT is employed. The CFD software aims to solve the fluid flow based on the solution that agrees with the 3 conservation equations: mass, momentum and energy. These equations have been highlighted in previous chapters. To solve these, the CFD software employs a finite-volume based method consisting of the following steps

- The domain is divided into discrete control volumes using mesh
- The governing equations are integrated on the individual control volume to obtain algebraic equations for the discrete dependent variables such as velocity, pressure, temperature etc
- The discretised equations are linearised and solution of the resultant linear equation yield updated values of the dependent variables.

### 7.2.1. Computational domain

The first step in any CFD analysis is to identify the fluid control domain in which the governing equations are solved. Deciding where the computational domain begins and ends has an impact on the accuracy of the model. For this study, the flow through the valve holder tubings have not been considered and only the flow internal to the valve chip has been analysed. The domain under study is the extracted fluid volume consisting of the internal flow domain that the flow passes through the valve, which can be seen in figures 7.2,7.3.

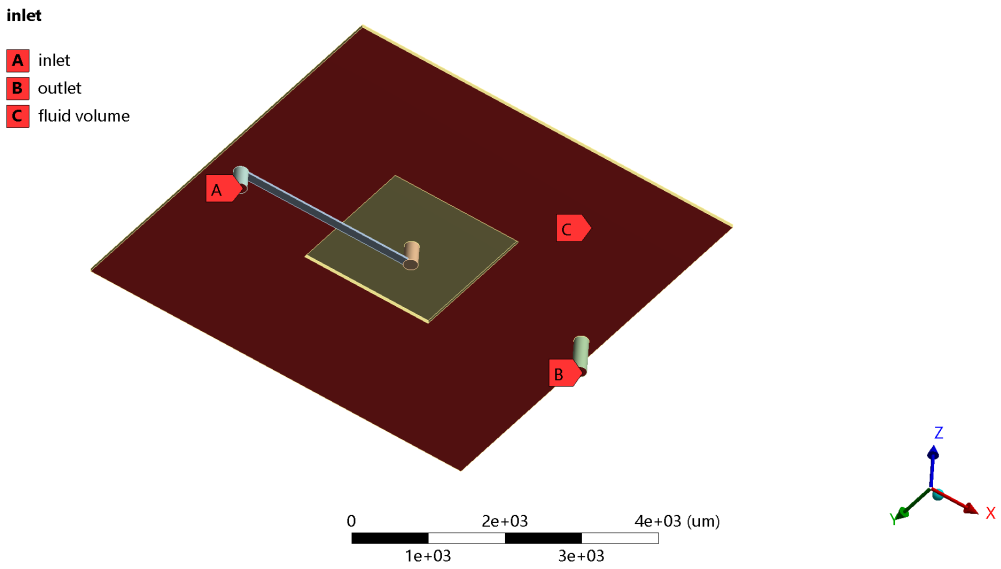


Figure 7.2: Computational domain for ANSYS Fluent

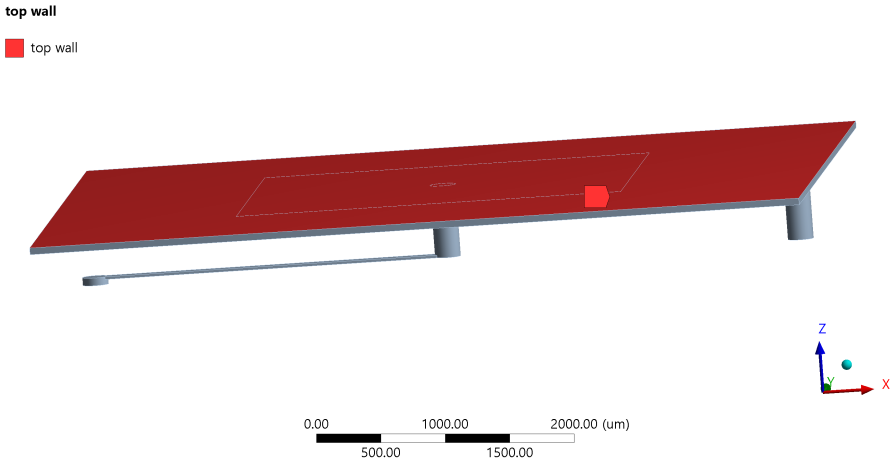


Figure 7.3: Computational domain for ANSYS Fluent

As mentioned earlier, the fluid simulation was carried out in steady state, which means the fluid control volume is the entire volume of space which will be occupied by fluid when it is fully opened.

The deflection denoted as 's' in 6.12 is the height that the membrane will be deflected by the actuator, keeping the internal fluid resistance constant, to achieve the mass flow requirement. As the fluid simulation is isolated from the structural simulation, this deflection is the height of the top plate relative to the outlet plane (denoted by C in figure 7.2). From the structural deformation, the deformation curve of the membrane can be seen in figure 7.25. The fluid control volume would mimic the deformed structural curvature. Therefore, an attempt was made to capture the structural deformation when creating the fluid geometry in SolidWorks. The STL results file from the ANSYS structural analysis was converted into a solid body in Spaceclaim. However, since the deflection (s) in question for this study were only in the order of microns compared to the lateral dimensions, many of the skin surface features were lost in the geometry, not reflecting accurate results. Therefore, the model geometry was simplified and a constant deflection (s) was assumed, hence the top plate in the figure 7.3 can be seen parallel to the outlet plane (referred to as fluid volume). Such a geometry is an over-estimation of the real schenario.

### 7.2.2. Boundary conditions

Choosing appropriate boundary conditions is indispensable in any CFD simulations. In this study, laminar flow is chosen with a pressure density solver. The material chosen is liquid water, where the density is constant. The inlet and outlet are set to be pressure type, where the value of the pressure is set according to requirement. The rest of the boundary are described as stationary wall and no-slip boundary condition (where the velocity at the boundary is zero).

| Surface | Boundary condition |
|---|---|
| Inlet | Pressure-inlet<br>P0 = 5 bar |
| Oulet | Pressure outlet<br>P = 0 bar |
| Remaining surface | Wall- no slip |

Table 7.1: Boundary conditions for the numerical model

### 7.2.3. Grid

Mesh generation is an important consideration in attaining numerical solutions to partial differential equation in CFD problem. Specific mesh for a given flow problem can determine the failure or success in obtaining a converged solution. The mesh should be fine enough so that important flow features can be captured with adequate resolution. The mesh for the fluid simulation is generated using in-built meshing software in ANSYS Fluent. A structured mesh with selective mesh refinement was created using multizone capability in Ansys, containing hexahedral swept regions. Structured mesh is made possible by dividing the entire geometry into several smaller geometries and then sweeping the domains accordingly to obtain a rather uniform mesh. For this, the geometry is edited in the Design Modeller and split surfaces are created to create multiple smaller domains to perform structured meshing. The structured meshes along the channel walls, inlet/outlet pipes can be seen in figure 7.4. However, due to curvature, the topology of the geometry is irregular, there are certain limitations in yielding a regular overlay mesh. For example, the face of a circular cylinder is meshed with body-fitted structured mesh, but the downside of it is that such a grid might produce skewed cells at the vertices resulting in numerical instabilities. An unstructured mesh is certainly well suited for handling arbitrary shape geometries, domains with high curvature boundaries. The mesh spacing in this geometry has been chosen such that the grid-size discontinuities can be removed as much as possible in regions in areas of flow changes.

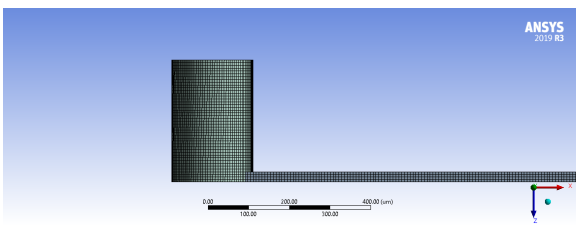


(a) Side view of the inlet pipe

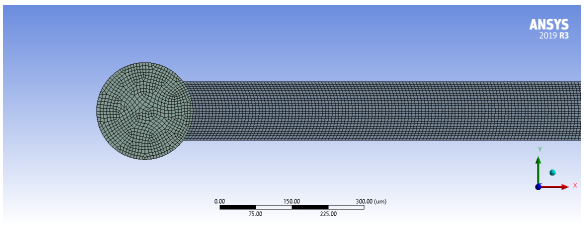


(b) Top view of the rectangular channel

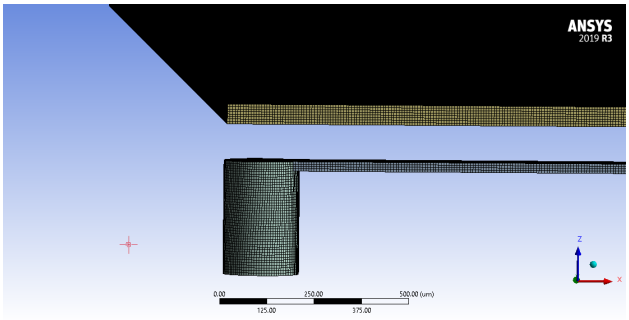


(c) Side view of the fluidic control volume

Figure 7.4: Structured hex mesh for the fluidic model

#### 7.2.3.1. Grid convergence

A grid convergence study is performed to determine the numerical error in the CFD solution. As the number of points in the grid increases, the numerical model will approach continuum representation of equations and error will tend to zero. As the mesh is refined, the solution becomes less sensitive to grid sizing. The error band for the quantities obtained from the finest mesh is determined. Due to limitation in computational resources, a different approach for meshing was employed. The author began by generating the finest mesh possible within the constraints of available resources. This fine mesh served as the starting point. Then, utilizing this fine mesh, the author derived an additional set of coarser grids.

This grid refinement study is based on the approach proposed by Roach [58], which uses a Grid convergence index (GCI). GCI is computed using three sets of mesh to estimate the order of convergence and to check if the results are within the asymptotic range of convergence. In other words, the solution from the computed numerical analysis approaching true numerical solution (asymptotic result) as grid resolution improves. However, there still might be errors between this asymptotic solution and true physical solution to the problem. A smaller value of GCI indicates that the computation is within the asymptotic range, and further refinement will not change the solution much. It is calculated using the parameter, average mass flow rate at the outlet.

Calculation is done using 3 grids, GRID_1, GRID_2, GRID_3, with a constant refinement ratio (r) of 1.5. GRID_1, GRID_2, GRID_3 represents the finest, fine and coarse mesh respectively. Assuming average grid spacing for finest grid (GRID_1) is h=1, then the average grid spacing for GRID_2 and GRID_3, normalised by finest grid spacing, will be h=1.5 and h=2.25 respectively. Calculating the order of convergence, p:

$$p = \ln\left(\frac{F_3 - F_2}{F_2 - F_1}\right) / \ln(r) \tag{7.1}$$

where F_i is the value of the function at Grid_i. Since the mass flow rate is used as the function, so F_i represents the value of mass flow rate at that grid. r is the refinement ratio which is constant for the three grid and is 1.5. After p is determined, the theoretical value of the function at grid spacing zero, is calculated using Richardson extrapolation method, this value will be the asymptotic function value.

$$F_{h=0} \approx F_1 + \frac{F_1 - F_2}{r^p - 1} \tag{7.2}$$

GCI is calculated between GRID_1 and GRID_2 using mass flow rate, which is given by:

$$GCI(\%) = 100\frac{F_s|\epsilon|}{r^p - 1} \tag{7.3}$$

$$\epsilon = \frac{F_2 - F_1}{F_1} \tag{7.4}$$

where (F_s) is the factor of safety and is recommended to be 1.25 for more than 2 grids [56]. The safety factor is an 95% confidence bound on the estimated relative error. Based on the above relations, the GCI for this study is calculated. Different grids and the respective function value can be found in the table below.

| **Grid** | Normalised grid spacing | **Average mass flow rate outlet (kg/m^3)** |
|---|---|---|
| Coarse mesh (Grid_3) | 2.25 | 5.89E-06 |
| Fine mesh (Grid_2) | 1.5 | 3.52E-06 |
| Finest mesh (Grid_1) | 1 | 2.90E-6 |

Using the above relations, the GCI% between grid 2-3 is 29%, whereas, the GCI% between grids 1-2 is 9.4%. In order words, it means the relative error in mass flow rate due to insufficient grid resolution is 9%. These indicate that on further refinement of the grid (with a ratio of 1.5), the change in the mass flow rate is around 9% or 0.09. In other words, the mass flow rate for this geometry is estimated to be 2.90e-6 kg/m$^2$ with an error band of 9% or 0.09.

Even though the GCI for this problem is relatively on the high side, and might suggest further refinement to obtain more accurate numerical solution. Generally, a GCI of less than 10% is considered acceptable in most CFD problems [58]. Therefore, since further refinement was not possible due to limited computational resources, the error percentage was within the acceptable range, hence the result was considered sufficiently admissible.

It is necessary to check if the grid convergence is within the asymptotic range of convergence. If we are in the asymptotic range, this means we are asymptotically approaching a converged answer and thus our solution is grid independent. With the three grids, it can be calculated as

$$\frac{GCI_{2,3}}{r^p \times GCI_{1,2}} \approx 1 \tag{7.5}$$

With $GCI_{2,3}$ as 29% and $GCI_{1,2}$ is 9.4%, this value comes to 0.85 ≈ 1, this confirms we are in asymptotic range. The graph in figure 7.5 plots the different function value at constant grid spacing along with the Richardson extrapolated value (estimated true value of the solution). GCI gives a measure of percentage the computed value is away from the value of the asymptotic numerical value. It indicates an error band on how far the solution is from the asymptotic value. It can be seen from the figure, that the GCI is decreasing as the grid is further refined, suggesting that the numerical solution is approaching a asymptotic numerical value.

It is important to note, that GCI value gives an assessment of how independent the numerical solution is to grid refinement. The likelihood of the reliability of the solution increases with a smaller GCI suggesting all important flow features were sufficiently captured, but it does not necessarily indicate accuracy of the solution. Since, that depends on a number of factors such as boundary conditions, numerical instabilities, numerical method, physical model used to describe the system, modelling assumptions: all of these contribute to the error of the simulation results.

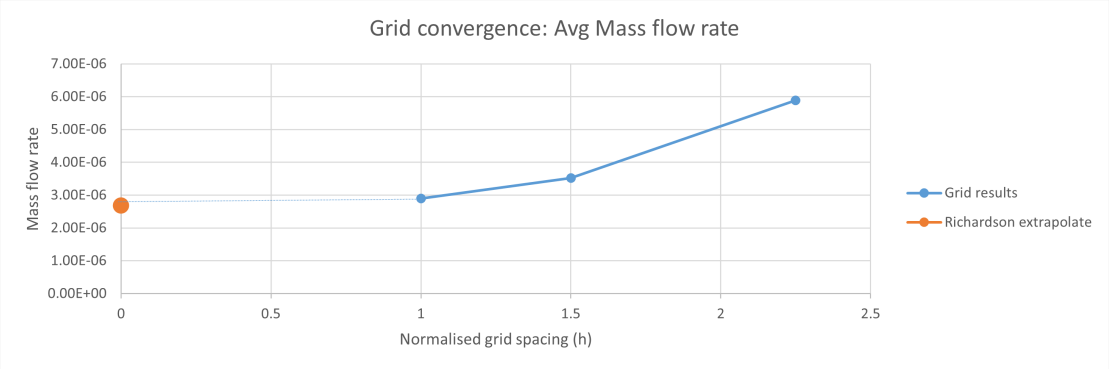


Figure 7.5: Grid convergence study indicating the Richardson-extrapolated value.

### 7.2.4. Solver details

For these simulations, a pressure-based solver with steady state formulation was used based on an iterative solving approach to calculate the solution. The pressure-based solver allows solving the flow problem either using segregated or coupled manner. For this case, the coupled scheme was chosen. Coupled scheme offers robust and superior performance over the segregated method, especially for implementation of steady-state flows. The coupled algorithm solves the continuity and momentum equation together, resulting in faster convergence compared to the segregated solver. In theory, the Coupled scheme gives most accurate results but is also computationally expensive. The interpolation scheme used with the coupled solver is second order upwind. For all the other controls, default Ansys fluent values are used.

### 7.2.5. Results

Once the numerical formulation is done, the results were used to validate the analytical model. To satisfy the MIC-PERF-100 requirement, the analytical model was used to calculate the fluidic path for the required pressure drop. However, it is essential to verify this analytical model to ensure that the model is performing the way it was intended and that it solves the problem it was designed to solve. Hence, subsequently a numerical simulation was performed. The results from flow field analysis are shown below, showing a non-linear flow behaviour.

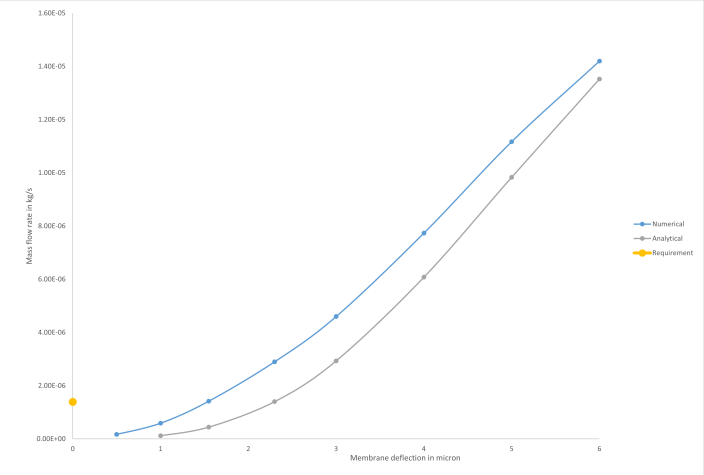


Figure 7.6: Comparison of predicted and measured flow rate in the microvalve for a pressure drop of 5 bar.

As can be seen from figure 7.6, the mass flow rate under varying membrane deflection trends well for both the calculated and simulation results.

However, the difference between the absolute value between the two can be attributed to a number of reasons. As can be seen from the graph that the mass flow rate for a given deflection is higher than analytical results. The primary reason anticipated by the author is the difference in fluidic path through which the flow study takes place. As highlighted earlier, solving the valve model is a structural contact problem in which the fluid is surrounding and acting on solid parts and an electrical signal is induced to cause structural movement. Modelling a situation like this, where two objects that are into contact will completely shut off the path of the flow, is particularly challenging. When the valve is closed, the topology will change so that one fluid domain is split into two disjoint domains. In various research papers, it was found that in order to avoid such topology change, a small offset is added to the contacting surfaces such that there is always a remaining small flow channel, even when contact has been established. Since, such a model would defeat the purpose of being able to simulate off-state condition. The author handled this model by simulating an open state condition at opening pressure, in other words by modelling the required offset between the contacting surfaces to achieve the necessary flow rate. The domain, which is immediately downstream to the membrane deflection is also included in the numerical model. However, in analytical results, the model approximating the flow field between the valve seat and the valve membrane is only a representation of region d as in figure 6.11, which is the region between the valve seat and plunger. However, the pressure drop downstream of this was not accounted for. Therefore, the case of numerical simulation leads to higher mass flow rate, the larger geometry can allow for a more gradual flow path, resulting in reduced pressure drop and lower resistance to fluid flow. The total fluidic resistance is a measure of how much the system impedes the flow of fluid. Higher resistance means it is more difficult for the fluid to flow through the system. As a result, in case of numerical, where the fluidic resistance is lower, the flow rate will be higher, leading to a higher mass flow rate compared to analytical.
Furthermore, from the GCI calculated earlier, it is predicted further refinement of mesh can lead to more accurate results. This could be another reason for the discrepancy. However, finer mesh finer was not possible due to computational limitation. In addition, the mesh convergence for a particular deflection configuration is optimised, and the same mesh was used to calculate the results for other deflections. This means, the model is not optimised for each changing geometry, which could have also added to the variation.

In summary, the trended line agree well with the similar valve design presented in literature, resembling the fluid modelling results presented by Olivier Smal in [64], [54]. The contour plots for the various cross-sections of the geometry are plotted below. The flow has a smooth parabolic velocity profile following the Hagen Poiseuille flow conditions, where the pressure drop along the direction of the flow is driven by viscous flow.

Similar to the inlet contour plots in figure 7.7, you can see the contour plots at the outlet plane in figure 7.8. As you see, as the pressure contours show a higher pressure at the inlet 7.9, subsequently a lower maximum velocity at the inlet compared to the outlet.

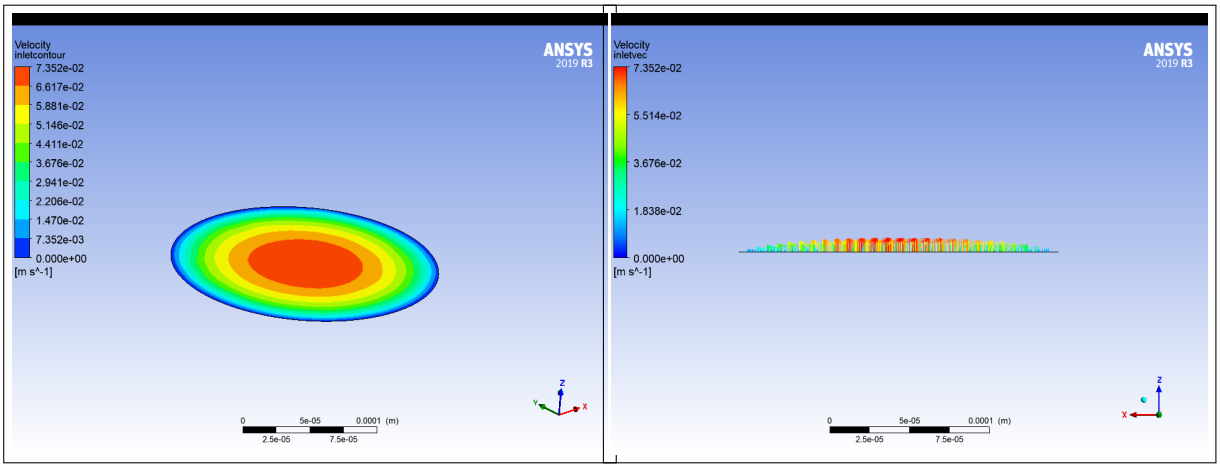


(a) Velocity contour at the inlet plane

(b) Velocity vectors at the inlet plane showing the parabolic flow

Figure 7.7: Contour plots and velocity vectors at the inlet

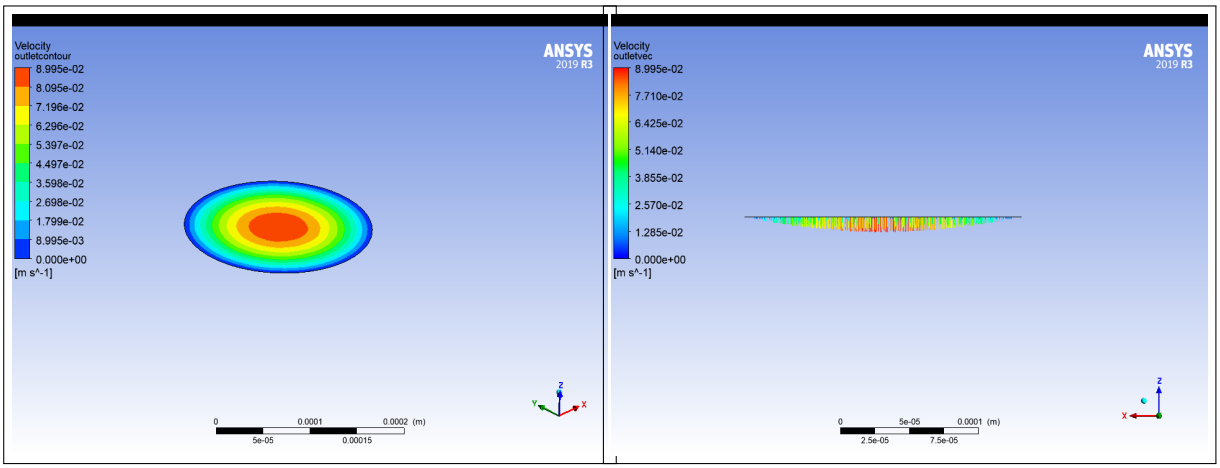


(a) Velocity contour at the outlet plane

(b) Velocity vectors at the outlet plane showing the parabolic flow

Figure 7.8: Contour plots and velocity vectors at the outlet

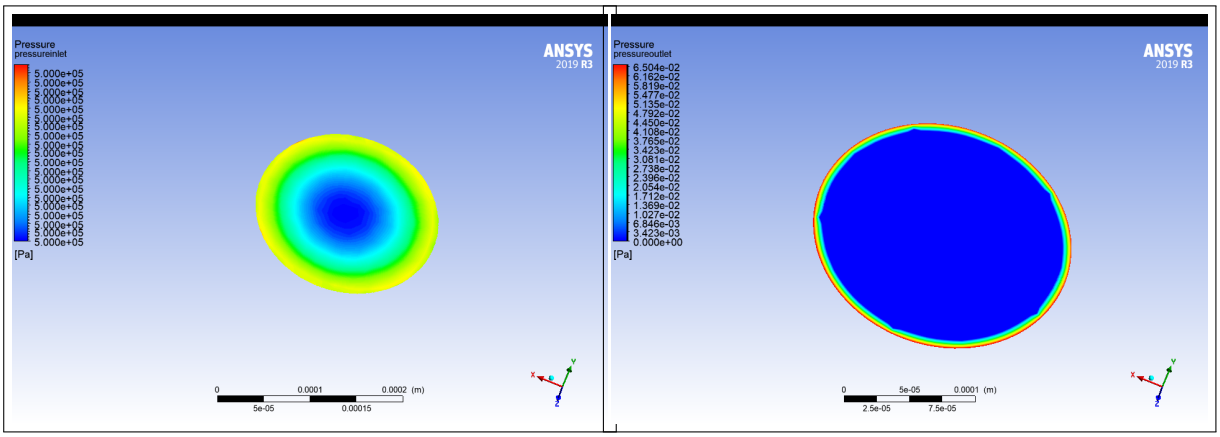


(a) Pressure contour at the inlet plane

(b) Pressure contour plots at the outlet plane

Figure 7.9: Pressure contour plots at the inlet and outlet, showing the local range of pressures at the respective location

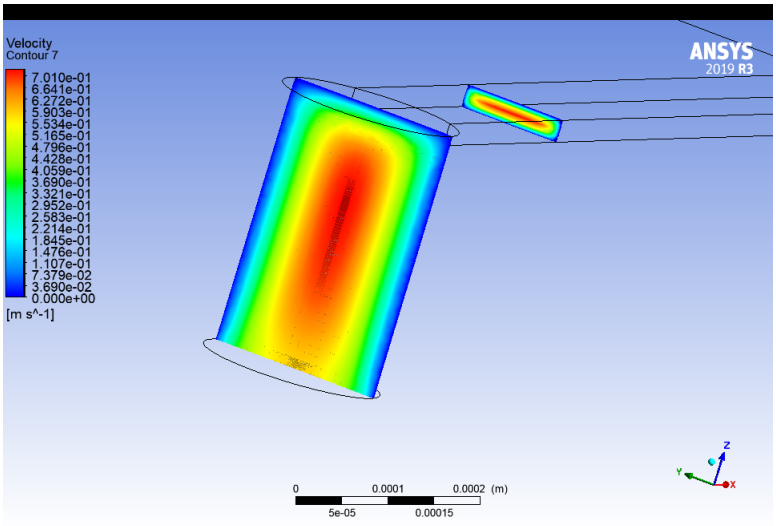


Figure 7.10: Velocity contours at the cross-sectional plane on the cylindrical pipe and rectangular channel

The plots, above 7.10, show the velocity contours at different planes along the fluid path-at a cross-section of cylindrical pipe and at the rectangular channel. From the contour plots, it can be seen that the flow follows the parabolic flow, with velocity maximum in the middle and zero at the walls fulfilling the no-slip boundary condition.

Furthermore, the pressure contour plot over the entire domain can be seen in figure 7.11. The pressure at the inlet is 5 bar and as it goes through the channel it experiences pressure drop, eventually the pressure at the outlet is close to 0 bar. The concentric contour lines in the middle indicate the pressure decreasing radially from the middle inlet towards the outlet, which also validates the radial flow modelling strategy adopted in the analytical model between the valve seat and the valve boss 5.5 in Chapter 5 and 6. This shows that the pressure drop through the system drives the flow and is dominated by losses due to viscous flow. The pressure drop in the circular and rectangular channels up to the valve seat is 5% of the total pressure drop.

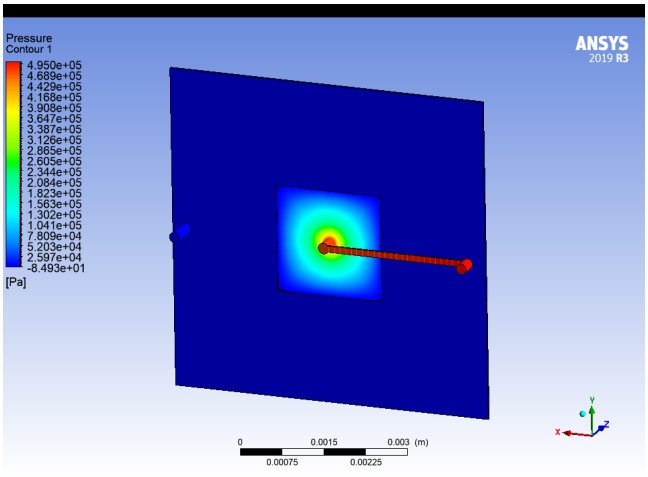


Figure 7.11: Pressure contours over the entire computational domain.

The streamline and particle vectors can be seen in figure 7.12, 7.13 , manifesting the path for the fluid flow across the entire domain.

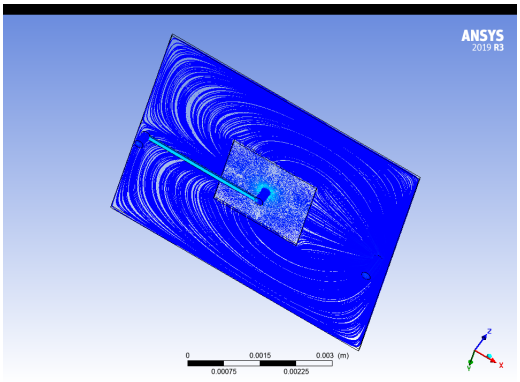


Figure 7.12: Streamline and velocity contours showing the path of fluid flow

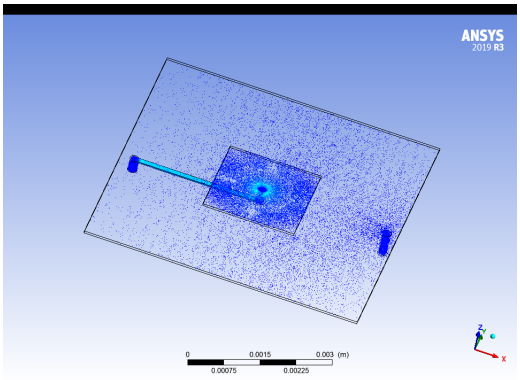


Figure 7.13: Streamline and velocity contours showing the path of fluid flow

One of the objectives of the work was also to show proportional control of fluid flow by the valve. This is shown in figure 7.14. This graph shows the valving behaviour of the valve at different deflections and different differential pressures. The mass flow rate of the valve for different stroke lengths at different inlet pressure is plotted, and it shows the range of flows that the valve can operate in.

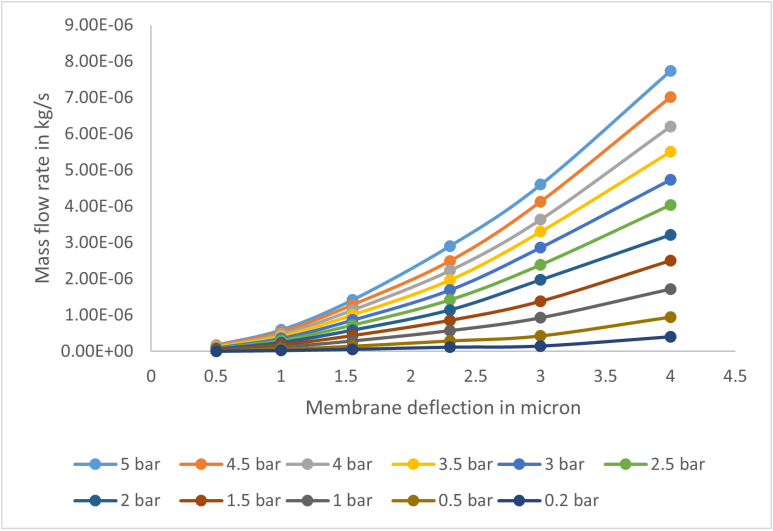


Figure 7.14: Proportional flow control at different differential pressures.

The results given in this section are based on analytical and numerical flow models. And this study shows the numerical simulation is well in accordance with the theory. While the analytical model is about using

existing flow models to achieve a valve design, numerical methods further refines the design while approximating the answer through iterations.

In summary, although the mass flow predicted by the two models differs in absolute value, the trend remains similar. However, this discrepancy does not compromise the validity of the design as it still meets the requirements. This is because from the graph 7.6, the analytical model suggests that a deflection of 1.6 microns would be necessary for the required flow rate, compared to 2.3 microns in the case of analytical simulations. Nevertheless, this discrepancy is inconsequential because the proposed piezo design offers a range of stroke possibilities, with a maximum free stroke of 4.5 microns. Therefore, regardless of the required stroke, the piezo will be capable of delivering it.

## 7.3. Structural simulation

Achieving functionality, safety and reliability are the main purposes in a structural simulation. Deformation, usually related to functionality and stress to safety and reliability. In this section, we will look into the stresses developed in the valve assembly due to loads on it. These stresses will be compared against the critical values and the failure criteria for the system will be explained. Care has been taken to have the model as close to the real geometry describing the contact surfaces, loading forces and the material. Due to the geometrical complexity, non-linear effects the analytical calculations are not so straightforward. The detailed design presented in Chapter 6 is further developed in this section and the structural simulations was performed in Ansys workbench.

### 7.3.1. Computational domain and methodology

The geometry used in the simulation can be seen in figure 7.15

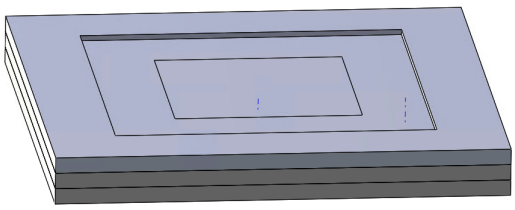

Figure 7.15: The valve geometry used in Ansys workbench for structural simulation

The 3D geometry was developed in SolidWorks, and then exported in spaceclaim to further add split surfaces for proper application of loads. As you can see, the geometry has three different layers. The top layer acts as the flexible membrane for the valve seat, whereas the bottom two layers have the fluid path inscribed. The cross section view of the geometry for the FE model can be seen below 7.16

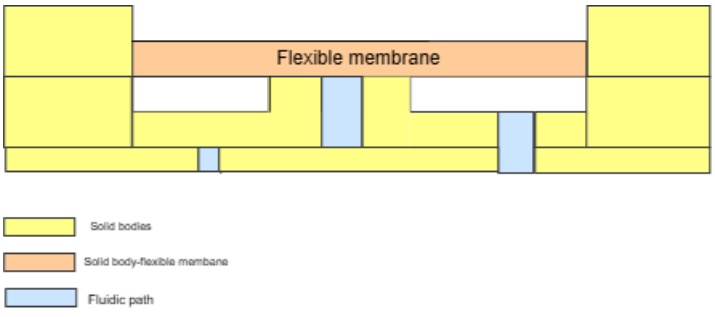


Figure 7.16: Cross-section view of the valve geometry used in Ansys workbench

In this mechanical simulation, the piezo is not introduced. The reason for it is that the piezo is going to be a commercially available one. The material, electrodes placement and other characteristics of the actuator are not known to accurately simulate the piezo behaviour. So, the methodology adopted for the mechanical simulation is as follows:

- The deflections needed from the fluid simulation for the design requirements are noted
- Appropriate piezo actuator will be selected to meet the stroke, frequency, and other requirements
- The deflection values are used as boundary conditions at the piezo-membrane interface to ensure the structure can withstand the stress generated

By doing so, the actuator can be isolated from the simulation without affecting the end results.

#### 7.3.1.1. Mesh

For the mesh, the geometry was divided into structured hex dominant meshing. Since the geometry is relatively simple, and can be easily subdivided, hex mesh was chosen because of its high accuracy and simple geometric properties. Symmetric surfaces and flat surface geometries can be better modelled with hexahedral elements. The domains which will be most affected by the boundary conditions are further refined using body sizing, which can be seen in the figure 7.17.

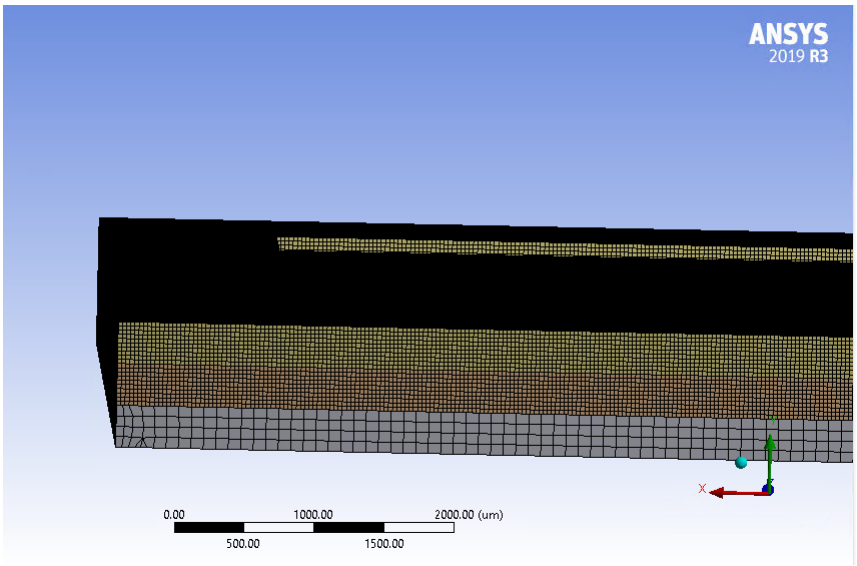


Figure 7.17: Mesh generation for the structural simulation

Mesh convergence study was conducted for this simulation just like for the fluid simulation. Same philosophy of GCI was adopted to study the accuracy and reliability of results. Since equations related to GCI was already explained in the preceding section, they are not repeated here. GCI is calculated using 3 grids, $GRID_1$,$GRID_2$, $GRID_3$. The factor of safety of 1.25 was used. The results from the grid convergence study are tabulated below.

| **Order of convergence (r)** | 9.76E-01 | |
|---|---|---|
| $\epsilon$ | 5.19E-03 | 7.67E-03 |
| **$GCI_{23}$** | | 1.97% |
| **$GCI_{12}$** | 1.34% | |
| **Grid** | **Normalised grid spacing** | **Force reaction at displacement boundary (uN)** |
| **Grid_1 (Finest mesh)** | 1 | 1.985E+07 |
| **Grid_2 (Fine mesh)** | 1.5 | 1.996E+07 |
| **Grid_3 (Coarse mesh)** | 2.25 | 2.011E+07 |

It can be seen, the GCI between grid 2-3 is 1.97% whereas, the GCI between grid 1-2 is 1.34%. This implies, the reaction force is estimated to be around 19N with an error band of 1%, which is relatively low. The results were found to be in the asymptotic range with a value of $0.98 \approx 1$. Hence the fine grid $GRID_1$ is deemed sufficient for these simulations.

### 7.3.1.2. Boundary conditions

The following boundary conditions are used:

- The bottom face is a fixed support-since it will be placed in the holder and will not move
- The boss face on the top layer is given the required displacement
- Force applied on the bottom face of the top layer-obtained from the post-processing of fluid numerical simulation

Furthermore, the contact interactions between the two bodies is important to capture since the behaviour of the material at the interface also affects the overall design. Two contact connections are accounted for in this model. Both of them are the bonded contact which means the two surfaces interact in such a way that they neither separate from each other no slide over each other. Usually the larger surface in contact is the target body and the smaller surface the contact body. The normal and tangential forces are very strong and they tend to resist any forces that causes relative motion between them. Such a kind of connection represent the adhesive contact between layers. The surfaces that are in contact can be seen in figure 7.18

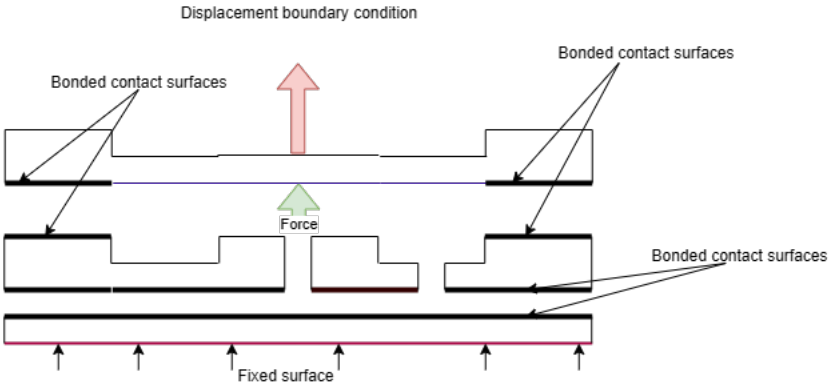


Figure 7.18: Contact interactions between the different layers representation the adhesive contacts and the other vboundary conditions on the FE model

## 7.3.2. Results

Stress-strain relation is one of the most important characteristics of the material. Understanding the material behaviour, i.e. deformation mechanisms enables prediction of Si failure during thermo-mechanical processing and device operation. Single crystal Si is brittle material at room temperature in which crack propogates without any appreciable plastic deformation. It exhibits ductile fracture when temperature is increased to 500 degree Celsius. The fracture of brittle materials is mostly due to tensile failure, which mostly occurs after cracking. And the fracture of ductile materials is due to shear forces. A brittle material fractures because the tensile stress (maximum principle stress) reaches fracture strength.

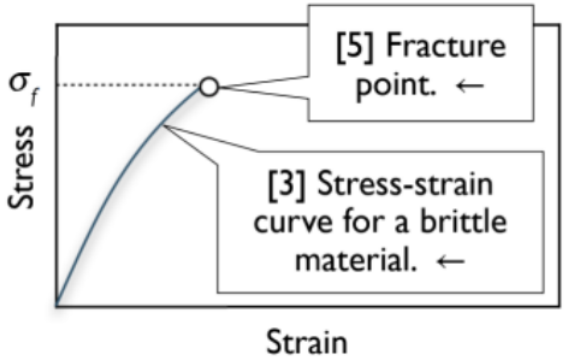


Figure 7.19: Stress strain curve for brittle material [33]

Therefore, to understand the stress behaviour of the system, static structural analysis was run and a parametric study for a range of displacement values was conducted.

A static structural analysis was performed on the model, revealing that the stress in the area where the piezo actuator would be bonded to the membrane is notably higher compared to other regions. This was not desirable and continuous cycles of operation may result in further fatigue and eventual failure.

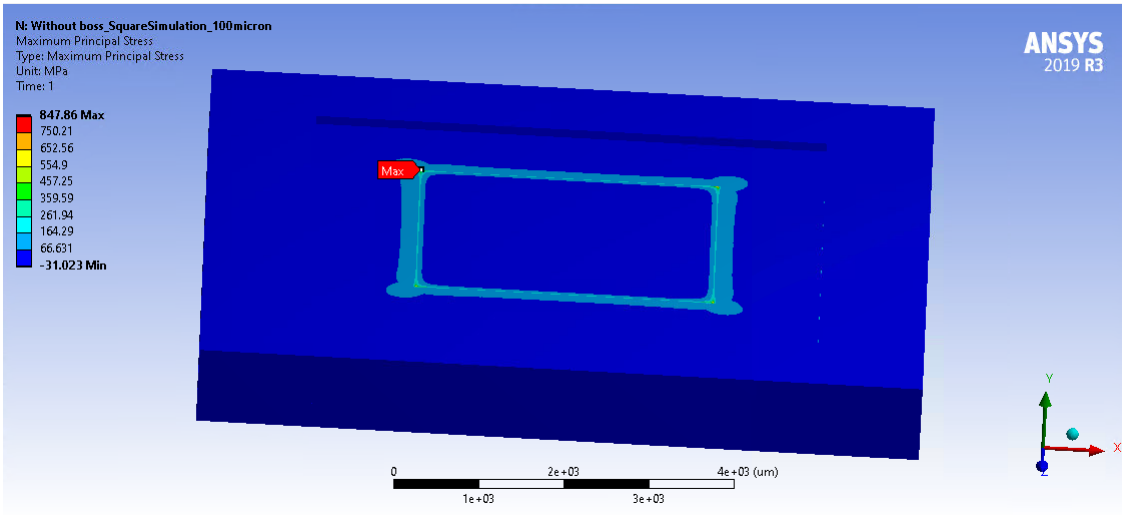


Figure 7.20: The graph shows Maximum principle stress on the plunger design for deflection of 3 micron

To mitigate this issue, the membrane was extruded to create a boss structure. This enhances the relative stiffness of the membrane in the region where the actuator would be bonded atop the boss. Given the piezo's stiffness relative to the membrane, all loads would be transferred to the membrane. To prevent structural failure, a boss structure was introduced. The dimensions of the boss are determined based on the footprint of the commercially available piezo actuator as described in Section 6.6. The bending force necessary for this new design was found to be comparable to that of the previous design case. Hence, moving forward, this modified design will undergo further analysis.

As discussed in Chapter 6, in open state condition, the actuator will drive the membrane to open. As the membrane is opening, the water will flow through the created passage and will exert force on the membrane. To simulate this state, the above force boundary conditions was defined. Since a fluid-structure simulation was not carried out, instantaneous force field is unknown. But to solve this, the forces on the membrane for each deflection were obtained from the fluid simulation. This can be seen from the figure 7.21. As the displacement increased, the force acting on the membrane decreased which seems obvious because as stroke length increases, the pressure reduces owing to pressure drop. This force represents the total force acting on the membrane.

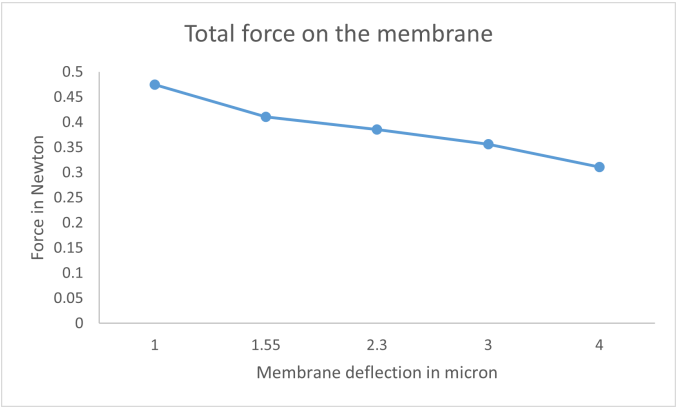


Figure 7.21: Force vs Deflection on the membrane obtained from Ansys fluent simulation

From the FE simulations, the Von Misses equivalent stress and principal maximum stress for the structure was studied. From figure 7.24 the stress distribution on the membrane can be seen on application of loads and displacement of 3 micron.

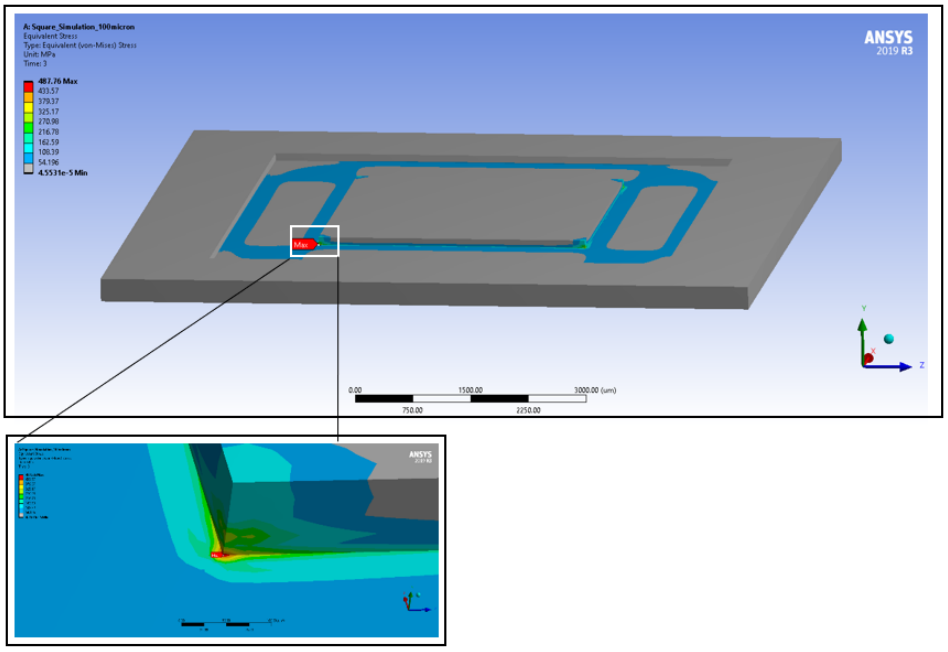


Figure 7.22: Equivalent stress distribution on the membrane on application of load

As can be in the above figure, the maximum stress appears to be at the edge of the boss. It can be suspected that this high concentrated peak value at the edge is not a real representative stress value and can be cause of numerical error as well. This area can either be stress hot spots or areas with stress singularity. However, further refinement of local mesh was not possible due to computational limitation.

From literature, silicon crystal have a fracture strength between 2-9 GPa [42]. As can be seen from the table 7.2, the maximum principal stress values seem to be much less than the fracture strength of silicon.

However, silicon is extremely brittle and high stress concentrations at the sharp edges under load application can cause micro-crack formation and decreases the mechanical stability of micro-structures. The corners rounding should be as large as possible. The author also calculated stress distribution with round boss and as expected the stress values decreases considerably, however having round boss is unfeasible due to unavailability of piezo actuator with circular cross section. So to address this issue, fillets were introduced and the corners were rounded off in areas of high stress gradients. These fillets distributed the stress over a broader area and increase the load bearing capacity. It should be noted that in MEMS micro-fabrication, most of the processes are optimised for anisotropic edge rates, selectivity etc but not for corner rounding. So, it should be included in the design so that required masks can be generated and can accordingly match the etching requirements for rounding.

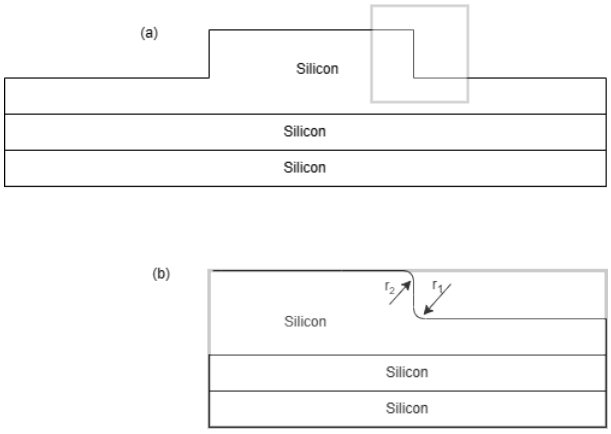


Figure 7.23: (a) Shows the simplified cross section view of the valve. Since the high stress points are near the boss region, the sharp edges near it will be rounded. (b) Figure shows one of the regions where the filleting is added to reduce stress concentration. $R_1$ = 200 $\mu$m, $R_2$ = 120 $\mu$m

.

The figure below shows the FEM stress distribution for the case (b). As you can see the high stress concentration still shows at the edges of the silicon boss which is usual in designs with corners and edges but we can see from the table below that the stress is significantly reduced by reducing the fillet. Further reduction in stress concentration could be possible by increasing the fillet radius.

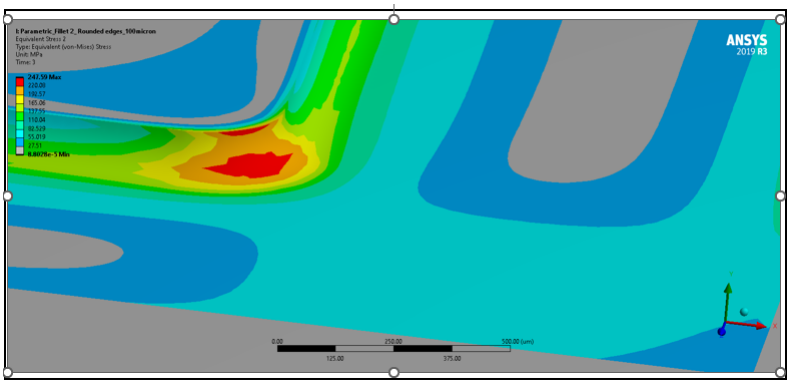


Figure 7.24: The equivalent stress for displacement of 3 micron with the fillet introduced at sharp corners

The below table compares the maximum principal stress for the two cases, it is evident that adding fillets reduces the stress more than by half.

| **Deformation in micron** | **Maximum principal stress @ 90 degree bent in MPa** | **Maximum principal stress @ rounding in MPa** |
|---|---|---|
| 1 | 213.41 | 94.852 |
| 2 | 428.66 | 190.64 |
| 3 | 643.76 | 286.35 |
| 4 | 858.86 | 382.06 |
| 4.5 | 966.48 | 429.96 |

Table 7.2: Comparison of maximum principal stress for the two cases for different displacement cases along with load addition

To conclude, it is not straightforward to predict stress values and even though in theory the fracture strength of Silicon is in GPa and the stress values from FE simulations are well under it. But in real life, there are quite a lot of factors that influence it such as edge cracking, chipping of wafers from production processes, surface roughness, presence of oxygen in the lattice from the mono-crystalline Si ingot production. Usually thin Si used as membrane with large pressure distributions can be easily supported but being brittle a very

small chip in the silicon wafer can cause it to break in one of the planes very easily. So, the dependence on the distribution of the stress in the surrounding Si is also critical which can be modified during the fabrication processes. Hence, it is imperative that the design is designed for lower stresses values. In summary, the design presented here offers the ability to handle the bending stresses induced while fulfilling the performance requirements.

From the FE simulations, the deformation curve for the design can be visualised from the figure 7.25. It can be seen that the deformation of the flexible membrane is maximum along the cross section of the boss and decreases until the edge of the membrane. This deformation on the parts of the membrane attached to the boss can vary based on the fluid force distribution. In the FE analysis, it was assumed to be constant along the entire membrane surface. It should be recalled that during the fluid simulation, this flexible membrane representing the fluid domain in open condition was assumed to be parallel to the valve seat. However, from the FE simulation it can be seen that it is not the case and deformation varies polynomial from the edge of the boss to the edge of the flexible membrane. In other words, the numerical simulation accounted for a larger fluid volume for a given deformation compared to real case and this will result in lower mass flow rate in the latter case. However, this can be easily compensated by having the same fluid domain which can be achieved by increasing the displacement. This is possible by selected piezo actuator which offers a maximum free stroke of around 4.5 micron.

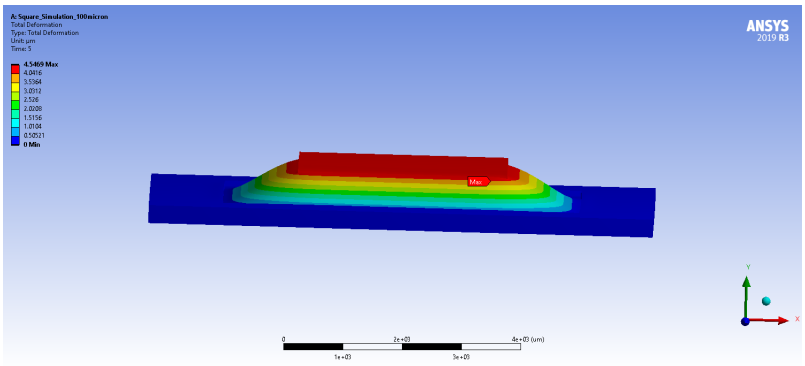


Figure 7.25: Visualisation of the deformed geometry under application of boundary conditions at 2x Auto scale. This presents the deformation curve upon actuation of piezo

.

## 7.4. Dynamic Response

In the earlier sections, we have discussed the general properties of PZT: design, mechanical etc. Another important consideration is the electrical characteristics. A PZT actuator is driven by electrical input from external source so it is necessary to know the drive voltage/frequency, capacitance which will facilitate the selection of the control circuitry. Piezo actuators are oscillating mechanical systems and are characterised by resonant frequency. The resonant frequencies of the piezo stack is dependent on the length of the piezo stack and is determined by stiffness and effective mass distribution within the actuator. Shorter the length of the stack, higher is the resonant frequency. Moreover, driving a load along with the piezo can considerably change the resonant frequency which is given by the following equation.

$$f_o' = f_o \sqrt{\frac{m/3}{m/3 + M}} \tag{7.6}$$

where m is the mass of the actuator, M is the mass of the load. $f_0$ is the resonant frequency. In the data sheet of the piezo actuators, manufacturers generally specify the unloaded resonant frequency and the mass of the actuator. It is recommended that the piezo actuators are not driven at or near the loaded resonant frequency, because this can cause the actuator to be driven beyond its rated maximum displacement leading to eventual mechanical fatigue. Thorlabs suggests that the actuators should be used with frequencies approximately 80% of loaded resonant frequency. For valve operation, piezo actuators are well suited for fast motions due to their high resonant frequency. As we know, the magnitude of the voltage applied determines the nominal extension of the stack. Applying quick changes to the applied voltage, fast dimensional changes of the piezo

stack can be achieved. This response time parameter is of significance for our application and is one of the requirements. The response time of the piezo is the time at which actuator reacts to change when subjected to electrical signal. This depends on a number of factors: resonant frequency, maximum current of the controller, capacitance of the piezo stack and the amplitude of the driving signal.
The actuator can be operated in static or dynamic conditions. During these operations, we need to understand the current consumption by the piezo. When the piezo is operated below its resonant frequency, it acts as a capacitor. The current needed for the actuator is given by:

$$I = \frac{dQ}{dt} = C\frac{dV}{dt} \tag{7.7}$$

where dV/dt is the slew rate. In static state, PZT consumes very less and the controller needs to compensate for the low leakage current from the PZT. Usually, for static or low dynamic operation the current necessary for the piezo is low and most of the controller can suffice. For dynamic operation, the actuator are driven by time varying signal such as sine wave, triangle or square wave. The circuitry must be able to source the current required by the PZT over the desired range of PZT action. The current, frequency and voltage values depend on the specifications of the piezo being used and the type of signal. The shortest time that the piezo takes to expand or contract is approximately given by:

$$t_{time} = \frac{1}{3f_0} \tag{7.8}$$

This describes the shortest time possible for a fast switch to make the piezo to displace. Attitude control systems often employ pulsed operation mode in order to provide impulse increments for the correction of orientation. This involves giving smallest possible repeatable impulse bits for attitude control. In order to achieve this, the response time of the fluid control should be minimised. And as stated earlier this is significantly influenced by valve characteristic. The valve is driven by the actuator, where it is important to minimise the response time of the actuator so that the displacement changes ( valve opens and closes) in a shortest time possible to make a fast switch. For these pulsed applications, response time down to micro seconds is possible, however that would require significant peak current from the controller for high resonant frequency PZT operation which can be seen in the table 7.3. Current and power values are too high that can be provided by most basic drivers. For most of the micro-controllers, the maximum current that can be drawn from any single I/O pin is 20/40mA. Based on the constraints on the driver bandwidth, the author assumed for an instantaneous voltage change from 0 V to 50 V, it would take 4 ms for the output voltage to reach 50 V to achieve desired deflection. This would require a current of 15mA for the PZT, which is within the driver specs.

| **Specifications** | **Value** | **Comments** |
|---|---|---|
| Capacitance | 850 nF | Specifications provided by manufacturer |
| Resonant frequency (without load) | 230 kHz | Specifications provided by manufacturer |
| Resonant frequency (with load) | 110 kHz | Using equation 7.6<br>Assumption: mass of actuator~0.9g<br>Mass of load ~1g (From CAD) |
| Recommended Resonant frequency | 88.3 kHz | 80% of loaded resonant frequency |
| Min Rise time | 3.7 $\mu$ s | Using equation 7.8 |
| Peak to Peak Voltage | 50V | Required voltage for 2.3 um deflection. This is an assumption from linear interpolation of voltage vs deflection curve excluding hystersis and reduced stroke due to load. |
| Current | 11 A | |
| Power | 0.5 kW | |
| **Since the current and power required is unrealistic for our system, so with response time of 4ms** | | |
| Current required | 10mA | Using equation 7.7 |
| Power required | 0.5 W | |
| Piezo Drive frequency | 250 Hz | |

Table 7.3: Design specifications for piezo circuitry

As depicted in Figure 7.6, the numerical results indicate that a deflection of 1.6 microns would be necessary to attain the desired flow rate. This implies that the operating voltage could be further reduced. Moreover, as illustrated in the table above, further reduction in the drive voltage could enable the attainment of the lower limit of the response time requirement.

It is necessary to match the PZT with an appropriate circuitry. The driver and the amplifier must be able to source the current required by the PZT over the range of the desired frequency ranges. The current drawn by the pzt over the varied range of frequency is given in figure 7.26. For this piezo design, it is recommended to not drive the PZT in the region after the orange line. By, doing so, concerns of longevity and durability arise.

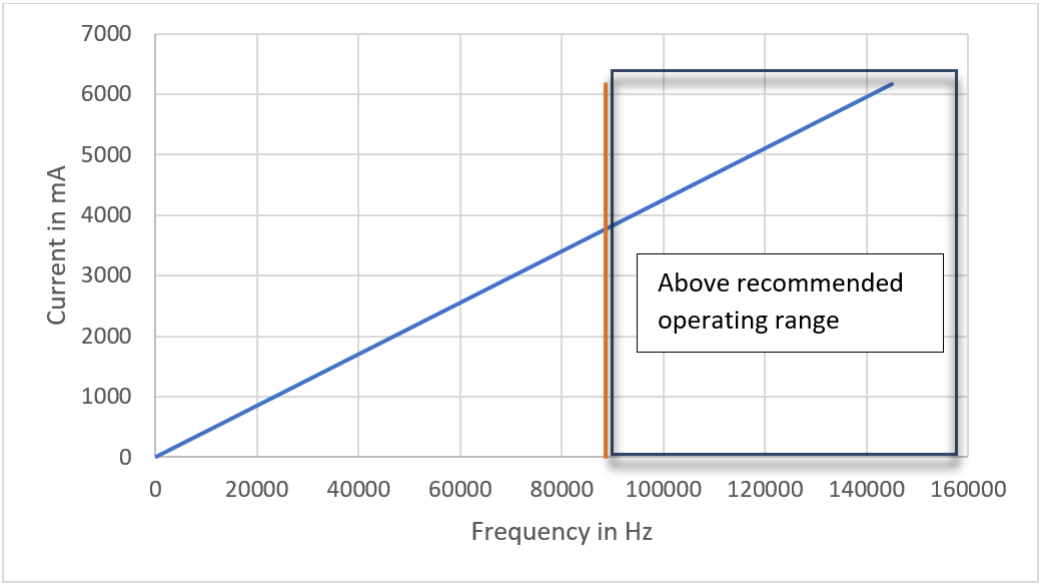


Figure 7.26: The graph shows the relationship between the drive frequency and required current to drive the piezo for peak voltage of 50V. Based on the max current rating of the driver, you can tune the frequency at which you can drive the piezo actuator. The orange line indicates the maximum allowable frequency at which you it is safe to drive the piezo

.

The graphs below (7.27) give an indication of the expected power and current that will be consumed by the piezo for different operating voltages. Based on the voltage supplied to the piezo, it is possible to modify the response time of the piezo. So, for example, if the piezo is driven at lower voltage, then for the same current consumption it can be driven faster, resulting in faster switching.

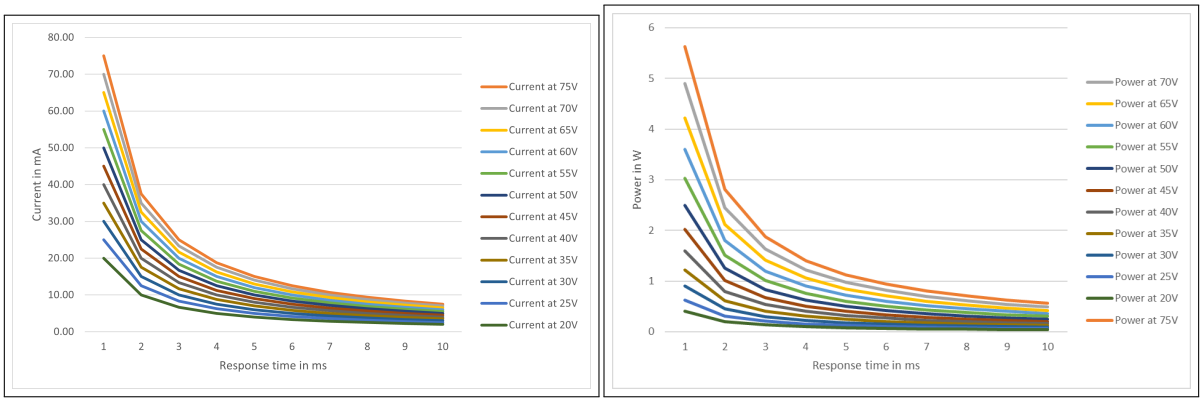


(a) Current vs Response time at a range of drive voltage levels

(b) Power vs Response time at a range of drive voltage levels

Figure 7.27: Variation of Power and Current with respect to the response time

In order to control the voltage supplied to the piezo, we need a controller. Most micro-controllers have an operating voltages of 5V. Using an input signal of 5V it is not possible to make the piezo work with such low

voltage. Multi-stack actuators typically operate at very high voltages. For driving the piezo at voltages in the range of 20V-75V, there is a need for an amplifier to boost the input voltage. Below you can find the proposed simplistic block diagram for the circuitry to drive the valve system.

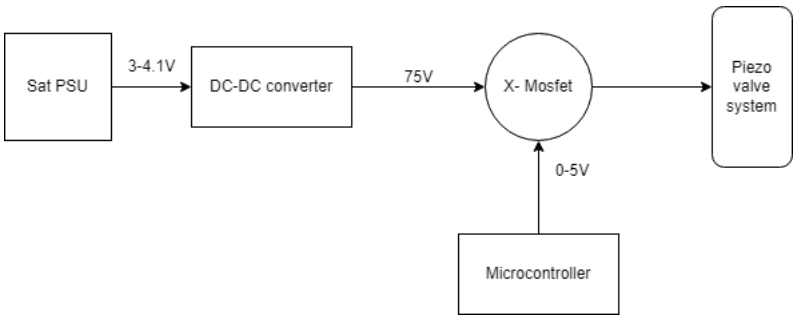


Figure 7.28: Simplified system block diagram

.

The Sat PSU refers to the satellite power supply unit which provides an input voltage of 3-4.1V, this will in turn drive the DC-DC converter which can provide uni polar high voltage rail in the range of 0-75V. To control this output voltage is the micro-controller which drives the X-MOSFET gate which act as a on-off switching switch. By controlling the amplification factor of the DC-DC controller, micro-controller can regulate the output voltage driving the piezo. This in turn will control the displacement of the membrane thus modulating the mass flow rate of the fluid. Many modern micro-controllers integrate PWM to the external pins for pulsed operation. The switching of the voltage and current supplied to the load between 0 and 100% happens at a rate faster than it takes piezo to change. The response time of the micro-controller nano for example is less than a 500ns-1ms. Duty cyle is one the primary component in defining the PWM signal. It is the fraction of the period when the system is active and is characterised as ON-OFF cycle. Response time of the system is an important parameter in deciding when and how long the system should be operational, in other words duration for which valve will be functioning, ergo the duty cycle.

To regulate the thrust level of the VLM device, the mass flow rate is adjusted to match the commanded output via the micro-valve. The initiation time of thruster operation hinges on when the established flow reaches a steady state. Hence, understanding the transient behavior is crucial to discern the settling time, given that many control features rely on the system's response time. As previously mentioned, numerous physical processes come into play during the actuation of a valve. Upon delivering the actuation voltage to the piezo actuator, an electrostatic interaction occurs between the moving plunger and the piezo, initiating motion in the plunger and subsequently opening the valve. This action allows the fluid to flow from the inlet, thereby establishing the flow. Two multiphysics coupling are at play in this behavior: the piezoelectric effect and fluid surface interaction. This renders the study of the behavior intricate and complex, as it necessitates the accurate setup of physics to simulate real-case scenarios. This process is cumbersome and demands substantial computational resources to address these nonlinear effects effectively.

Hence, it was decided to decouple the physics, and only perform a simplified fluid study. For this, the 2D model of the geometry was conducted in COMSOL. The geometry mirrors that discussed in the fluid simulation section (7.2.1). Similar to what was discussed earlier, the valve opening was introduced by creating a offset (0.8 micron) to the contacting surfaces. Segregated solver was used with default settings.

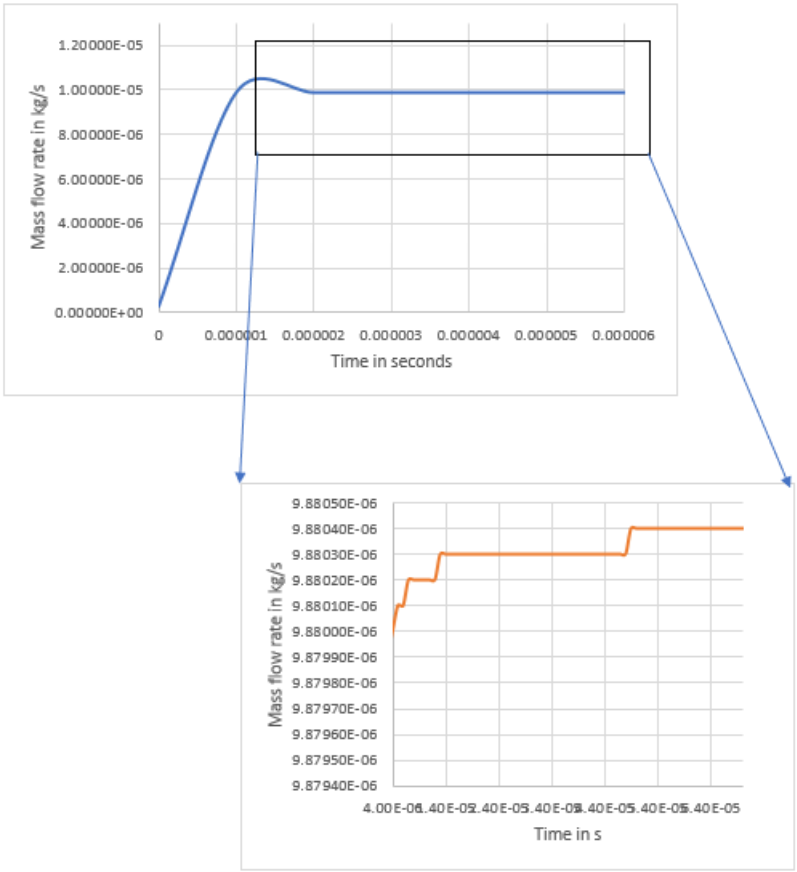


Figure 7.29: Transient flow behaviour of the 2D geometry, indicating the setting time

.

From first glance it seems like the flow reaches steady behaviour in around 2 $\mu$s, however, on closer inspection there were still very minute flow changes until flow reached steady state in about 40 $\mu$s. This suggests that the fluid flow reacts instantaneously to changes in the valving chamber. However, caution is warranted as dynamics related to plunger behavior and the effects of moving mesh in response to actuation voltage are neglected which could further dampen the flow and affect the response time.

Nonetheless, one could argue that this provides insight into the response behavior of the valve system. Also, it can be inferred that the piezo response time is the limiting factor in achieving response times on the order of microseconds. Although literature on simulating the response time of microvalves is scarce, achieving such low response times is not uncommon [31].

For an in-depth analysis of transient behavior, sophisticated models can be developed that accurately represent the geometry and account for the various physics involved.

Therefore, in summary, the response time of the system can be adjusted by changing other driving parameters for the piezo actuator. The estimated response time of 4ms is well within the system requirements for this design while meeting constrains on power and voltage levels.

# 8

# Proposed design

The complete 3D design of the valve along with the actuator and holder which would be able to tested to slot into with the micropropulsion system is shown in Figure 8.1 This prototype design is envisioned to be used in tests described in section 10.2. The microvalve along with the valve housing fits within the volume requirements put forth for this thesis. Adjustments may be needed to the holder design if different interconnectors are used than the one designed for as mentioned in section 6.7 .

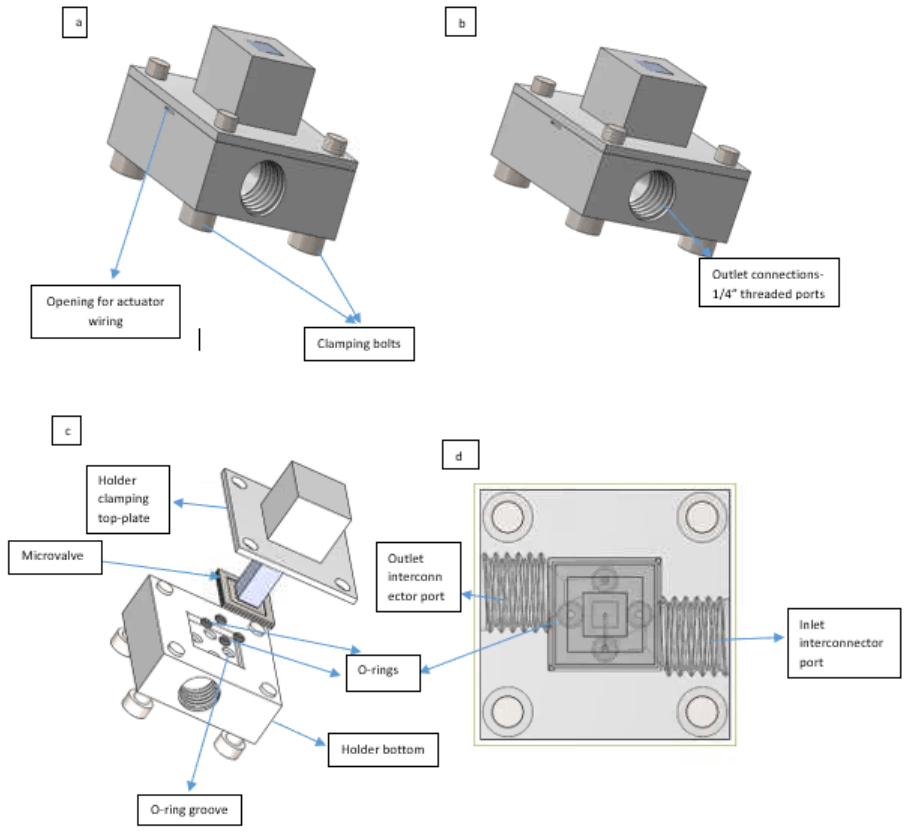


Figure 8.1: (a) Top isometric view of the microvalve in the 3-D printed valve holder (b) Bottom isometric view of the holder with threads to enable connections with other systems (c) Exploded view of the entire design along with holder and microvalve (d) Cross-section of assembled microvalve holder

The overall size of the microvalve along with the holder is 20mm x 20mm x 17 mm. As can be seen from

the figure, an opening is provided for the actuator wiring, along with that the clamping bolts will help with the pre-stressing of the actuator when it is installed. This pres-stress should be carefully managed to ensure that the structure is not damaged due to excessive stress.

A breakdown of the mass estimation of the engineering model of the microvalve assembly in the propulsion system can be seen in Table 8.1.

| Component | Mass | Comment |
|---|---|---|
| Microvalve-silicon chip | 0.1 g | From CAD model |
| Piezo actuator | 1 g | COTS |
| Orings+Fastners | 2.4 g | From CAD model |
| Holder | 6.5 g | 3D printed PTFE material- From CAD mode. However note that this can vary significantly if you use any other material like transparent resin ( which is the preferred choice for this thesis) |
| Total | 10 g | |

Table 8.1: Mass estimation of the microvalve assembly

As can be seen from the table above, the mass of the whole microvalve is 10g which is above the requirement set forth for this study. However, this is primarily due to the large valve housing that is required for the valve. This housing is suitable for the test model and at this level of the maturity of the overall propulsion design, it meets the interfacing requirements. As the design maturity increases, attempts must be made to explore chip to chip bonding for the thruster and valve which will then eliminate the bulky valve housing bringing the mass well within the requirement. One thing to note is that the overall mass budget for the propulsion system should also be checked to see if there is any margin available within the total mass requirement of 75g. The numbers for the rest of the propulsion system are derived from the micropropulsion payload demonstrator report from Leon Turmaine. [68]. The relevance of Leon's study to this thesis was discussed at the beginning of the report. The main objective of this research is to come up with a MEMS valve design to be manufactured in-house replacing the COTS valve. It can be seen that it satisfies the overall mass budget. As previously stated, the design should be further optimised for the final flight model.

| Component | Mass | Comment |
|---|---|---|
| Aluminium metal plate | 4 g | From Leon Turmaine thesis |
| Sensor, PCB +electronics | 15 g | From Leon Turmaine thesis |
| VLM & LPM thruster | 20 g | From Leon Turmaine thesis |
| Valve | 20 g | The valve has been designed for VLM thruster, assuming the same design is modified for LPM |
| Tubing | 1 g | From Leon Turmaine thesis |
| Wiring | 5 g | From Leon Turmaine thesis |
| PEEK manifold | 1 g | From Leon Turmaine thesis |
| PEEK check valve | 1,5 g | From Leon Turmaine thesis |
| Propellant | 0,5 g | From Leon Turmaine thesis |
| Delfi-PQ interface structure | 5 g | From Leon Turmaine thesis |
| Propellant storage | 2 g | From Leon Turmaine thesis |
| Total mass | 75 g | Meets the mass budget |

# 9

# MEMS fabrication process

## 9.1. Introduction

MEMS technology is the process to fabricate tiny devices or systems with electrical and mechanical components combined in a single circuit to perform different tasks. They are fabricated using Integrated Circuit batch processing technology. These MEMS devices have the ability to control, actuate and sense objects at the micro level. They are usually fabricated by sophisticated manipulation of silicon or other substrates using micro-machining processes wherein IC technology exploit the electrical properties of silicon, MEMS makes use of both the mechanical and electrical properties of silicon to fabricate electro-mechanical components. MEMS generally comprises of micro-sensors, micro-actuators, micro-electronics and micro-structures all on the same silicon ship. micro-sensors senses the change in the system environment's by measuring physical, magnetic, electrical, chemical properties and send the signal in response to the measured parameter. These signals are then processed by the micro-electronics which sends the command to the micro-actuators to respond to the environment. This chapter will discuss the various fabrication techniques used for manufacture of micro or nano devices. This will also entail the challenges involved in fabrication and various reliability issues that need to be accounted for in the design or overall working of the system.
Recent innovations in the field of micro and nano fabrication have created an array of technologies which have achieved an adequate level of maturity for the manufacture of commercial products of micro or nano level with dimensions less than $1\ \mu$m. These available techniques are used to fabricate wide variety of equipments right from novel electronics, sensors, gyroscopes, accelerometers, magnetic to biological and chemical devices. Generally most of the MEMS microvalves are fabricated using surface, bulk micro machining or high-aspect-ratio micro-machining (HARM). They employ the use of patterning, adding or subtracting additional layer on the substrates using a variety of lithography, thin film deposition, bonding and etching techniques. [5],[52].

Before diving into the different fabrication process which are commonly used, it is important to investigate the different materials used as the substrate for micro-machining. The primacy of the use of silicon in the MEMS industry will be discussed in the next section along withe the other commonly used materials as substrate or additional layers using bonding techniques [2].

## 9.2. Materials used for micro-machining

Silicon continues to be the most prevalent substrate in MEMS from past few decades and will continue to dominate the areas of miniaturisation. The desirable characteristics that make silicon the widespread material for the micro-scale devices are listed below:

1. Being abundantly available it is an inexpensive material and highly reliable making it an ideal material for sensors

2. The crystalline structure of the silicon provides for adequate electrical and mechanical properties to be used in microelectronics and microstructures.

3. Having high yield strength hence does not rupture or fracture easily with repeated cycles of mechanical stress

4. Due to large know-how and infrastructure of the Silicon Integrated circuit industry, high level of precise fabrication and reproducibility can be achieved in batch fabrication of devices on wafers

5. Having low thermal expansion silicon is mostly insensitive to thermal shock and inert with most acidic compounds making the thermal and chemical properties greatly suited for the MEMS industry

6. The homogenous crystal structure of silicon makes anisotropic and isotropic etching easily realisable for creating microstructures.

7. The electrical properties can be tuned by doping silicon with impurities which makes it a great material for various applications.

8. Due to the mechanical properties and available fabrication technologies creating patterned and raised structures can be achieved to a high degree of precision.

9. Silicon is highly compatible and hence can easily be integrated with the electronic components and other circuitry making it a great hit as MEMs substrate

10. Extensive technology portfolio available to glue the silicon chip to substrate material

The technical know-how to produce micro scale devices is readily available on silicon making it the desired substance in MEMS industry. Other materials used for MEMS devices are Germanium (Ge), Silicon Germanium (SiGe) or Gallium arsenide (GaAs) since the crystalline structure of these semiconductors is analogous to silicon [52]. However, the machining technologies available for these materials is not fully realised to make patterns and structures with grooves. Moreover, the other non-semiconductor substrate that are being realised for MEMS include glass, ceramics, polymers. Glass substrates is another common substrate for bonding silicone rubber in case of membrane valves. For membrane valve composite of silicone/parylene is most common material used in various designs especially for thermo-pneumatic actuation. But still the development and research for the use of these substances has a long way to go. The feasibility, precision, the technology readiness level and the cost of machining the materials plays an important role in MEMS. The capabilities and the technologies to support the fabrication process on silicon substrate has been appreciably developed leading to the explosive growth of silicon in the industry. The range of other materials used as additive films and materials in MEMS as sacrificial layer for further patterning include polymers, silicon compounds, and other metallic compounds ( Au, Cu, Al)

The above section gives the general overview of the materials commonly used for the fabrication of microvalve. Since the micro-machining process involving silicon is highly matured it is a commonly used substrate. But that does not limit the use of other materials for substrates like glass, pyrex. Various other materials would be required to realise the overall design of the microvalve right from Al layer to provide for the electrical connection, Silicon Carbide (SiC) to provide for the electrical isolation between Si and Al or using thin membranes like PDMS or other polymers for the plunger. The different wafers would need be bonded which could involve using high temperature gold (Au bonding) or other epoxy bonding.

## 9.3. Bulk micro-machining

This is the most common type of process used to produce MEMS. It defines structures by selectively etching inside a substrate or in other terms removing a part of the substrate. It is one of the oldest and most commercially successful techniques used for the manufacture of MEMS components. It is a subtractive process which employs techniques like wet etching, dry etching and substrate etching to make pits, channels or grooves.
Usually silicon wafers are used as substrates, since they can easily be wet etched anisotropically to produce highly regular structures. Silicon anisotropic wet etch constitutes an important technique in bulk micromachining.

### 9.3.1. Wet Etching

This is one of the common techniques to thin down silicon wafer. It involves the etching of material by immersing it in liquid etchants. Etching is generally used to etch out thin films that were deposited during

masking process or passivity. Besides thin film etching it can also be used to selectively remove a part of the substrate layer to create microstructures (plates, beams, etc). Selectivity and directionality plays an important role in etching. Selectivity refers to the degree to which the etchant can differentiate between the masking layer and the etching layer. Directionality refers to the etch profile under the mask. The etchants can be anisotropic or isotropic as seen in figure 9.2. In anisotropic etching the etchants attacks the material differently in different directions which depends on the dissolution rate of the etchant, concentration and the temperature, with etching being faster along preferred crystallographic direction. The structures formed in the substate depend on the crystal orientation of the material. In isotropic etching the etchant attacks the material in all the directions. For Isotropic etching of silicon a combination of $HF/HNO_3/ CH_3COOH$ is usually preferred. Usually glass plate (transparent) coated with chromium or Gold plate (opaque) is used for masking purposes. Glass can be isotropically etched using the $HF/HNO_3$ combination with etches having considerable roughness. Longer etching time require robust masking for which bonded silicon is used.
Silicon anisotropic wet etch is one of the preferred methods for bulk micromachining process. The three most important silicon etchants are potassium hydroxide (KOH), ethylene diamine pyrochatechol (EDP) and tetramethyl ammonium hydroxide (TMAH). All three etchants attack silicon along preferred crystal direction. Usually KOH is used to etch the silicon layer or the silicon nitride layer used as passivation layer [77]. Dopant levels can affect the etch rate by KOH with effectively stopping it at high doping levels. To selectively etch the silicon substrate, boron is doped in the structure which leads to the doped region unaffected. This helps in creating controllable thickness microstructures. Common masking materials for anistropic wet etchants are silicon dioxide and nitride with the latter being preferred for longer etch time. The crystallographic plane which shows the slowest etch is the (111) plane. These characteristic can be used to employ beams, membranes and other mechanical structures. Fig.9.1 shows an anistropic etch profile for (a) profile in which the (111) plane shows the slowest etch rate forming a trapezoidal or V groove in a (100) silicon wafer, whereas in (b) profile the (111) profile forms a vertical sidewalls in the (110) silicon wafers.

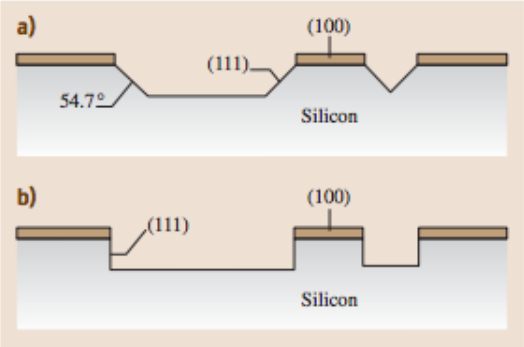


Figure 9.1: Anisotropic etch profiles for (a) 100 and (b) 110 silicon wafers [5]

.


Figure 9.2: Profile for isotropic (a) and anisotropic (b) etch through a photoresist (PR) mask [5]

.

### 9.3.2. Dry Etching

This process is another attractive alternative to wet etching. They offer several advantages over wet etching in terms of possibility of smaller lines to be patterned and higher anisotropicity. However, the selectivity of dry etching is lower than wet etchants and moreover the masking materials have finite etching rate. There are three types of dry etching techniques: high pressure plasma etching, reactive ion etching (RIE) and ion milling. Ion milling is a physical process that uses accelerated inert ions striking the surface to be etched

perpendicularly to remove the substrate. The main characteristics are very low etch rates and poor selectivity therefore, used to etch very thin layers. In High pressure plasma etching highly reactive species react with the material to be etched. The end products are volatile which diffuses the old material exposing the new material to the reactive material. This method provides directionality leading to higher vertical etch rate than lateral one. In RIE etching also known as ion assisted etching is a combination of chemical and physical processes. On collision of the incident ions from the plasma the surfaces to be etched get activated that is when reactive species react with the material. Like the previous technique the etch rate for the vertical direction is faster than lateral direction. To increase the etch anisotropy, sidewall passivation methods like deep reactive ion etching (DRIE) are used. In this method, passivation deposition and etching steps are performed sequentially in a 2 cycle process. One of the designs presented in previous chapter by NASA employed this technique as microvalve fabrication technique.

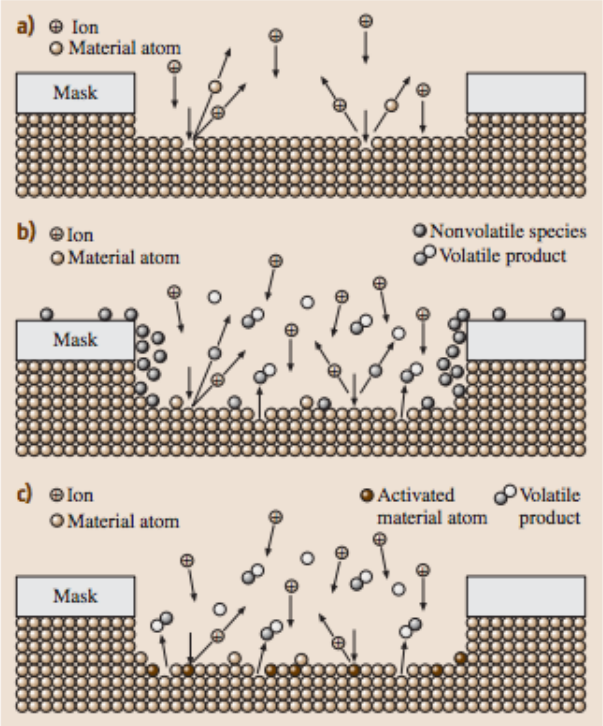


Figure 9.3: Simplified representation of etching mechanism: (1) ion milling, (b) high-pressure plasma etching (c) reactive ion etching (RIE) [5]

.

## 9.4. Surface micro machining

Unlike the bulk micro-machining this process creates micro structures on top of a substrate.This process employs the use of thin film deposition and selective etching over a substrate to produce structures. One of the main advantages of this process over the bulk micro-machining is the extremely small sizes that can be obtained. This technique also provide easy integration with the on-chip electronics for increase functionality. However, this process limits the number of layers that can be deposited. Various micro-actuators, micro-sensors employ this technique. The basic surface micro-machining process is illustrated in figure **??**. First step of this process is the growth of sacrificial layer on the silicon substrate which is then patterned. After which the structural material is deposited and patterned which is anchored to the substrate through the openings created in the sacrificial layer in the previous step. Later the sacrificial layer is removed resulting in the creation of required microstructure.

Dissolved water process sequence (a) KOH etch (b) deep B diffusion (c) shallow B diffusion (d) silicon-glass anodic bon (e) release in EDP The most common sacrificial and structural material are phosphosilicate glass (PSG) and polysilicon whereas low temperature oxide is generally used as sacrificial layer. There are other combinations available as well but based on the design and the choice of the sacrificial layer plays an

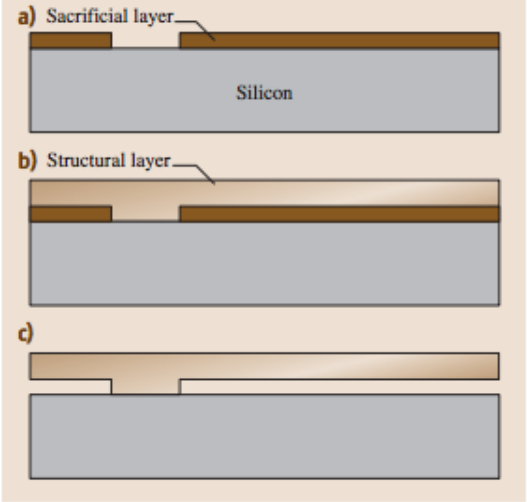


Figure 9.4: Basic surface micro-machining process [5]

.

important part for desired properties and specific applications. Some of the important requirements include

1. Ease of deposition

2. Mechanical properties

3. Deposition rate

4. Electrical conductivity

5. Thermal budget

For the success of surface machining process successful removal of all the sacrificial layer is necessary to free all the structural elements that will be actuated. This step is responsible for curtailing the yield and MEMS reliability issues due to stiction. It occurs when the structural elements stick to the substrate. Capillary forces from the liquids as well as electrostatic forces also produce permanent adhesion after the system has dried.

All the methods mentioned here are important MEMS fabrication techniques which are commonly used to build microstructures. This section dealt the more important techniques used in the EKL lab for MEMS manufacturing. The next section will detail the fabrication steps to be undertaken for producing the design. Due to these steps, the constraints imposed on the design itself have been envisioned and explained in the previous chapters.

## 9.5. Fabrication Plan

Since the design of the microvalve needs to be fabricated in-house it is essential to understand the processes followed by Else Kooi Lab. On discussion with Professor Henk van Zeijl and Francesco Stallone, from Else Kooi Laboratory at TU Delft, the specific process steps are presented in the next paragraphs. The cross sectional view of the valve can be seen in figure 9.5

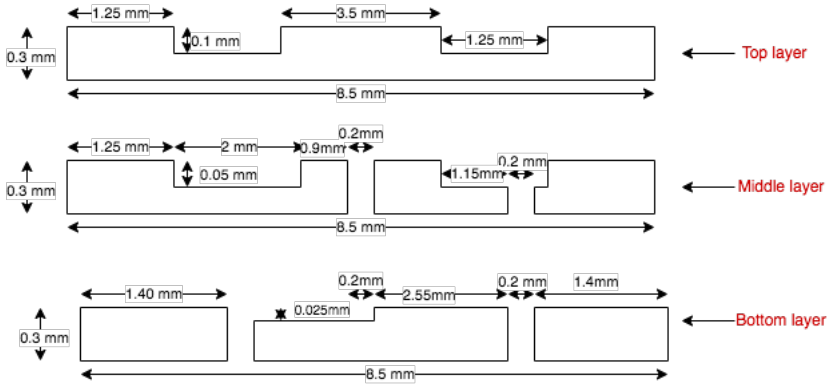


Figure 9.5: Cross sectional view of the valve design: not drawn to scale. Note: Aspect ratio of the rectangular channel is 0.2

The complete diagram with the steps for the fabrication of the three different layers is shown in figure 9.6. The 3 different layers can be processed in the same single wafer with multiple masks which can then be diced and stacked on top of each other. A single wafer can yield more than 50 valve chips. The micro-fabrication process involves two main steps: photolithography and etching.

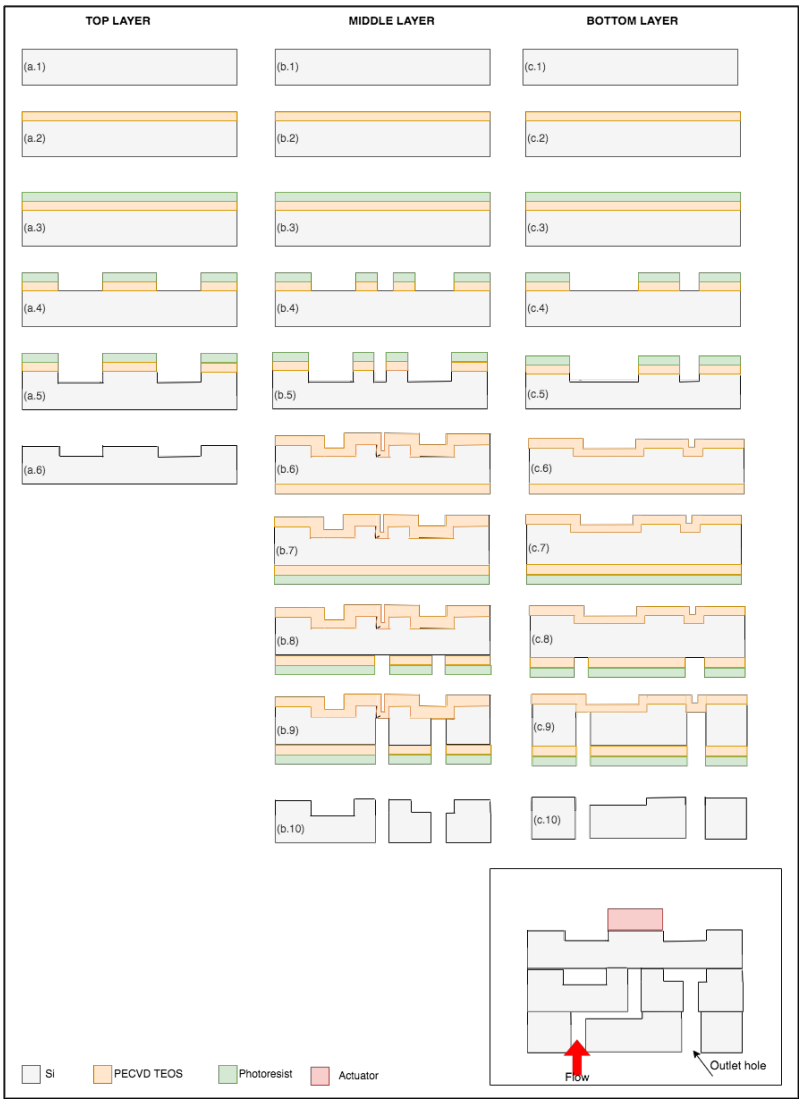


Figure 9.6: Process flow diagram showing the steps of manufacturing for the three layers. On the bottom right, cross section of the valve with all three layers bonded together along with the actuator

Please note: The starting steps for the three layers shown in the above figure 9.6 follow the same general process flow which will be described below, however each will require different photomask based on the pattern required. The steps for the manufacturing for the above process flow diagram is given below:

a.1,b.1,c.1 The starting material is a 100 mm double sided polished silicon wafer with thickness of 300 $\mu$ m. The specifications of the silicon wafer used at EKL are given in table 9.7

| | | | |
|---|---|---|---|
| Diameter: | 100 ±0.3 mm | Surface Finish: | Double Side Polished |
| Grade: | Prime | Flats: | 2, SEMI-Std. |
| Growth: | FZ | TTV: | <5 µm |
| Type/Dopant: | P/B | Bow: | <30 µm |
| Orientation: | <100> ±0.5° | Warp: | <30 µm |
| Resistivity: | >1000 Ohm-cm | Particles: | <10@0.3 µm |
| Thickness: | 300 ±10 µm | **Quantity:** | **25 pcs** |

Figure 9.7: Silicon wafer specification from EKL lab

a.2,b.2,c.2 On top of the silicon wafer, a masking layer of 2 $\mu$ PECVD TEOS (Plasma Enhanced Chemical Vapour Deposition tetraethoxysilane) silicon oxide is deposited. This step usually takes around 5-10 mins. This is done, so that during the etching process, only the exposed silicon surfaces gets etched while the rest can remain un-attacked. For larger etching cavities, usually the photoresist does not survive the entire etching process. It is typically not resistant to harsh plasma etching conditions hence to ensure that the unexposed silicon also does not also from get etched, a hard-mask of oxide is used.

a.3,b.3,c.3 Photoresist (AZ3012) is deposited on the substrate as a next step.

a.4,b.4,c.4 This coated wafer is then placed in a mask aligner in very close proximity to the photomask (with the pattern required on the silicon wafer). The photomask is patterned opaque layer of chromium on an optically flat glass plate. The relative positions of the photomask and the wafer needs to be correctly lined up with the reference masks or pre-existing pattern on the wafer. Mask alignment is an important step and is required to be accurate to within 0.5-1 micrometers.
Ultraviolet (UV) light is then turned on and the clear areas of the wafer that are not covered by the opaque areas of the photomask are exposed to light. The exposure time is generally between 3-10 seconds and should be carefully controlled to the required amount. The areas of the photoresist ( positive photoresist) that were exposed to light become readily soluble and then removed in the developer solution. This step creates the replication of the photomask pattern.
After the photoresist is stripped off from the required area, the TEOS oxide layer is etched by immersing the wafers in Buffered Hydrofluoric acid (BHF). It is a mixture of a buffering agent, such as ammonium fluoride $NH_4F$ and HF. This solution normally etches thermally grown oxide at approximately 120 nanometers per minute.

a.5,b.5,c.5 Now the exposed area of the silicon wafer, the trenches are anisotropicaly DRIE ( deep- reactive ion etching) etched.

a.6 The first layer is ready after the photoresist layer is removed using oxygen plasma etching and TEOS with BHF, standard wafer cleaning is carried out with $HNO_3$.

b.6, c.6 After stripping the photoresist with plasma cleaning and removing TEOS with BHF, a layer of 2 $\mu$m of silicon dioxide is deposited on both sides of the wafer to form the hard mask of the cavities. This hard mask on the top surface acts as a landing layer for the etching step for the through-holes. The etching stops at the oxide layer preventing the etching machine from being damaged.

b.7,c.7,b.8,c.8 For fabrication of through-holes, a photoresist layer is deposited at the bottom surface and the desired pattern is created through exposure of photomask to UV light, after which TEOS layer is stripped with BHF.

b.9,c.9 the inlet and outlet holes are anisotropicaly etched

b.10,c.10 Following cleaning and removal of hard masks and photoresists layers, the different silicon dyes are sliced and are ready to be bonded together.

11. Bonding between the silicon wafers and Si-PZT occurs via a eutectic bonding process using Die Bonder-T-3000-Pro equipment in which a patterned Ti/Au layer is deposited on the micro-machined silicon wafer. After proper alignment and clamping of the wafers, gold eutectic bonding at 400 celsius temperatures followed by annealing at 1100 degree celsius is carried out for ensuring bond strength.

12. Once the silicon structures are ready, the bonding between the piezoelectric components and silicon components was achieved using a titanium-platinum-gold multilayer film and heating to approximately 300°C in a reducing atmosphere. The bonding technology allows thin, electrically conductive bonds to be formed between dissimilar materials with minimal amounts of applied pressure during bonding. The process was optimized to produce mechanically robust, void-free bonds. The absence of voids can be verified through scanning electron microscope examinations of bond cross-sections.

After the 2D design of the microvalve defining the different layers and materials, L-edit is used to create the different masks which is then supplied to the EKL laboratory.
The fabrication process involved, the thickness of the layers used, the design rules, etching rates, exposure times, mask alignment play a major role in the successful design and operation of the device. Hence, designing a microvalve with less complex fabrication steps would be desirable. This would also reduce the risk of failure.

### 9.5.1. Fabrication of Valve Housing

The fabrication approach put forth for this thesis is a hybrid integration method, using a combination of 3-D printing and micro machining techniques to achieve the desired device. Rapid prototyping involving 3D printed valve holder allow for faster and easy interconnection of the valve to the other fluidic accessories. This can be seen in figure 9.8 which depicts the prototype of the holder based on the aforementioned design. The resin 3D printed holder provides structural support, helps in better visualisation of the fluid and the most importantly ensures tighter clamping to reduce leakage loss. It also makes it easier to make modifications to the holder design as and when required. Whereas, for the flight model steel or other material for the holder design may be considered.

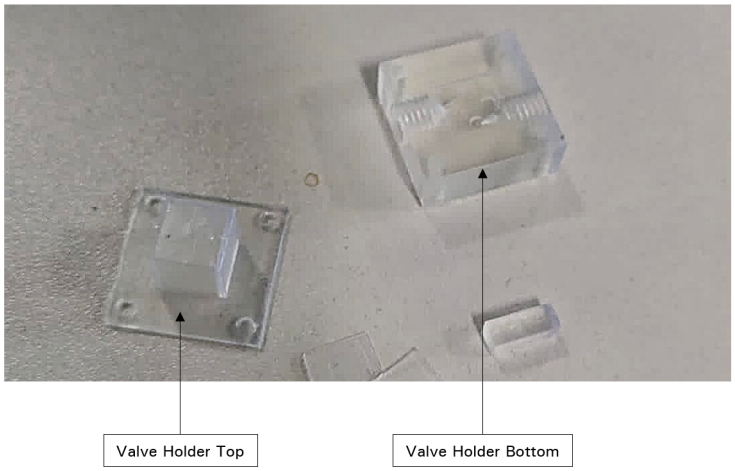


Figure 9.8: Prototype of Resin 3D printed valve housing based on the design presented in this study

## 9.6. Risk Analysis

In this section, a number of potential challenges involved in the development of the valve system are discussed. The analysis is done by using a risk assessment matrix, which combines the likelihood of occurrence and the consequence of the occurrence to provide an indication of the risk. Although some of the risks have already been mitigated to an extent in the design choices made in the Chapters 4, 5 and 6, there could still be problems in the manufacturing phase of the system. Since, the fabrication process deals with MEMS micro-machining and due to different masks sets, etch tolerances, and complex processes a number reasons can contribute to device failure. In keeping with Systems Engineering design philosophy, risks are defined as low, moderate and high probability. Furthermore, a marginal consequence is seen as small reduction in

technical performance of the fabricated chip, a critical consequence as the design performance questionable and catastrophic is seen as system failure. These risks will be mitigated to eliminate or reduce the chance of occurrence while some of these risks are to be assessed and modified during the testing phase.

Some of the potential failure modes during and after the fabrication process are:

1. With multiple lithography steps being performed on the wafer, accurate alignment of wafer and mask every time an exposure is performed is a critical step to match the relative position of the structure. Misalignment of marks for the design features on the wafer can lead to faulty designs and it's extremely crucial to have correct position and angle of the mask feature on the wafer

2. During photolithography a number of fabrication issues can occur such as the wafer might incomplete contact or poor adhesion of the photoresist film with the Si sample or residuals of the photomask itself left on the substrate during expose phase. Further, the conditions of exposure dose and incorrect development time can also lead to non-uniformity of the patterned structures.

3. The developer solution in the lithography step might remove the photoresist from the unwanted regions of the silicon wafer, losing more photoresist than required which can impact the succeeding etching steps.

4. Coating a non-uniform and non-conformal photoresist film on a silicon wafer can be another fabrication risk which can ultimately impact end result.

5. The DRIE process is a pulsed and time-multiplexed etching, requiring repeated sequence of etching and passivation. This iterative cyclic processing methods manifests in scalloped sidewalls in trenches as seen in image 9.9.The different sizes of these scallops formed depend on DRIE recipe conditions. These rough surfaces can affect the fluid flow and cause small turbulences in the fluid passing through them.

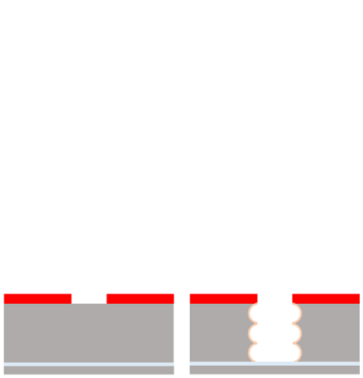

(a) Creation of scallop figures during dry etching process [51]

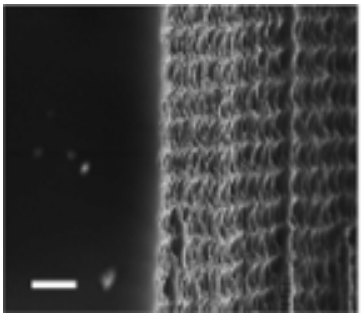

(b) SEM imaged of the wafer tranches where the scalloping is visible. The author mentioned that with more RF power applied during the etching process, the smoother the cavities [51]

Figure 9.9: Cross sectional image of the fabricated DRIE scallop

6. The oxide layer from the exposed parts of the silicon after the photolithography step might not be fully removed, which might affect the etch rate during DRIE step. Hence, the etching will vary from wafer to wafer and also on the success of the preceding steps making it difficult to achieve good reproducibility across devices.

7. Precision in etching process to achieve really low tolerances of the etched membrane cavities/trench and through holes etching in comparison to desired dimension can be challenging. Dry etching process is based on ion bombardment, it is dis-homogenous process and achieving high uniformity is challenging. The edges might etch faster than the centre, usually the machines try to maintain 3% variation limit between central and outer edges. Main challenges associated with dry etching include achievable anisotropic/vertical sidewall profile, uniform etch rate across the wafer and good selectivity.

8. Silicon wafers suffer from bow (deviation of the surfaces from centre point), having small convex/concave surfaces are not inherently perfectly flat, this can hamper valve sealing, causing leakage.

9. Wet etching is an isotropic and anistropic etching process and can lead to unwanted release of structure due to over etching or under-etching during wet-etching. It occurs at the extruded corners and can cause curved edges of the mask pattern on the silicon wafer. This can then lead to faulty features or additional Si substrate being etched away causing bigger structures than desirable. In case of important faulty feature profile, the device can be rendered completely faulty.

10. Stress concentration at the edges due to residual or fabrication induced stress in layers can lead to device failure. Etching process is required for creating trenches in the membranes. If etching recipe is not controlled, this can lead to thin areas or corners where stress can build up due to multiple load cycling leading to breakage.

11. Precise alignment when bonding the three layers is extremely critical for device success.

12. High residual stress can be generated at the bond interface due to local volumetric expansion during the eutectic formation. This can cause a bond failure

13. In case of eutectic bonding, a gold layer of few hundred nanometers is deposited conformally on the entire patterned silicon wafer, so this intermediate layer has a finite thickness and can change the eventual channel height of the device.

14. Assembly of piezo on the silicon structure can lead to membrane breakage if not aligned properly. Piezo stack actuator are a highly stiff material compared to membrane structures, careful but tight assembly of the two is crucial for the device performance

15. The distance between the membrane and piezo structure when prestressing not fine tuned can lead to loss of stroke and can also cause higher forces on the membrane than designed for. This is a risk and can cause the structure to deform permanently.

16. Slight Mismatch in mating faces (piezo to holder surface) can cause edge squeezing and high pressure at localised spots, often resulting in PZT ceramic damage. When using to secure load to piezo actuator, excess glue should be avoided and should only contact the mounting plates. Otherwise, it can cause mechanical failure.

| | | | | |
|---|---|---|---|---|
| **Likelihood** | High | 5,13 | 1 | |
| | Moderate | 8,9 | 12 | 14,15,11 |
| | Low | 2,3,4 | 7,10,6 | 16 |
| | | Marginal | Critical | Catastrophic |
| | | **Impact** | | |

Figure 9.10: Risk matrix, showing the risk each poses to the development of the system

The probability of occurrence of mask misalignment is determined to be high because it is a complex step increasing chances of poor alignment. This is an important step which also impacts subsequent fabrication processes. Using alignment features and contact aligner tool, likelihood of misalignment can be reduced but not completely negated. In best case scenario, alignment upto 1-1.5 $\mu$m is achievable relative to hole structures of 200 $\mu$m is not significant, but if it becomes couple of micron difference, the impact for the design can be critical but not catastrophic.

Risk 2, 3, 4 have been given low probability of occurrence because of the wide knowledge bank of EKL process engineers. These steps have been improved over the time at EKL and have proven to give good results. Risk 4 employs a spin coating method to deposit a thin layer. The acceleration step of the spinner ensures spreading of the liquid resist layer until the edge of the wafer during which most of the solvent evaporates. The thickness is controlled by the viscosity, evaporation rate and the spin rate which is generally uniform across the substrate. In addition, these standard steps are first characterised on the test wafer for required dosage and exposure parameters so these steps can be corrected to achieve desired features so as to not complicate associated processing. The non-uniformity of the photo-resist can be easily inspected through naked eye due to different reflectance and colour variations, making it easy to correct for it. These high order effects lead to either decrease in feature size or loss of sharpness of corners which does not have a major impact on

the design performance.
Risk 5 has been identified as high chance of occurrence because it is almost not possible to have smooth DRIE trench walls since it is inherent to the process itself. The 2 step etching process repeats many time and rotates between silicon etching and polymer deposition step (to protect the sidewalls from further etch), creating distinctive undulating sidewalls. It is possible to optimise the DRIE etch process parameters, predominately the etch cycle time to minimise scalloping, but not completely. Another way to flatten out the edges is thought high temperature ( > 1000 °C) treatment in hydrogen environment, but such temperatures can lead to other problems. Some literature have studied the impact of channels with rough side-elements [82],[35]. It was observed that the surface roughness increased the friction factor, with increased pressure drop than predicted and causing early transition to turbulent flow. However, the fabricated result of the DRIE process with bumpy surface in the form of the scallops in micro-units, rather than an ideal vertical plane has been listed as minimal impact. Since the Reynold's number for the design was very low, chances of turbulent flow was low. Moreover, they have only been validated with very limited data by the authors. To provide a more reliable guide for various micro-channel applications, this needs to be tested to study the effect of the surface roughness on the fluid flow.

Risk 6 is likely to not occur because the even after the BHF treatment to remove oxide, the wafer is still cleaned with $HNO_3$ buff and water buff to ensure all the unwanted layers are removed. However, the impact of occurrence can be critical since it will also affect the subsequent process recipe and etch cycles.
Impact of risk 11,14, and 15 can have damaging effect, since the actuator and the valve needs to work in harmony for proper valve performance. The probability of occurrence is high since it will require sophisticated tools and adept skills to ensure precise alignment of different parts of the valve design and fine-tuning of the pre-stress when loading the piezo. Manifestation of residual stresses in micro-systems, as highlighted in risk 12 can have high impact on the device behaviour. The multiplicity of complex and interrelated causes that can cause the residual stress during bonding process, particularly caused due to unequal thermal expansion coefficients in different materials. However, a lot of research suggest that the likelihood of residual stress development is relatively high [57], [26], [13]. Since, the design presented in this thesis involves bonding of multiple layers including PZT and Si. However the extent of impact shows the most variability, with very high impact in some cases while none in some. If the stresses are high, it affects the mechanical behaviour of the material: lowering the material stiffness, or in some cases also cause buckling of the component. Silicon are brittle materials, if the stress is sufficiently large it can cause a crack or result in fracture of the substrate rendering the device useless. However, it is difficult to quantify the residual stresses owing it its dependence on a number of causes.
The result of bowing in silicon wafer can cause interference with the resultant quality of processing steps. For example, bowing in chips means not having correct focal distance across the entire substrate during photolithography steps resulting in features being out-of-focus and having reduced resolution. It also impacts the uniformity of etching process. Bowing is commonly present in most of the silicon wafers, however the impact of can be few nanometers gaps which can render the device not being fully leakage prone, which would mean lesser lifetime of the mission than anticipated. But it would not classify the mission a failure, so risk 8 is marked low on impact.
Risk 13 is an inherent cause of the eutectic bonding process and cannot be avoided but the effect of it is not detrimental for system performance. This is because the intermediate layer of gold that is deposited on the silicon substrate is few nanometers which means, it will change in the aspect ratio of the channels but the influence is not mission failure. The undercut during wet etching is quite common in wet etching process, mostly caused by isotropic nature of the process or either by the long exposure of the substrate to the etchant. This can lead to more removal of the oxide layer than required, exposing the silicon substrate to ion bombardment during DRIE. This leads to bigger features than required, which relatively might not deliver on it's functionalities however, with reduced performance. So risk 9 is of moderate likelihood with minimal impact.
Risk 12 mentioned stress specifically during bonding process, however stress are also generated along various steps of the fabrication process. These stresses if not generated evenly along the entire substrate can concentrate at weak spots causing the device to break altogether during operation. Since, attempts have been made to avoid extremely thin structures in the design, lowering the possibility of stress concentration at corners or edges in case of risk 10. However, if generated can be detrimental hence critical. Across-wafer uniformity in the plasma etching is difficult to achieve, since it is challenging to produce similar plasma conditions on every location on the wafer to achieve uniform process control and usually this variation at EKL is around 3%. DRIE etching is typically a tradeoff between rate, uniformity and selectivity, which is contradictory in

itself. High etching rate is achieved by using high-energy ion bombardment whereas for high selectivity and good critical dimension control low energy plasma is required. It is important that the recipe for DRIE and the process parameters are optimised on a test wafer so that near tight tolerances on critical dimensions can be achieved, especially for channels in the bottom layers. Since the etching process at EKL is quite mature and capable of achieving relatively good etching profiles, risk 7 is assigned as low in likelihood but it is still an important step and can be critical to the overall device performance itself, hence impact is critical and must be monitored. Risk 16 has low likelihood of occurrence since the mating of the flat face of the holder is designed to be centered on and applied uniformly over on the flat surface of the piezo. The surfaces are flat and smooth by ensuring good parallelism between the two, improper mounting can be avoided. Further, using any epoxy cured at temperature lower than 80 °C or using Thorlabs High temperature or vaccuum epoxy should be used. Mitigating this risk is important as edge squeezing as shown in image 9.11, can lead to failure of the actuator which is catastrophic to reliable operation hence comprising the mission.

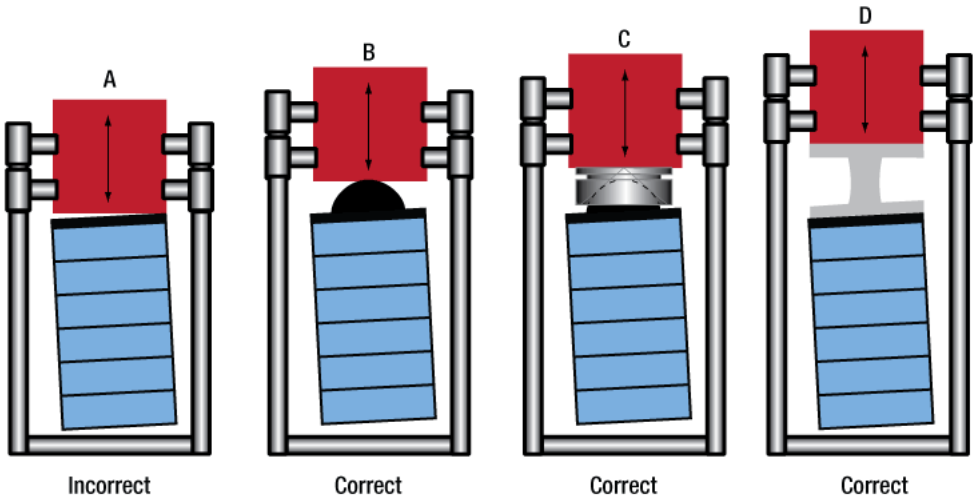


Figure 9.11: Reference of proper and improper mounting of PZT actuator (Thorlabs)

### 9.6.1. Mitigation strategies

The conclusion for the risk analysis is that risks 1,11,12,14,15 have higher chances of occurrence and are critical to mission success. Therefore, these needs careful monitoring and mitigated to eliminate or reduce the chance of occurrence. All the risks should also be watched to ensure they are kept in check. Risk 1- can be addressed by incorporating proper alignment markers on the mask layout. Contact aligner machine is used at EKL for photolithography step where the wafer and mask are brought close to each other and aligned relative to one another using the feature marks, there are two sets of optics to aid in the alignment process. So these high precision reference alignment features should be large, distinct and easily identifiable ( example having open window region to easily find them on the wafer) and locatable ( for example having pointers). Reference of these alignment markers can be found in image 9.12. Furthermore, these alignment markers should be located within the travel range of the alignment equipment. Typically, two alignment marks are necessary to correct for x and y and also fine offset in rotation between wafer and mask. Even though this risk might not be fully eliminated, the impact can be significantly reduced.

The amount of stress in risk 12 is difficult to quantify since it is process specific and can also vary case to case, hence, it needs to be watched and will require testing of the valve design itself in the clean room. Risk 14 and 15 need to be mitigated by careful monitoring of the integration process, and employing advanced tools for alignment using expert skills either at EKL. The best case scenario would be to send the fabricated chip to piezo actuator companies themselves and getting it aligned, pre-stressed and integrated by them. Risk 11 can also be addressed by careful monitoring of the integration and bonding process itself and ensuring it is executed precisely either by research student or EKL process engineers.

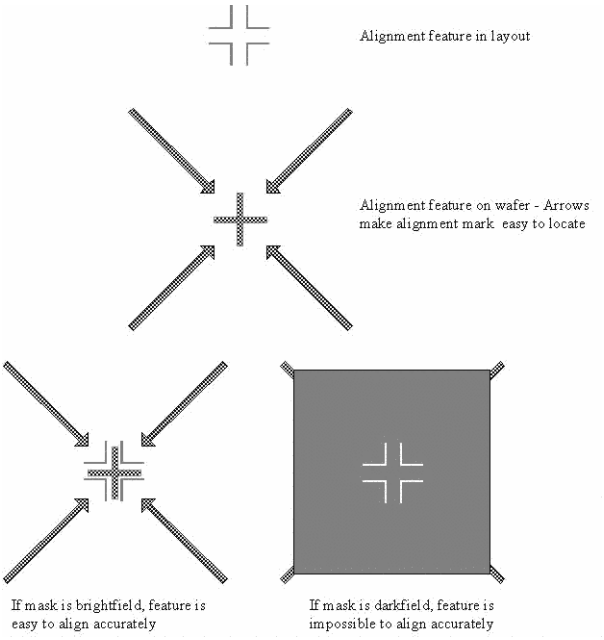


Figure 9.12: Reference of alignment marker design such that they are easy to identify and locate [1]

Overall probability of all risks mentioned above can be reduced if they are executed by the EKL process engineer, since they have wide knowledge of the devices and fabrication techniques, possibility of mistakes can be eliminated. A research collaboration between EKL and TU Delft Space engineering department can be formed, to employ the expertise of the process engineers at EKL. After talking to Francesco Stallone, he is keen on supporting the activity, this will be beneficial reduce the time of development and reduce the risks of failure.

# 10

# Design Verification and Test Plan

## 10.1. Verification of Design

Verification of the design adhering to the requirements set forth at the start of the report is the final step of this thesis. For this, each requirement is taken individually and a method of verification is given to each which can be seen in table . The four sets of verification are test, analysis, inspection and review of design.

| Identifier | Requirement | Verification |
|---|---|---|
| MIC-SYST-100 | The total mass of the valve shall not be higher than 4g | Review of design + Inspection Scale-test |
| MIC-SYST-200 | The total size of the propulsion system shall be within 42 mm x 42 mm x 30 mm (including thrusters, valve, electronic board, harness, connector and propellant storage tank | Review of design + Inspection Fit test |
| MIC-SYST-300 | The total microvalve chip size shall be within 10mm x10mm x 1mm | Review of design + Inspection |
| MIC-SYST-400 | The valve shall be able to handle a maximum operating differential pressure of 5 bar when closed | Analysis + Testing |
| MIC-SYST-500 | The peak consumption of the valve shall not be higher than 5W | Testing |
| MIC-SYST-600 | The system shall be able to operate on a single unregulated supply bus voltage of 3 [VDC] to 4.1 [VDC] | Testing |
| MIC-PERF-100 | The mass flow rate delivered by the system shall be 5g/hr at a maximum differential pressure of 5 bar | Analysis+ Testing |
| MIC-PERF-200 | The maximum response time of the system shall be between 0.3ms-8.3ms | Testing |
| MIC-PERF-300 | The maximum leak rate shall be $<10^{-5}$ scc/s at maximum operating pressure | Testing |
| MIC-FUN-100 | The system shall supply no propellant to the thruster in idle mode or when no power is supplied to the system | Review of design + Testing |
| MIC-FUN-200 | The system shall be able to operate on liquid $H_20$ | Review of design + Testing |
| MIC-FUN-300 | The valve system shall be able to provide proportional flow control | Review of design + Testing |
| MIC-INT-100 | The microvalve shall stay at a temperature range of +5 °C and +85 °C during all mission phase when the propulsion system operation are required | Thermal cyclic Test |
| MIC-INT-200 | The fluidic interface of the valve system shall be compatible with the thruster housing and the propellant tank | Review of design + Testing |
| MIC-INT-300 | The mechanical and electrical interface with the valve system and other micro-propulsion components shall respect payload's technical budgets | Review of design + Testing |

Table 10.1: Verification method for the valve requirements

## 10.2. Proposed Test Campaign

The contingent objective of the thesis is to check compliance of the valve in design for the preliminary configuration of the micro-propulsion system. This section covers all the tests that will be required to be carried out to verify that the design meets the requirements and exhibits desired performance. Moreover, since an in-house MEMS based microvalve design at the space department is first of its kind and due of lack of experience in operation and testing of this kind of valves, these tests will also help the team learn of any of the potential causes of failures or drawbacks that was not anticipated in the design phase. This can be used to optimise the current design further eventually leading to the development of flight model of the design. So the tests proposed in this section are for the engineering model of the design to qualify that the design meets the performance requirements. Four stage testing is proposed to be conducted: component testing, fit check of the assembly to ensure all the physical and software interfaces between the valve and the rest of the components are in place, section test with just the valve and VLM thruster and finally full system testing.

However, please note since this is new design with advanced fabrication techniques the valve component itself should be thoroughly tested before moving to full assembly testing ( with thruster and propellant tank). Results from the analysis conducted in Chapter 6,7 should be tested to characterise the valve behaviour. The stand-alone test of the valve is crucial to ensure that design is behaving as intended to before it is integrated with other components of the propulsion system. The test plan will answer the following questions

- Where will the test be conducted?
- Which instruments will be required for the test?
- What is the proposed test set-up?
- What is the expected outcome of the test?

### 10.2.1. Component testing

Testing of the valve component is required to check whether it lives upto the required specifications and to also eliminate/address potential damage to the rest of the system.

**TEST-COM-01: Visual inspection**:
The objective of this test is to ensure that the silicon chips are properly fabrication with visual signs of damage.
**When**: TBD
**Where**: 3ME
**Components**: Microscope, Microvalve
**Procedure**: When the silicon chips are fabricated, keep them under the under the microscope, and then observe each chip to locate for any visible micro-cracks, blocked channels, inlet/outlet holes, breakage of the chip. Chips with any signs of damage will be rendered useless on testing hence those chips can be already discarded.

**TEST-COM-02: Mass-Test**:
The mass of the microvalve should be measured to ensure it meets the mass budget of the propulsion system.
**Which Requirement- MIC-SYST-100**
**When**: TBD
**Where**: Anywhere
**Components**: Scaltec SBC33 digital weighing scale, Microvalve
**Procedure**: Once all the components are fabricated, place the components on the scale and weigh them individually and then weigh the entire valve assembly together.

**TEST-COM-03: Microvalve-Static measurement**:
The microvalve presented in this thesis is an active microvalve, with opening and closing being controlled by an actuator. Before carrying out fluidic testing, the static testing of the valve without the propellant needs to be carried out to ensure that the microvalve structure actuates when all the parts of the microvalve are integrated together. **Which Requirement**- MIC-SYST-600
**When**: TBD
**Where**: Optics lab in 3ME

**Components**: Probing station, displacement sensor, DC supply, Microvalve chip
**Procedure**: For this fluidic connections are not required. The actuation is controlled by a DC power supply and the displacement of the microvalve is measured using a displacement sensor. Due to the size of the chip, it is recommended to observe the valving mechanism under a microscope with a camera. For this it is preferred to use the probing station at the Optics lab in 3ME, the instrument consists of probing connectors to allow for electrical connections with the piezo, the wafer is placed in the chuck and the displacement (actuation) can be observed under the microscope and measured using displacement sensors. This allows to test the response of the wafer to the external electrical stimulus. Voltage-up sweep and voltage down sweep should be carried out to characterise the displacement response of the actuator. Even though the piezo-actuator used is a commercially available design whose specifications are already provided by the manufacturer. But since, the actuator will be integrated to the silicon devices, the characterisation of the membrane displacement to the voltage applied is required. These results also feeds in to the fluidic test to test the required mass flow rate at the predicted actuator stroke.
**Expected Output**: Static displacement of the assembled PZT stacked actuator and valve membrane to the applied voltage were measured

**TEST-COM-04: Leak test:**
The leak test needs to be completed first before moving on to mass flow test in order to find any possible leakage in the system. If leak test is not performed first it might render the mass flow test useless in case of leakage. Furthermore, since this is the first test with fluidic connections, the valve will also tested to check if it can hold pressures upto 5 bar. Incluidng the test for the leakage rate which occurs over time within the system. This is necessary to ensure the propulsion system can be operated in space for the required lifetime duration. In short, the goal of this test is to determine the leak rate of the feed system. Ideally the leak rate of the feed system should be lower than the requirement of the valve given in Section 2.5.1. This is to ensure majority of the propellant will through the valve and not leak into the environment.
**Which Requirement**:MIC-SYST-400, MIC-PERF-300
**When**: TBD
**Where**: Clean room in 3ME or Aerospace
**Components**: Valve, reservoir with water, Tubings, empty reservoir, mass flow sensor, pressure sensor
**Procedure**: Valve leakage is tested using a hydrostatic test (i.e, the test medium is water). The reservoir was first filled with predetermined amount of water. The No power is supplied to the valve, i.e., the valve is left in closed off. The required pressure is applied and is held constant for an extended period of time ( atleast 1 day). The rate of flow through the flow sensor is measured at the valve upstream and downstream at the start and stop times. This will give the leakage though the valve assembly. The pressure drop across the system also should be detected after the testing time. Both external leakage to the environment through visual inspection and internal leakage using measuring instruments must be performed. The leak rate against different differential pressure should be characterised as well, for this the applied pressure should be varied and the test should be carried out again.

**TEST-COM-05: Microvalve-fluidic measurement**:
This test will be completed to characterise the valve in terms of flow rate for different pressure and voltage levels and leakage. Schematic of the components used for the test setup in shown in Figure 10.1
In addition, the figure 10.2 shows the proposed setup that can be utilised as the test setup to characterise the valve performance. **Experimental setup:**

- Propellant tank: A cartridge/reservoir filled with water and attached to the micro-valve inlet line
- Pressure supply/pressure controller to pressurize the water in the tank
- 5 bar pressure sensor located at tank outlet compatible with water
- Power supply for valve actuation
- Microvalve with the customised holder interface to allow for fluidic connection
- A mass flow sensor in the valve downstream
- An empty reservoir

- Sensor signal readout ( A computer containing the software program capable of controlling, monitoring and communicating to the different components, so that all the control signals to the pressure source, voltage source and measurement signals from the sensors can be routed to the computer)

**Which Requirement**: MIC-PERF-100, MIC-FUN-100, MIC-FUN-200, MIC-SYST-500
**When**: TBD
**Where**: Clean room in Aerospace or 3ME
**Expected Output**: The flow rate-actuation voltage characteristics of the voltage under constant differential pressure conditions. Since, it is a normally closed valve, when the voltage is zero the expected flow rate should be close to zero and as the voltage is increased, the mass flow rate will increase until a point the actuator reaches its maximum stroke length. Furthermore, the mass flow measurements at varying differential pressure values can be recorded.

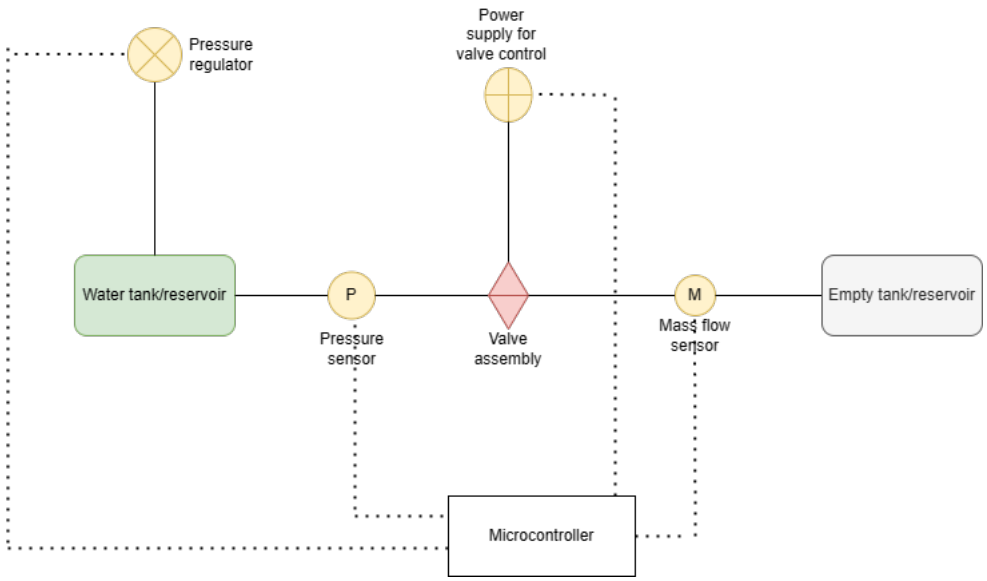


Figure 10.1: Schematic for the test setup for testing the valve assembly along with electronic and data interfaces

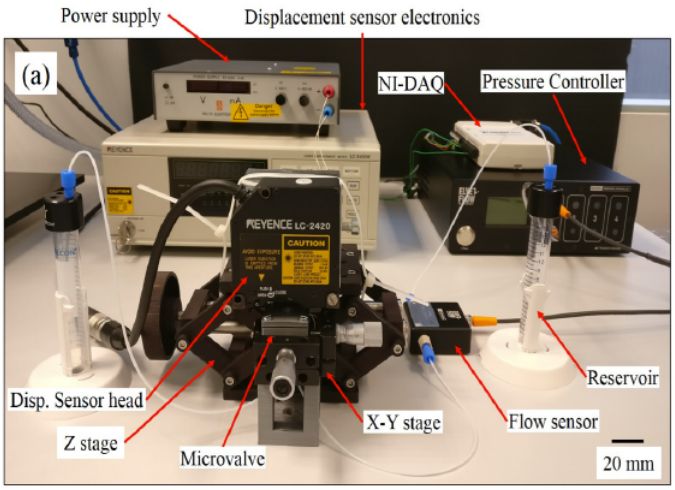


Figure 10.2: Proposed test setup [[25]]

**TEST-COM-06: Response time:** The goal of this test is to determine the spike time required to open the valve at the required operating pressure. From the analysis it is seen that the response time of the valve assembly is determined purely by the response time of the actuator itself. Hence, this must be verified with

this test. The time required to open the valve and achieve the steady mass flow rate at the operating pressure. Furthermore, it will also validate the power consumption of the system.
**Which Requirement**: MIC-PERF-200
**When**: TBD
**Where**: Clean room in Aerospace or 3ME
**Components**: The test setup in figure 10.1
**Procedure**: The response time of the microvalve can be measured by using a square wave that can be varied from 0-150V. A functional generator with an amplifier can be used to generate this input signal. The valve opening time must be measured at the operating pressure. Simultaneously once the valve is fully opened, the valve closing time must be recorded. The response time of the valve assembly is dictated by the piezo actuator and there is an inherent hysteresis observed in these actuators hence the opening and closing time will be different. Subsequently, the test must be repeated multiple times to test the repeatability since there are possible occurrences of stiction of the membrane to the valve seat delaying the opening time or possibility of fine particles which might affect the valve closing time.
**Expected Output**: Graph of mass flow rate over time. The mass flow rate should be measured at different on and off cycle to test for the spike time.

### 10.2.2. Fit test

After the valve is characterised separately and checking for performances between actual and expected. The next step must be integration of the entire propulsion assembly. This test is to confirm that all the components fit the designated volume requirements and that the different components can be properly integrated with each other in terms of physical and software connections. The inlet and outlet port of the valve holder has been designed for specific kind of tubings and fluidic interconnections. If different components are used, the valve holder must be re-designed to meet the mating requirements between the valve, tubings, thruster and other fluid accessories.
**Requirement**: MIC-INT-100
**When**: TBD
**Components**: water feed system, tubings, micro-controller, pressure sensor, mass sensor, valve assembly, VLM thruster.
**Procedure**: Place all the components in the correct location and connect all the wirings from the valve, thruster and pressure sensors to the micro-controller. Check that all components adhere to the requirement using measurement equipment.

### 10.2.3. Assembly and Integration Testing

After the individual components-valve and the thruster are individually tested followed by the fit test, the integration between the components needs to be tested to ensure a fully functional assembly of the system. The tests listed for these include the fill and leak test, electrical testing and mass flow test, thrust profile test and pressure profile testing. The scope of this thesis is only valve design and testing of the engineering model of this valve design. However, to address the integration capability of the valve with the thrusters which is part of the research question for this study, a proposal is provided on how the valve housing can be evolved to interface with the thrusters, which can be seen in figure 10.3. The concept design is given as reference that the valve housing can accommodate two thrusters. Even though, in the design two VLM thrusters are shown, but in the future studies it can be evolved to fit LPM thruster. The dimensions of the housing are 35mm x 31mm x 17mm.

Tests with the full propulsion system are not detailed but only highlighted. For details for the test campaign for the full propulsion system, the thesis of Leon Turmaine [68] should be referred, with a modification of replacing the Lee valve with the MEMS valve mentioned in this thesis. Furthermore, the valve is only designed to work with water, however research by Fazal [16] with a comparable design have been tested with gas flows. Hence, the author thinks this MEMS valve could also work for gas flows and hence should be tested for. The same valve design could work for both water and gas flows, with some design modification to accommodate the performance requirement for gaseous flows. The test setup for testing of the valve with the entire propulsion system can be seen in figure 10.4. The setup can be used to test the entire system or modified to test just the valve with the VLM thruster.

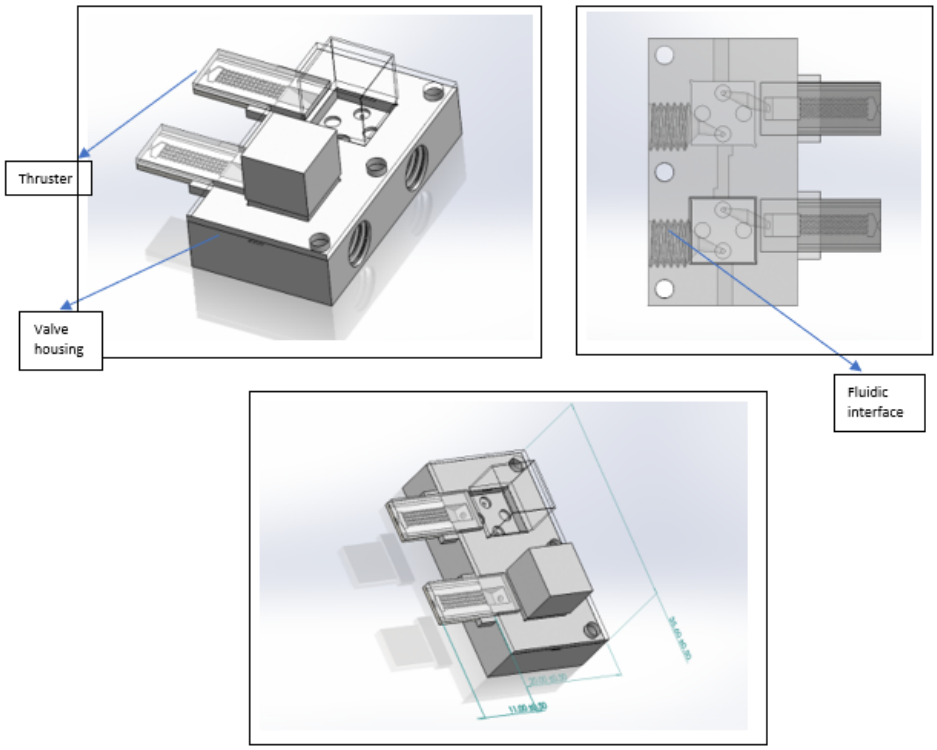


Figure 10.3: Different isometric view of the design proposal for interfacing the valve with the thruster

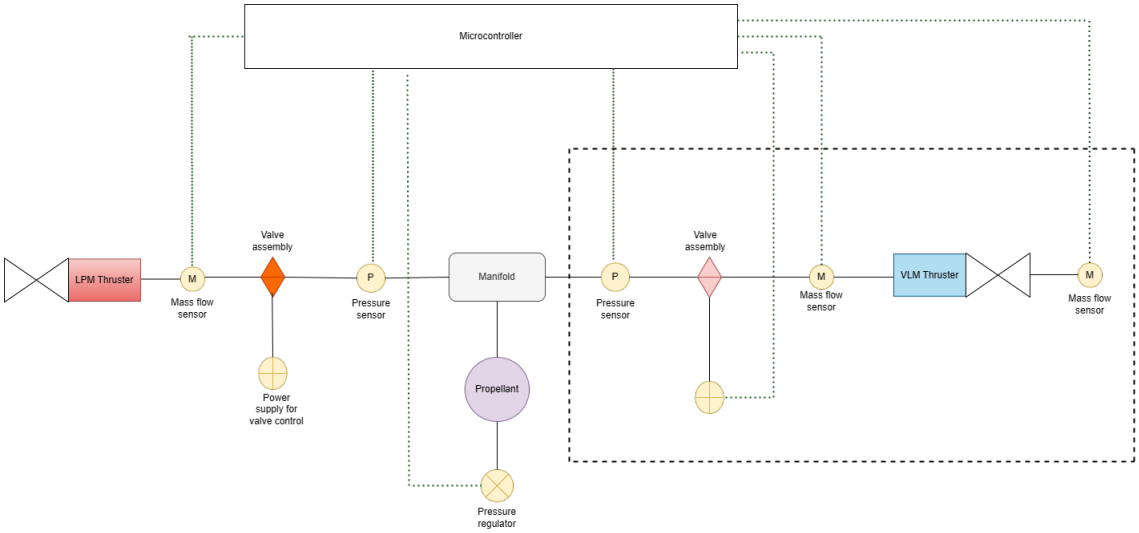


Figure 10.4: Schematic for the test setup for testing the valve assembly along with electronic and data interfaces

## 10.3. Risk Analysis

The engineering model once manufactured needs to be tested to ensure it meets the requirements and to assess if further changes are required to be qualified for the flight model. So in this section, the risks involved with the testing and operation of the engineering model of the valve are discussed. The risk analysis is done by use of a risk matrix, which will combine the likelihood and consequences of occurrence to provide an indication of the risk. Although, some of the risks have been mitigated in the design choices made in Chapter

5 and 6, whereas the problems that could arise in the manufacturing stage have been identified in Chapter 8. However, a number of risks can arise at the testing stage, affecting the test campaign. Identifying these risks early on, will allow mitigating or de-risking them. In keeping with Systems Engineering design philosophy, risks are defined as low, moderate and high probability. Furthermore, a marginal consequence is seen as small reduction in technical performance, a critical consequence as the mission success questionable and catastrophic is seen as system failure. These risks are to be iteratively assessed and modified during the testing phase of the system.

The risks mentioned here are mostly related to the component testing phase based on figure 10.4, some of the other risks that can arise during full propulsion system testing have not been included here. Please note, additional risks can arise when testing the full system.

| Risk | Probability | Consequence |
|---|---|---|
| Misalignment of the valve chip to the valve housing | Moderate | Catastrophic |
| Insufficient clamping force to the valve | Moderate | Catastrophic |
| Incompatible tubing and connector attachments between the valve and other components | Moderate | Critical |
| Manufacturing error of the valve components | Low-Moderate | Critical |
| Leakage at valve connections/fittings | Moderate | Marginal |
| Pressure sensor failure | Low | Critical |
| Mass sensor failure | Low | Critical |
| Valve stiction issue affecting valve closing and opening | Moderate-High | Critical |
| Valve leakage | Moderate-High | Critical |
| Bubble formation inside the valve causing flow rate instability | Moderate | Marginal |
| Fluidic resistances introduced by the path elements ( tubings between the valve and other components) | High | Critical |
| Test system inaccuracies | High | Critical |
| Valve breakage due to excessive force/pressure application | Low | Catastrophic |
| Debris/particle accumulation in valve causing seal issues | Low-Moderate | Critical |
| Repeatability issues | Moderate | Marginal |
| Valve hysteresis | Moderate-High | Marginal |

Table 10.2: Identified potential risks for the successful test campaign of the valve system

The probability of occurrence of the misalignment between valve chip and the housing is deemed as moderate since it is a manual work with possibility of human error. The consequence of this risk is catastrophic because the interfacing between the valve and the housing is an important step for being able to not just connect with the other components but also for fluid leakage which is undesirable. If the interconnection and the clamping force by the screws and pre-stress is not enough, there will be fluid leaking to the environment through gaps (least-resistance passage) with possibility of no water flowing to the outlet. This deems the entire system useless. Hence, risk 1 and 2 are critical steps in the testing phase. Risk 3 is about incompatibility with external tubings and interconnections, in which case operation of the propulsion system will pose a problem. The coupling interface has been designed to fit the existing components ( as in the 3ME cleanroom) hence, the likelihood of occurrence of this risk is moderate. However, if the components and tubings are changed the interconnections between them and the valve needs modification accordingly which can affect the overall valve design.
Risk 4 has been identified as lower occurrence probability, because the probable risks associated with manufacturing of valves have been identified in 9.6. There are still chances that some other manufacturing issues might arise that is not previously identified hence the risk is given low-moderate risk of occurrence. Depending on the kind of error, the risk can either be marginal or catastrophic. In general, this risk needs to be monitored since the impact of it is critical to the success of the testing. Chances of leakage at valve connections and other fittings is high but the overall consequence of it would be reduced test time for the overall mission which does not render the mission a failure hence not catastrophic. Risk 6 and 7 have lower probability of occurring since widely tested COTS components are used for the sensors. However, if these sensors fail, risk to the operation of the valve seems significant which would then require replacement of the sensors. However, if the failure occurs in flight, the consequence of these risks becomes catastrophic for the thrust control loop.

Risk 8 is given a high probability of occurrence because the stiction is a common problem in micro-devices, where a thin liquid layer between the silicon plates will work as adhesive due to capillary forces, which cannot be avoided during operation especially in this case, where the device is made with contact between the moving parts desirable. Impact of this risk can cause malfunctioning of the devices, however since the contact area is fairly reduced. The author predicts that if stiction occurs, it would cause problems in proper closing and opening of the valve either causing more leakage than desired during closing, or more force required by the piezo to open it to the required distance. This would be mean reduced performance of the valve than desired. Leakage in valves is a common problem, which is almost impossible to fully eliminate the chances of leaking. There are various reasons why leakage can occur, for example lack of tight connections, valve stiction, misalignment, manufacturing error, human error etc. Leakage is unfavourable and depending on how much the leakage occurs, the impact can be critical or catastrophic for the success of the system behaviour.
Risk 10 has a marginal impact on the valve performance, increasing the time needed to reach system equilibrium. And this effect can cause issues when precise and fast flow control is required. Occurrence of air bubbles inside micro-fluidic channels can occur because of several different origins and preventive measures should be taken right at the start of the test to eliminate them. In the design phase described in the previous chapters, calculate the mass flow rate for a given pressure based on the fluidic resistance of the valve alone. However, during the testing phase as shown in schematics 10.1, all the tubings between different components (shown in black lines) will add fluidic resistance. So the total flow resistance of the whole circuit ( pipe, sensor etc) is the sum of all the individual resistances of the elements. Then, the necessary pressure at the inlet to produce the desired flow rate is calculated from 6.28. Therefore, since the flow resistance has increased, more pressure would required at the inlet to produce the same mass flow rate compared to the designed value. It is anticipated that the fluidic resistance of the tubings would be fairly negligible compared to the valve resistance therefore the impact on the performance would marginal for risk 11.
Risk 12 has a high probability of test systems inaccuracies. Since the system and the design is to be tested for the first time, there can be many unknowns that are not accounted for. Some of the system inaccuracies can be un-calibrated sensors leading to inaccurate results, low detection limits of the selected sensors, human errors etc. Depending on the type of the inaccuracy during the test phase, the result can be marginal or critical. Risk 13 will cause catastrophic failure of the valve system rending the test campaign a failure. However, it has been awarded a lower occurrence probability since the valve has been designed to meet the pressure requirements with a certain factor of safety. If the pressure is applied above the maximum limit, then the system will break.
Most of the research papers mention about the particulate contamination in valves. Even though deionised water is used for the rest, there might be chances of particle residues, which are hard to remove. Various methods have been presented in the papers from having a filter in the fluidic circuit to having a concentric trench design to capture the debris. Having particles in the valve seating is not ideal, as these particles might get accumulated and would cause the two silicon plates to not have a proper contact between them leading to leakage issues. Even small micro gaps can lead to huge leakage which is certainly not desirable. Microfluidics devices suffer from repeatability issues as mentioned in risk 15. Since the MEMS fabrication techniques are employed, having the exact same features in all the chips is unheard of. Hence, performance characteristics of different chips might slightly vary. Moreover, due to stiction and hysteresis experienced in piezos as mentioned in risk 16, achieving consistent performance with the same parameters each time a test is performed can be difficult. This might lead to some loss of technical performance. Risk 16 is difference between the time/pressure at which the valve will open and then close again. Since the valve is driven by piezo actuators, which suffer from hystersis. This lag in reaction force affects the response time of the valve which also determines the control loop for the thruster. Higher response time is not catastrophic for the mission success but it does affect the system performance. Even though it can be mitigated, it cannot be totally eliminated and hence should be thoroughly tested for.

| | | | | | |
|---|---|---|---|---|---|
| **Likelihood** | High | | | 11,12 | |
| | Moderate-high | | | 4,8,9 | |
| | Moderate | | 5,10 | 3,15,16 | 1,2 |
| | Low-Moderate | | | 14 | |
| | Low | | | 3,6,7 | 13 |
| | | Negligible | Marginal | Critical | Catastrophic |
| | | **Impact** | | | |

Figure 10.5: Risk matrix showing the danger each risk pose to the test and development of the system

The conclusion of this risk analysis is that risks 1,2,3,15,16 need careful monitoring and mitigation during the test campaign and further development stage for the system. Risk 1, 2, 3 even though have been given as moderate chance of occurence, but since for the testing phase the valve holder is proposed to be 3-D printed. Any issues and changes required during the test phase itself, can be easily implemented due to faster development and turn-around times for 3D printed devices. Risk 3 will need careful monitoring especially when the entire propulsion system ( along with the thruster) is being tested. Since the design of the holder presented in Chapter 6 is only compatible with the Elveflow 1/4”-28 TPI microfluidic connectors and it should be ensured that the sensors selected also fit these connectors and the thruster housing. Finally risk 15 and 16 can be watched and followed as mitigation method. Priority should be given to thoroughly testing the valve alone first as this is the main focus of this study.

# 11

# Conclusion and Recommendation

## 11.1. Conclusion

The need for propulsion systems for small satellites like the PocketQubes initiated the requirement for a low thrust controllable thruster for attitude control, formation flying etc. For this, there was a need for fast acting propellant valves. In response to that, this thesis presents the design of a valve that shows the most promise of meeting the requirements for the propulsion system.

This thesis aims at answering the formulated research question: **How can a MEMS based valve be designed to be able to fit within the PocketQube volume budget and offer the advantage of in-house fabrication and proper integration with thruster housing?** With this primary objective in mind, the study presented the design considerations and selected a design solution that both adheres to the requirements and that is producible.

The major design criteria considered for this study were: performance, material compatibility, weight and reliability. The primary requirements are flow characterisation, propellant leakage and dynamic operation. The research questions mentioned in section 1.3 are deemed to be answered in a satisfactory manner. Question 1 was answered in chapters 4,6 and the motivation behind those choices are also detailed. The selection of the piezo actuator and the integration with the valve system are done to control a range of flows over a range of operating voltage. Proportional flow control of the propellant is achieved by controlling the extend of the upward displacement of the membrane by changing the applied voltage. There is a 4W peak power restriction for the propulsion system, and the power requirement for the proposed design is well below the budget. The power drawn by the valve system can also be adjusted by adjusting the drive frequency. Proportional flow control of the propellant is achieved by controlling the extend of the upward displacement of the

Reliability is also of utmost importance to achieve the mission objective because a malfunction could result in the risk of mission failure. One of the sub-questions listed in section 1.3, is obtained by having a simple design that is also easy to manufacture. At this stage of the study, there are no indications that the design presented in this report is unsuitable for meeting the requirements of a propulsion system for the picosatellite. However, this cannot be confirmed until the valve undergoes a testing campaign to understand the valve behaviour and the system performance. A careful review of the potential modes of failure both during manufacturing and testing was made in section 10.3, 9.6 and the probability of their occurrence. The extent to which these risks are design limitations can be understood from their effect on the mission.

To answer research question 2, chapter 9 details the fabrication plan to manufacture the valve, along with the different materials used for it. The design was conceptualised adhering to the possible manufacturing techniques and their limitations, which was done with continuous communication with fabrication engineer at EKL. The author has also anticipated possible manufacturing risks that should either be eliminated or mitigated for a functional design. Finally, research question 3 was answered by writing a verification plan for each of the system requirements, followed by the test plan for the system.

The valve has been designed as a fail safe in an event of power failure. When the voltage supply is switched off, the preload by the holder should ensure that the membrane shuts against the valve seat. However, it is essential that the prototype is built and undergoes substantial cycles of tests to ensure the reliability of the system. Leakage characterisation is another topic that needs test validation. Valve leakage represents another

critical requirement, challenging to analyze solely through theoretical means and necessitating validation through testing. Given that, at this stage of the study, leakage is only quantified analytically, and pre-stress on the actuator has been proposed in the design, there remains a possibility of impacting design reliability. One operational concern could be the susceptibility of microvalves to particle contamination from the fluid flow, which may cause these particles to adhere and compromise the sealing capability, subsequently leading to leakage. Utilizing high forces from the piezo actuator can aid in crushing the contaminants, thereby improving the situation.

Since an in-house active microvalve system is not tested in the department before, it is imperative to undergo full characterisation testing before it is assembled and tested with the thrusters. Furthermore, the conceptual design of the piezo actuator proposed in this study underwent many iterations and technical discussions with the supplier. This design would require testing on the part of the manufacturer to put forward tested performance specifications of the actuator. After having tested the design presented in this report, further optimisations and other incremental improvements to the design can be made as and when required in the future studies.

For the conceptual design of the system, the overall size of the microvalve with the holder from the CAD model is 20mm x 20mm x 17mm, which is limited due to the size of the piezo actuator whereas the size of just the microvalve is designed to be 8.5mm x 8.5mm x 0.9mm. Future studies can explore the possibility of compact package solutions of the microvalve. Chapter 9 and 10 provide a framework for future work on the design which will prove the feasibility of the design.

In conclusion, the design presented in this report has the potential to result in a functioning microvalve that can be relatively easily manufactured, has a good reaction time, low power consumption and a good dynamic range of flow control for liquids and, potentially for gases too.

## 11.2. Recommendations

Some of the recommendations for future studies are highlighted below:

- An attempt was made to set up a 2D simplified FSI model with piezoelectric, structural and fluidic physics to understand the transient flow behaviour. However, due to time and computational resource constraints it was not fully developed. Although tricky, future studies can investigate on developing FSI numerical models for the design to learn about the transient fluid characteristics in the microvalve that affect the overall propulsion system.

- As highlighted in the study, the holder is an important component for interfacing with other components as well as that its design is crucial to ensure leak tightness. At this stage, the holder design presented fulfils the requirements set forth for this research. It is able to provide interconnections with the thruster holder and the tank etc. It is imperative for testing purposes. However, as the thruster interfaces are evolved, dye attach technology or other zero-level packaging techniques (example reference 11.1) could be explored for valve holder interfaces to ensure a smaller device footprint.

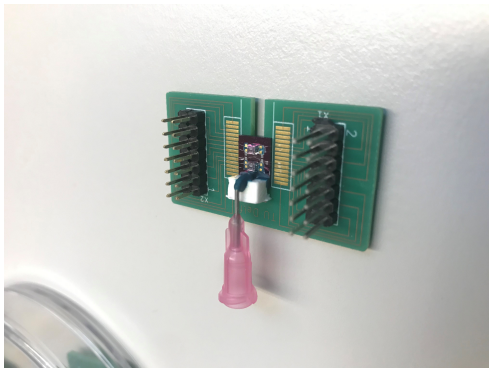

Figure 11.1: Thruster on the PCB with pressure sensor from Prof Henk van Zeijl at EWI

- The first version of the valve design put forth meets the volume and mass requirements, but it is still of a considerable size. And this is limited due to the size of the piezo actuator. Future optimization studies can explore the use of smaller piezo actuator configurations that meet the requirements.

# A

# Valve Seat Design Results

```
%% Input parameters
m_dot= 5; %  required mass flow rate in g/hr
m_dotkg = 5/(1000*3600); % in kg/s
d_in=0.0002;   % minimum inlet diameter in m
d_out=0.0002; % minimum outlet diameter in m
rho=1000; % density of water in kg/m3
mu=8.90e-4;  % dynamic viscosity of water in Pa-s
deltap=500000;  % differential pressure in Pa
k=1.1;  % for 90 degree bend
uncertainty= 0.05*deltap;

%% Reynolds number calculation
A=(pi*d_out^2)/4;
v=m_dotkg/(rho*A);
Re=(rho*v*d_out)/mu;  % Reynolds number

%% hydraulic resistance- static region
l4new=3e-4;      % length of circular pipe
d4new=2e-4;      % diamter of the circular pipe
r4new=d4new/2;  % radius of circular pipe
R4new=(8*mu*l4new)/(pi*(r4new^4));   % hydraulic
resistance
% Transistional Reynolds number is 15
Re1=(m_dotkg*d4new)/(mu*pi*(r4new^2));   % reynolds
number

% rectangular channel
lcase4=2.59e-3;
wcase4=1.2e-4;
hcase4=2.5e-5;
```

```
Acase4=wcase4*hcase4;
Rcase4=(12*mu*lcase4)/(wcase4*((hcase4)^3)*(1-
0.63*(hcase4/wcase4)));
Pcase4=2*(wcase4+hcase4);
hdia2=(4*Acase4)/Pcase4;
Re2=(m_dotkg*hdia2)/(mu*Acase4); % reynolds number
 % transistional reynolds number for rectangular
channels 30L/D<Ret<2300
LbyD=lcase4/hdia2;   %length to hydraulic diamter
ratio

%inlet in the middle
l7case4=3.3e-4;
d7case4=2e-4;
r7case4=d7case4/2;
R7case4=(8*mu*l7case4)/(pi*(r7case4^4));
Re3=(m_dotkg*d7case4)/(mu*pi*(r7case4^2));

% outlet pipe
l8n=5.5e-4;
d8n=2e-4;
r8n=d8n/2;
R8n=(8*mu*l8n)/(pi*(r8n^4));
Re4=(m_dotkg*d8n)/(mu*pi*(r8n^2));

preloss1=2*k*1/2*rho*v^2;

%% variable resistance
a32=1e-3;    % r1
a31= 1e-4;    % r0
s32=[0.001e-6,0.005e-6,0.01e-6,0.05e-6,0.1e-
6,0.23e-6,0.5e-6,1e-6,1.5e-6,1.55e-6,1.6e-6,1.75e-
6,1.8e-6,2e-6,2.3e-6,3e-6,3.5e-6,4e-6,4.5e-6,5e-
6,5.5e-6,6e-6,6.5e-6,7e-6,7.5e-6,8e-6,8.5e-6,9e-
6,9.5e-6,10e-6];
for i=1:length(s32)
%3.8046e-8;%2e-6;%2.5e-6;
R32(i)=(6*mu*log(a32/a31))/(pi*((s32(i))^3));
```

```
end

%% static resistance zig zag channel
l2n=7.5e-4;
w2n=1.2e-4;
h2n=2e-5;
R2n=(12*mu*l2n)/(w2n*((h2n)^3)*(1-0.63*(h2n/w2n)));

l3n=7.5e-4;
w3n=1.2e-4;
h3n=2e-5;
R3n=(12*mu*l3n)/(w3n*((h3n)^3)*(1-0.63*(h3n/w3n)));

l4n=1.09e-3;
w4n=1.2e-4;
h4n=2e-5;
R4n=(12*mu*l4n)/(w4n*((h4n)^3)*(1-0.63*(h4n/w4n)));

l5n=7.5e-4;
w5n=1.2e-4;
h5n=2e-5;
R5n=(12*mu*l5n)/(w5n*((h5n)^3)*(1-0.63*(h5n/w5n)));

l6n=7.5e-4;
w6n=1.2e-4;
h6n=2e-5;
R6n=(12*mu*l6n)/(w6n*((h6n)^3)*(1-0.63*(h6n/w6n)));

%% mass flow rate
R_case4=R4new+Rcase4+R7case4+R32+R8n; % with
straigh rectangular channel
R_case3=R4new+R2n+R3n+R4n+R5n+R6n+R7case4+R32+R8n;%
with zig zag channel
Rvar=R7case4+R32+R8n;
Qcase4=(deltap-2*preloss1-uncertainty)./R_case4;
%straight channel
Qcase3=(deltap-6*preloss1-uncertainty)./R_case3;
% zig zag
Qvar=(deltap)./Rvar;
```

```
mdotcase4=Qcase4*rho*3600*1000;    % straight
mdotcase3=Qcase3*rho*3600*1000;    %zigzag
mdotvar=Qvar*rho*1000*3600;        % only variable
value4=[s32*10^6;mdotcase4];
value3=[s32*10^6;mdotcase3];
%plot(s32*10^6,mdotvar)
%%
%plot(s32*10^6,mdot)
%hold on
plot(s32*10^6,mdotcase3)
hold on
plot(s32*10^6,mdotvar)
hold on
plot(s32*10^6,mdotcase4)
legend('zigzag+static','only variable
resistance','static+variable resistance')
%legend('zig zag rectangular channle','straight
rectangular resistance')
xlabel('Deflection in in micron')
ylabel ('Mass flow rate in g/hr')
title (' Effect of changing static resistance on
mass flow rate at constant inlet pressure')
%title (' Effect of incoporating static resistance
on mass flow rate at constant inlet pressure')

%% for straight+variable case
deltapminor=(2*preloss1/deltap)*100;
%Deltapstatic=Q*(R1n+R2n+R3n+R4n+R5n+R6n+R7n);
%Deltapstatic=Qcase3*(R1n+Rcase3+R7n+R8n);
Deltastat=Qcase4*(R4new+Rcase4+R7case4+R8n);
Deltapvariable=Qcase3.*(R32(15));
deltapper=(Deltastat(15)/deltap)*100;
deltapvariableper=(Deltapvariable(15)/deltap)*100;

%% Reynolds number calculation
A=(pi*d_out^2)/4;
v=m_dotkg/(rho*A);
Re=(rho*v*d_out)/mu;   % Reynolds number
```

# B

# Plunger Design Results

```
%% Input parameters- CASE 1
t1=[50e-6,100e-6,150e-6,200e-6,250e-6,300e-6];  %
thickness of the membrane in m
r=100e-6;  % radius of the valve seat inlet
W=5e5*pi*r^2;  % fluid force
b=6e-3;  % side length of the membrane
E=170e9;  % Young modulus of silicon

%deflection when force is applied at a cocentric
circle-- Closed case
for i=1:length(t1)
ymax(i)=(0.0611*W*b^2)/(E*t1(i)^3);  % max centre
deflection
end

value=ymax(4)*10^6;
% yyaxis left
 plot(t1*10^6,ymax*10^6)
xlabel('Thickness of the membrane in micron')
ylabel('Max centre deflection of the membrane in
micron')
title ('Deflection induced on the membrane by 5 bar
fluid pressure')


% Case when there is 10% assumed deflection->
stroke= 2.3e-6;  % required stroke calculated in
valve seat design-> assuming max centre deflection
of 2.3 micron
```

```
gap=0.1*stroke;  % assuming manufacturing defect
causes 10% gap height
t2=[50e-6,100e-6,150e-6,200e-6,250e-6,300e-6];

% Force required to be applied on the membrane to
produce a deflection of
% 10% of stroke
for i=1:length(t2)
F(i)=(E*(t2(i)^3)*gap)/(0.0138*b^2);
end
value=F(4);
pressure=value/(6*6*10^-6);
plot(t2*10^6,F);

%% Input paramters- CASE2- OPEN CONDITION
A3=3.5*3.5*10^-6;  % Area of the membrane cross-
section where the force is acting
b3=6*10^-3;  % side-length of the membrane
y3=2.3*10^-6;  % deflection between valve seat and
plunger-computed from valve seat model
E=170e9;
Ps=1;  % Pre-stress force from valve seat;

% for plunger -> force required to pull membrane up
by 2.3 micron in the centre- force acting just on
3.5x3.5mm. choice of 200mm
t=[50e-6,100e-6,150e-6,200e-6,250e-6,300e-6];
for i=1:length(t)
F(i)=(E*(t(i)^3)*y3*A3)/(0.0138*b3^4);
F_total(i)=F(i)+Ps;
k(i)=F_total(i)/y3;
end

yyaxis left
plot(t*10^6,F_total)
xlabel('Thickness of the membrane in micron')
ylabel('Required force in N')
yyaxis right
```

```
plot(t*10^6,k)
set(gca, 'YDir','reverse')
ylabel('Stiffness of the membrane in N/m')
legend('required actuator force','stiffness of the
membrane')
title ('Deflection of 2.3 micron: Required force
and stiffness of the membrane for different
membrane thickness')


%% Calculating fluid force for 10% manufacturing
defect and Case 3- derived from valve seat design
model
R_caserun=R4new+Rcase4+R7case4+R32;  % from valve
seat design matlab model
Deltahello=(Qcase4).*(R4new+Rcase4+R7case4+R32); %
form valve seat design matlab model
P2=5e5-Deltahello;  % fluid pressure acting on the
membrane
F2=P2*6*6*10^-6;  % fluid force on the
membrane/pre-stress force required
```

# C

# Piezo Results

```
%% Piezo results

d31=-320e-12;  %dielectric constant from
manufacturer
s11=17e-12;   % piezo compliance from manufacturer
S31=0.05/100;  % strain from manufacturer
A33=3*3*10^-6;  % cross-section area
l1=[5e-3,6e-3,7e-3,8e-3,9e-3]; % piezo length
kl=16/(2.3*10^-6);  % stiffness of membrane- from
numerical simulation

for i=1:length(l1)
stroke(i)=l1(i)*S31;
ka(i)=A33/(s11*l1(i)); % stiffness of piezo
F(i)=ka(i)*4.5*10^-6;  % free blocking force
end
newstroke=stroke*(ka/(ka+kl)); % reduced stroke due
to spring load
delta=(stroke-newstroke)*10^6;  % change in stroke
hysteris=(15/100)*stroke;
actualstroke=(newstroke-hysteris)*10^6;

plot(l1*10^3, actualstroke, 'o')
xlabel('Length of the piezo actuator in mm')
ylabel ('Maximum stroke of the actuator in micron')
%title (' Effect of changing static resistance on
mass flow rate at constant inlet pressure')
title ('Deflection vs Length curve for the piezo
actuator')
```

# Bibliography


[1] Mems nanotechnology exchange. https://www.mems-exchange.org/users/masks/intro-equipment.html. Accessed: 2023-03-20.

[2] Silicon as a mems material.

[3] Mohsen Akbari, David Sinton, and Majid Bahrami. Pressure drop in rectangular microchannels as compared with theory based on arbitrary cross section. *Journal of Fluids Engineering*, 131(4), 2009.

[4] Phillip W Barth. Silicon microvalves for gas flow control. In *Proceedings of the International Solid-State Sensors and Actuators Conference-TRANSDUCERS'95*, volume 2, pages 276–279. IEEE, 1995.

[5] Bharat Bhushan. *Springer handbook of nanotechnology*. Springer, 2017.

[6] ET Carlen and CH Mastrangelo. Paraffin actuated surface micromachined valves.

[7] Jorge Alejandro Carretero Benignos. *Measurement and modeling of the flow characteristics of micro disc valves*. PhD thesis, Massachusetts Institute of Technology, 2001.

[8] A Cervone, B Zandbergen, DC Guerrieri, M De Athayde Costa e Silva, I Krusharev, and H van Zeijl. Green micro-resistojet research at delft university of technology: new options for cubesat propulsion. *CEAS Space Journal*, 9(1):111–125, 2017.

[9] Angelo Cervone and Marsil AC. Silva. Micro-propulsion: State-of-the-art and challenges.

[10] Indrani Chakraborty, William C Tang, David P Bame, and Tony K Tang. Mems micro-valve for space applications. *Sensors and Actuators A: Physical*, 83(1-3):188–193, 2000.

[11] Allen Cowen, Greg Hames, D Monk, Steve Wilcenski, and Busbee Hardy. Soimumps handbook. *MEMSCAP Inc*, pages 2002–2011, 2011.

[12] Ravi A Deepak and Robert J Twiggs. Thinking out of the box: Space science beyond the cubesat. *Journal of Small Satellites*, 1(1):3–7, 2012.

[13] Elizabeth C Dickey, Colleen S Frazer, Thomas R Watkins, and Camden R Hubbard. Residual stresses in high-temperature ceramic eutectics. *Journal of the European Ceramic Society*, 19(13-14):2503–2509, 1999.

[14] Claudia Patricia Durasiewicz, Sophia Thekla Güntner, Philipp Klaus Maier, Wolfgang Hölzl, and Gabriele Schrag. Piezoelectric normally open microvalve with multiple valve seat trenches for medical applications. *Applied Sciences*, 11(19):9252, 2021.

[15] Eui-Hyeok Eh, Choonsup Lee, and Juergen Mueller. Normally-closed, leak-tight piezoelectric microvalve under ultra-high upstream pressure for integrated micropropulsion. In *The Sixteenth Annual International Conference on Micro Electro Mechanical Systems, 2003. MEMS-03 Kyoto. IEEE*, pages 80–83. IEEE, 2003.

[16] I Fazal and Michael Curt Elwenspoek. Design and analysis of a high pressure piezoelectric actuated microvalve. *Journal of micromechanics and microengineering*, 17(11):2366, 2007.

[17] Germán Ferreira, Artur Sucena, Luís L Ferrás, Fernando T Pinho, and Alexandre M Afonso. Hydrodynamic entrance length for laminar flow in microchannels with rectangular cross section. *Fluids*, 6(7): 240, 2021.

[18] Takashi Fukuda and Makoto Ryo Harada. Analysis of aspect ratio in a miniature rectangle channel for low frictional resistance. *Micromachines*, 12(12):1580, 2021.

[19] Paul Galambos, Jeffrey Lantz, Michael S Baker, Jaime McClain, Gregory R Bogart, and Robert Joseph Simonson. Active mems valves for flow control in a high-pressure micro-gas-analyzer. *Journal of Microelectromechanical Systems*, 20(5):1150–1162, 2011.

[20] Thomas George, Sam Young Bae, Indrani Chakraborty, Hillary Cherry, Christopher Evans, Beverley Eyre, Amanda A Green, Allan Hui, Kevin King, H Lynn Kim, et al. Mems technology at nasa's jet propulsion laboratory. In *Photonics for Space Environments VII*, volume 4134, pages 16–25. International Society for Optics and Photonics, 2000.

[21] Murali K Ghatkesar. Lecture 1 and 2 introduction thinfilms-bb, lecture 9 eklmumps jiawei, lecture 10 masks and design.

[22] Peter Gravesen, Jens Branebjerg, and O Søndergård Jensen. Microfluidics-a review. *Journal of micromechanics and microengineering*, 3(4):168, 1993.

[23] Maarten Groen. *Microvalves for precise dosing: proportional flow control on a chip*. PhD thesis, University of Twente, Netherlands, 11 2015.

[24] Maarten S Groen, Dannis M Brouwer, Remco J Wiegerink, and Joost C Lötters. Design considerations for a micromachined proportional control valve. *Micromachines*, 3(2):396–412, 2012.

[25] Arun Gunda. A proportionally controlled microvalve using a piezoelectric unimorph microactuator. 2019.

[26] Michael Huff. Residual stresses in deposited thin-film material layers for micro-and nano-systems manufacturing. *Micromachines*, 13(12):2084, 2022.

[27] Michael A Huff, Michael S Mettner, Theresa A Lober, and Martin A Schmidt. A pressure-balanced electrostatically-actuated microvalve. In *IEEE 4th Technical Digest on Solid-State Sensor and Actuator Workshop*, pages 123–127. IEEE, 1990.

[28] JP Khatait, W Lin, and WJ Lin. Design and development of orifice-type aerostatic thrust bearing. *SIMTech Technical Re-ports*, 6(1):7–12, 2005.

[29] Brian J Kirby. *Micro-and nanoscale fluid mechanics: transport in microfluidic devices*. Cambridge university press, 2010.

[30] Chandramoulee Krishnamoorthy and Afshin J Ghajar. Single-phase friction factor in micro-tubes: A critical review of measurement, instrumentation and data reduction techniques from 1991-2006. In *International Conference on Nanochannels, Microchannels, and Minichannels*, volume 4272, pages 813–825, 2007.

[31] Choonsup Lee and Eui-Hyeok Yang. A piezoelectric liquid-compatible microvalve for integrated micropropulsion. 2004.

[32] Curtis D. Lee and Ellis Meng. Mechanical properties of thin-film parylene–metal–parylene devices. *Frontiers in Mechanical Engineering*, 1:10, 2015. ISSN 2297-3079. doi: 10.3389/fmech.2015.00010. URL https://www.frontiersin.org/article/10.3389/fmech.2015.00010.

[33] Huei-Huang Lee. *Finite element simulations with ANSYS Workbench 18*. SDC publications, 2018.

[34] M.C. Louwerse. *Cold Gas Micro Propulsion*. PhD thesis, University of Twente, Netherlands, 10 2009. 10.3990/1.9789036529037.

[35] Hui Lu, Minghai Xu, Liang Gong, Xinyue Duan, and John C Chai. Effects of surface roughness in microchannel with passive heat transfer enhancement structures. *International Journal of Heat and Mass Transfer*, 148:119070, 2020.

[36] Andréas Manz, N Graber, and H áM Widmer. Miniaturized total chemical analysis systems: a novel concept for chemical sensing. *Sensors and actuators B: Chemical*, 1(1-6):244–248, 1990.

[37] M Micci. Low-power solid-state microwave thruster systems. In *Spacecraft Propulsion*, volume 465, page 203, 2000.

[38] David Mikaelian and Ben Jones. Modeling of capillary-driven microfluidic networks using electric circuit analogy. *SN Applied Sciences*, 2(3):1–19, 2020.

[39] Gian Luca Morini. Laminar-to-turbulent flow transition in microchannels. *Microscale Thermophysical Engineering*, 8(1):15–30, 2004.

[40] Juergen Mueller. A review and applicability assessment of mems-based microvalve technologies for microspacecraft propulsion. *Micropropulsion for Small Spacecraft, M. Micci and A. Ketsdever, Eds., Reston, VA: AIAA*, 187, 2000.

[41] Juergen Mueller and Juergen Mueller. Thruster options for microspacecraft-a review and evaluation of existing hardware and emerging technologies. In *33rd joint propulsion conference and exhibit*, page 3058, 1997.

[42] H-D Ngo, A-T Tham, M Simon, and E Obermeier. Corner rounding to strengthen silicon pressure sensors using drie. In *SENSORS, 2008 IEEE*, pages 1576–1579. IEEE, 2008.

[43] Nam-Trung Nguyen, Steven T Wereley, and Seyed Ali Mousavi Shaegh. *Fundamentals and applications of microfluidics*. Artech house, 2019.

[44] Kwang W Oh and Chong H Ahn. A review of microvalves. *Journal of micromechanics and microengineering*, 16(5):R13, 2006.

[45] Kwang W Oh, Kangsun Lee, Byungwook Ahn, and Edward P Furlani. Design of pressure-driven microfluidic networks using electric circuit analogy. *Lab on a Chip*, 12(3):515–545, 2012.

[46] T Ohnstein, T Fukiura, J Ridley, and U Bonne. Micromachined silicon microvalve. In *IEEE Proceedings on Micro Electro Mechanical Systems, An Investigation of Micro Structures, Sensors, Actuators, Machines and Robots.*, pages 95–98. IEEE, 1990.

[47] Rijk Edwin Oosterbroek. *Modelling, design and realization of microfluidic components*. Citeseer, 1999.

[48] V. Pallichadath. Propulsion subsystem requirements for the delfi-pq satellites, 12-05-2017.

[49] V. Pallichadath. Propulsion subsystem mass, volume and power budgets, 16-2-2018.

[50] Vidhya Pallichadath, Leon Turmaine, Marsil A. C. Silva, Daduí Cordeiro Guerrieri, Sevket Uludag, Barry Zandbergen, and Angelo Cervone. In-orbit micro-propulsion demonstrator for pico-satellite applications. In *69th International Astronautical Congress, Bremen, Germany*, volume IAC-18, C4.8-B4.5A, 6, x44909. IAF, 10 2018.

[51] Jin Soo Park, Dong-Hyun Kang, Seung Min Kwak, Tae Song Kim, Jung Ho Park, Tae Geun Kim, Seung-Hyub Baek, and Byung Chul Lee. Low-temperature smoothing method of scalloped drie trench by post-dry etching process based on sf 6 plasma. *Micro and Nano Systems Letters*, 8:1–8, 2020.

[52] Prime Faraday Partnership. An introduction to mems (micro-electromechanical systems). *Prime Faraday Partnership*, 2002.

[53] Mukund R Patel. *Spacecraft power systems*. CRC press, 2004.

[54] B Pramanick, S Das, and TK Bhattacharyya. Mems based normally closed silicon microregulator for gas and water. *Sensors and Actuators A: Physical*, 205:15–25, 2014.

[55] Jin-Yuan Qian, Cong-Wei Hou, Xiao-Juan Li, and Zhi-Jiang Jin. Actuation mechanism of microvalves: A review. *Micromachines*, 11(2):172, 2020.

[56] Sampath Raghunathan Srikumar. Les of a novel wing/body junction: Anti-fairing. 2019.

[57] TD Riney. Residual thermoelastic stresses in bonded silicon wafers. *Journal of Applied Physics*, 32(3): 454–460, 1961.

[58] Patrick J Roache. Perspective: a method for uniform reporting of grid refinement studies. 1994.

[59] Jürgen Rödel and Jing-Feng Li. Lead-free piezoceramics: Status and perspectives. *MRS Bulletin*, 43: 576–580, 2018.

[60] John Saliba, Arij Daou, Samar Damiati, Jessica Saliba, Marwan El-Sabban, and Rami Mhanna. Development of microplatforms to mimic the in vivo architecture of cns and pns physiology and their diseases. *Genes*, 9(6):285, 2018.

[61] Shuchi Shoji and Masayoshi Esashi. Microflow devices and systems. *Journal of Micromechanics and Microengineering*, 4(4):157, 1994.

[62] Joachim Sihler. *A low-leakage 3-way silicon microvalve*. PhD thesis, Massachusetts Institute of Technology, 2004.

[63] Stefano Silvestrini. Closed-loop thrust magnitude control system for nano-and pico-satellite applications. 2017.

[64] Olivier Smal, Benoît Raucent, and Hervé Jeanmart. Fluid flow modelling of a micro-valve. *International Journal for Simulation and Multidisciplinary Design Optimization*, 3(2):356–362, 2009.

[65] Todd M Squires and Stephen R Quake. Microfluidics: Fluid physics at the nanoliter scale. *Reviews of modern physics*, 77(3):977, 2005.

[66] Niels Tas, Tonny Sonnenberg, Henri Jansen, Rob Legtenberg, and Miko Elwenspoek. Stiction in surface micromachining. *Journal of Micromechanics and Microengineering*, 6(4):385, 1996.

[67] M Tittu Varghese, BTC Zandbergen, M Mihailovic, JF Creemer, and PM Sarro. A silicon-based mems resistojet for propelling cubesats. In *IAF 62nd International Astronautical Congress, Cape Town*, 2011.

[68] Leon Turmaine. A technology demonstration payload for micro-resistojet thrusters on delfi-pq. 2018.

[69] Wouter van der Wijngaart, Håkan Ask, Peter Enoksson, and Göran Stemme. A high-stroke, high-pressure electrostatic actuator for valve applications. *Sensors and Actuators A: Physical*, 100(2-3):264–271, 2002.

[70] C Vicider, Ove Ohman, and Hgkan Elderstig. A pneumatically actuated micro valve with a silicone rubber membrane for integration with fluid-handling systems. In *Proceedings of the International Solid-State Sensors and Actuators Conference-TRANSDUCERS'95*, volume 2, pages 284–286. IEEE, 1995.

[71] Lisa R Volpatti and Ali K Yetisen. Commercialization of microfluidic devices. *Trends in biotechnology*, 32 (7):347–350, 2014.

[72] Zhihong Wang, Jianmin Miao, Chee Wee Tan, and Ting Xu. Fabrication of piezoelectric mems devices-from thin film to bulk pzt wafer. *Journal of electroceramics*, 24(1):25–32, 2010.

[73] T Watanabe and H Kuwano. A microvalve matrix using piezoelectric actuators. *Microsystem technologies*, 3(3):107–111, 1997.

[74] Keiichi Yanagisawa, H Kuwano, and A Tago. Electromagetically driven microvalve. *Microsystem Technologies*, 2(1):22–25, 1995.

[75] Eui-Hyeok Yang, Nishant Rohatgi, and Larry Wild. A piezoelectric microvalve for micropropulsion. In *NanoTech 2002-" At the Edge of Revolution"*, page 5713. 2002.

[76] Eui-Hyeok Yang, Choonsup Lee, and JM Khodadadi. Development of mems-based piezoelectric microvalve technologies. *Sensors and Materials*, 19(1):001–018, 2007.

[77] Xing Yang, Charles Grosjean, and Yu-Chong Tai. Design, fabrication, and testing of micromachined silicone rubber membrane valves. *Journal of microelectromechanical systems*, 8(4):393–402, 1999.

[78] Jong-Chul Yoo, YJ Choi, CJ Kang, and Yong-Sang Kim. A novel polydimethylsiloxane microfluidic system including thermopneumatic-actuated micropump and paraffin-actuated microvalve. *Sensors and Actuators A: Physical*, 139(1-2):216–220, 2007.

[79] Warren C Young, Richard G Budynas, and Ali M Sadegh. *Roark's formulas for stress and strain*. McGraw-Hill Education, 2012.

[80] A Cengel Yunus. *Fluid Mechanics: Fundamentals And Applications (Si Units)*. Tata McGraw Hill Education Private Limited, 2010.

[81] N Zaidon, AN Nordin, and AF Ismail. Modelling of microfluidics network using electric circuits. In *2015 IEEE Regional Symposium on Micro and Nanoelectronics (RSM)*, pages 1–4. IEEE, 2015.

[82] Guobing Zhou and Shi-Chune Yao. Effect of surface roughness on laminar liquid flow in micro-channels. *Applied Thermal Engineering*, 31(2-3):228–234, 2011.